Schweizerische Eidgenossenschaft
Confédération suisse
Confederazione Svizzera
Confederaziun svizra

Federal Department of the Environment, Transport,
Energy and Communications DETEC

Swiss Federal Office of Energy SFOE
Energy Research and Cleantech Division

Final report dated 15th August 2023

Optimal integration of electric vehicles fast charging stations into medium voltage power distribution grids

Source: GoFast

Date: 15 August 2023
Location: Bern

Publisher:
Swiss Federal Office of Energy SFOE
Energy Research and Cleantech
CH-3003 Bern
www.bfe.admin.ch

Subsidy recipients:
EPFL/STI/I EL/DESL
Station 11
1015 Lausanne

GridSteer Sàrl
c/o EPFL STI IEM DESL
ELL 038 (Bâtiment ELL)
Station 11
CH-1015 Lausanne

Romande Energie SA
Rue de Lausanne 53
1110 Morges

Gotthard FASTcharge Ltd
Via Industria 16
6826 Riva San Vitale

Authors:
Max Chevron, GridSteer, max.chevron@gridsteer.ch
Rahul Gupta, EPFL, rahul.gupta@epfl.ch
Sherif Fahmy, EPFL, sherif.fahmy@epfl.ch
Enea Figini, GridSteer, enea.figini@gridsteer.ch
Mario Paolone, EPFL, mario.paolone@epfl.ch
Georgios Sarantakos, EPFL, georgios.sarantakos@epfl.ch

SFOE project coordinators:
Karin Soderstrom, karin.soederstroem@bfe.admin.ch
Michael Moser, michael.moser@bfe.admin.ch
SFOE contract number: SI/502045-01

The authors bear the entire responsibility for the content of this report and for the conclusions drawn therefrom.

Résumé

Au niveau mondial, l'**utilisation de combustibles fossiles** pour le transport routier représente 12% des émissions de gaz à effet de serre (GES). En Suisse, le transport routier représente 30 % des émissions GES, avec une tendance à la baisse en raison de l'électrification progressive du secteur. Depuis 2020, la part des **véhicules électriques** (VE) dans les nouvelles ventes est passée de 20 % à plus de 50 %. Cependant, la nature stochastique de la **recharge des VE** et de la **production d'énergie renouvelable** a un **impact sur l'équilibre du réseau électrique à la fois pour les réseaux de transmission et de distribution**. La littérature récente a montré comment l'intégration proactive des véhicules électriques dans les systèmes électriques, alimentés par des sources de production renouvelables, peut améliorer le fonctionnement global du réseau pour répondre aux besoins locaux et globaux. À cet égard, le **projet vise** à améliorer le fonctionnement d'un réseau de distribution d'électricité hébergeant des ressources renouvelables stochastiques (de puissance nominale de l'ordre des MW), des systèmes de stockage d'énergie par batterie(BESS - de puissance nominale de l'ordre des MW), et des bornes de recharge rapide de niveau 3 pour les véhicules électriques (EVCS), afin de répondre à de multiples objectifs opérationnels du réseau. À cet égard, **quatre groupes de questions de recherche** ont été définis en relation avec : (a) le comportement des utilisateurs de VE, (b) la contrôlabilité des EVCS de niveau 3, (c) la capacité du réseau de distribution d'électricité hébergeant une production renouvelable stochastique substantielle d'EVCS à être dispatché et contrôlé avec succès en temps réel, et (d) la fourniture de services auxiliaires multiples par les réseaux de distribution d'électricité hébergeant des BESS et des EVCS contrôlables. **Les principaux résultats** du projet sont les suivants : (i) la combinaison d'EVCS et de BESS contrôlables présente des avantages mesurables pour le dispatching, l'exploitation et le contrôle du réseau locale de distribution, (ii) le contrôle des EVCS peut réduire le besoin d'investissement dans les BESS (c'est-à-dire réduire la puissance et l'énergie nominales) sans pour autant réduire de manière significative le niveau de satisfaction des utilisateurs de l'EVCS, (iii) le déploiement de contrôles spécifiques des EVCS peut réduire de manière significative leur impact négatif sur le réseau électrique (i.e., congestions et réglage de tension), et encore plus lorsque ces EVCS sont associés à la charge programmée de flottes d'EV commerciales, (iv) la rentabilité économique des BESS couplés aux EVCS est spécifique à chaque cas et, dans les conditions du marché actuelles et la configuration du projet, les services système fréquence est le contrôle qui offre le meilleur retour sur investissement.

Summary

The **utilization of fossil fuels'** for the road transportation accounts for 12% of the global greenhouse gas emissions (GHGs). In Switzerland, the road transport account for 30% of Swiss GHGs emissions with a decreasing trend due to the sector's progressive electrification. Since 2020, the **electric vehicles' (EVs)** share in new sales has increased from 20% to over 50%. However, the stochastic nature of both **EV's charging** and **renewables generation** has **an impact on the power grid** for both **transmission and distribution networks**. The recent literature has shown how the proactive EV integration in renewable-based power systems can enhance the overall power system's operation to satisfy local and bulk grid needs. In this respect, the **project aims** to enhance the operation of a power distribution grid hosting stochastic MW-class renewable resources, MW-class battery energy storage systems (BESSs), and level-3 EV fast charging stations (EVCSs), to serve multiple grid operational objectives. In this respect, four sets **of research questions** were defined in relation to: (a) the EV users' behavior, (b) the controllability of level-3 EVCSs, (c) the ability of the power distribution grid hosting substantial stochastic renewable generation and EVCSs to be successfully dispatched and controlled in real-time, and (d) the provision of multiple ancillary services to the power transmission grid by power distribution grids hosting controllable BESSs and EVCSs. The main project **outcomes** are the following: (i) combining controllable EVCSs and BESSs has measurable benefits for grid dispatching, operation and control, (ii) the control of EVCSs can reduce the need for BESS investment (i.e., reduce both power and energy ratings) without significantly affecting EVCS users' satisfaction, (iii) the deployment of specific controls of EVCSs can significantly lower their negative impact on the power grid, and even more when these EVCS are associated with scheduled charging of EV commercial fleets, and (iv) the economical profitability of BESSs coupled with EVCSs is case-specific and, under the current market conditions and the projects' setting, the frequency containment reserve (FCR or primary frequency regulation reserve) is the control with the best return on investment.

Contents

Abbreviations

ADMM	Alternating Directing Methods of Multipliers
ADNs	Active Distribution Networks
BESS	Battery Energy Storage System
CFCS	Commercial Fleet Charging Station
CPCs	Controllable Power Converters
CPs	Charging Profiles
CSC	Current Source Control
DESL	Distributed Electrical Systems Laboratory
DoD	Depth of Discharge
DP	Dispatch Plan
DSO	Distribution System Operator
EMS	Energy Management System
EVC	EV Chargers
EVCSs	Ev Charging Stations
EVs	Electric Vehicles
FCR	Frequency Containment Reserve
FE	Forecasting Error
GHI	Global Horizontal Irradiance
GIT	Global Irradiance and Temperature
GMM	Gaussian Mixture Model
LER	Limited Energy Reservoirs
MABI	Maximum Absolute BESS Injections
MAE	Maximum Absolute Error
MBU	Maximum BESS Usage
MEVUS	Minimum EV User Satisfaction
MPC	Model Predictive Control
MPP	Maximum PCC Power
MSBC	Multi-Service Battery Controller
O&M	Operation and Maintenance
OP	Optimization Problem
PFCS	Public Fast Charging Station
PCC	Point of Common Coupling
PLCC	Pearson's Linear Correlation. Coefficient
PMUs	Phasor Measurement Units
PPS	Peak Power Shaving
SCs	Sensitivity Coefficients
SoC	State of Charge
TSO	Transmission System Operator
UEE	Uncovered Energy Error
VSC	Voltage Source Control

1. Introduction

1.1 Background information and current situation

The worldwide **utilisation of fossil fuels'** as primary source of energy accounts for most global greenhouse gas emissions (GHGs). International efforts, such as the **Paris agreement** [1], aim to address this issue, requiring countries to develop national GHGs emissions targets and associated actions for their achievement. Switzerland has already undertaken several steps in this direction. On January 1st, 2018, the **Swiss Energy Strategy 2050** came into force, and on 27 January 2021, the Federal Council adopted the climate strategy for Switzerland, aiming for a net zero emissions target by 2050 [2]. Since **energy usage represents 75%** of the national GHG emissions [3], fossil fuels need to be replaced by renewable energy resources for the achievement of this strategy. This would require the electrification of several sectors (e.g., private heating and mobility along with several industry processes) and the massive integration of distributed renewable energy resources into the power grid.

Regarding the **road transport**, it accounts for 30% of Swiss CO_2 emissions [4]. In recent years, significant progress has been achieved in the electrification of this sector, via the massive rollout of low-emission vehicles, including electric vehicles (EVs)[1] (Figure 1) [5]. It is indicative that, since the beginning of the MESH4U project, in 2019, the EVs' share in new sales has increased from 20% to over 50%.

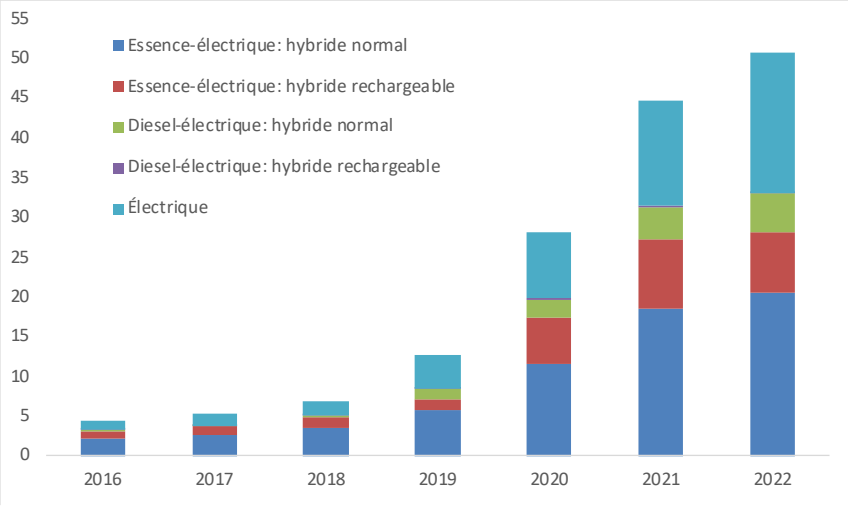

Figure 1: Trend of the new sales of low- or zero-emission vehicles in Switzerland

The transport sector electrification entails several challenges for the power grid. Indeed, this transition should be paired with the massive integration of renewable energy resources to positively affect the GHGs of the sector. However, the stochasticity of both EV's charging and renewables generation both have an impact on the power grid equilibrium. In this respect, proactive EV integration in renewable-based power systems can serve as grid-connected small-scale distributed battery systems capable to enhance the overall system's operation. As a matter of fact, EVs can adapt their charging patterns to provide ancillary services to both transmission and distribution grid operators such as: dispatchability of the aggregated local resources, frequency containment and restoration reserves, as well as support to voltage control and line congestion management of the local distribution grid. They can further facilitate the integration of renewable energy resources, especially if coupled with stationary battery energy storage systems (BESSs).

1.2 Purpose of the project

The synergy between EVs and renewables allows for a reduction of fossil-fuel dependency in both the electricity generation and transportation sectors. The deployment of smart grid solutions, including EV charging strategies, along with the optimal coordination of distributed energy resources, requires a multi-disciplinary approach and the solution of complex control problems of stochastic nature. Furthermore, a suitable validation

[1] By EVs, we refer to vehicles with a full electric power train and an on-board battery energy storage system (BESS).

in realistic scale pilot and demonstration sites can be made possible via close collaboration between academia and industry.

The MESH4U project capitalizes on the existing infrastructure in two demo sites: one in Aigle developed in the frame of the SFOE P&D REeL project, and another one represented by the smart grid demonstrator on the EPFL campus. For the purpose of the project, these sites have been expanded by adding to the EPFL smart grid platform a high-power EV fast charging station and establishing in Aigle links with various energy actors, notably the local distribution system operator (DSO), Romande Energie, and the local municipality of the city of Aigle. This setup is ideal to develop specific and advanced control frameworks aiming at: (i) optimizing the EV integration in renewable-supplied power grids, (ii) analyzing the performance of the developed tools in a real environment, while (iii) considering insights and feedback from the DSO's and the society's perspectives. In view of the above, the aim of this project is to enhance the operation of a power distribution grid hosting stochastic MW-class renewable resources, MW-class BESSs, and EV fast chargers, in order to maximize multiple grid operational objectives and by leveraging the controllable power electronics converters of the considered resources.

1.3 Objectives

For the achievement of the above-mentioned project's multiple aims, the research activities focused on the development of advanced control algorithms for optimal resources control. These algorithms have been developed and validated in different settings, namely: (a) off-line simulations, (b) experiments on the EPFL smart grid platform, and (c) simulations based on the real-scale experimental setup in Aigle.

The developed control algorithms interact with the controllable resources' power electronic units to enable the provision of power system ancillary services, even in the presence of large stochastic EV charging. A centralized master-level controller is designed for the coordination of the controllable resources for the optimal provision of these services, while respecting the single units' and grid operational constraints. For example, when controlling the EV fast-charging station, the EV batteries' wear and tear associated with a variable power charging process are minimized with the objective of maximizing the users' energy demand while respecting all operational constraints of EVs and their batteries. The inputs of the main controller are: (i) the actual status of the available controllable resources (such as the information on the equivalent virtual battery of the aggregated available EVs given the users' needs and the real-time status of the controllable BESS) and (ii) the real-time power grid conditions, e.g., system frequency, nodal voltages and loading levels of lines/transformers. These last are made available via a cutting-edge sensing infrastructure based on advanced phasor measurement units (PMUs) specifically developed for power distribution grids. These devices have already been installed in both experiment sites at the EPFL campus and Aigle demo (see Section 2).

Since the existing literature has largely proven that the uncontrollable EV charging can severely and negatively impact the power-grid, we envisage that through the joint control of BESSs and EVCSs, our proposed control algorithms are capable to guarantee the provision of the above-listed power system services even in the presence of a large stochastic EV charging patterns.

More specifically, the elements of the proposed control methodology are the following:

- *Type of measurements*: nodal voltages, branch currents, active/reactive powers, resource-specific data.
- *Method of measurements*: measurements at the BESS, PV and EVCS grid connection points and for the electrical grid by means of a PMU infrastructure. Further resource-specific data are also be pulled in order to create databases that can be used for forecasting purposes.
- *Objective of the measurement*: input and validation of control approaches for real time congestion, load profile management and voltage control of MV power distribution grids.
- *Duration of each measurement*: during the entire activity.
- *Frequency of measurements*: minimum 1 Hz
- *Planned evaluation of efficiency*: ability to control the EVCSs according to the objectives set in all stages of the control algorithm (see Section 3 where it is explained that the proposed framework includes both a day-ahead and real-time phases).

2. Description of facility

As mentioned in *1.3 Objectives,* the control algorithms are validated through simulations both at the EPFL and in Aigle as well as on a real hardware at the EPFL smart grid platform. This iterative process enables the implementation and control's benchmarking first in a simulation setup and then in a real-scale experimental environment before assessing, via simulations, its impact at the Aigle demo site. In this respect, both the demo site in Aigle and the one at the EPFL possess similar assets, namely PV generation, a MW-class BESS and PMUs for the real-time situational awareness of the local power distribution grid. Yet, the laboratory facilities possess a wider variety of controllable elements such as supercapacitor bank, heat pump, and fuel cells, allowing the development of a control framework applicable in a wide range of use cases. Furthermore, since the infrastructure is connected to the EPFL power grid, there is more flexibility to study and validate future business models that cannot be tested in a real-life grid. In what follows, details about the two experimental set-ups are provided.

2.1. The EPFL smart grid platform at the EPFL Distributed Electrical Systems laboratory (EPFL-DESL)

A dedicated hardware infrastructure has been developed at the EPFL-DESL with a similar structure to the Aigle demo site (meaning REeL + MESH4U infrastructure). This enables the iterative process of validating and improving the developed controls. This infrastructure includes the following elements (see Figure 2):

a) A low-voltage Cigré benchmark microgrid connected to a 21kV busbar through a 630 kVA 21kV/400V transformer that hosts the following resources (non-exhaustive lists of the relevant resources that are used in this project):
    a. 40kW (peak) photovoltaic (PV) system, divided in three separated power plants supported by measurement units of meteorological quantities (e.g., solar irradiance, environmental temperature etc.);
    b. 25 kW – 25 kWh BESS based on Lithium Titanate Oxide electrochemistry;
    c. fast dynamic AC electronic load emulators up to an overall rated power of 30 kVA;
    d. a level-2 charging station combining two type 2 EV plugs (up to 22kW) and a bidirectional (up to 10 kW) CHAdeMO-type charging station.

b) A GoFast EV fast charging station equipped with the same technology of the foreseen installation in the Aigle site. It is connected to the same 21kV busbar of the microgrid through a 630 kVA 21kV/400V transformer (see Figure 6 and Figure 7).

c) A 720kVA / 560 kWh Lithium Titanate Oxide BESS connected to the same 21kV busbar of the microgrid through a 0.72 MVA 21kV/300V transformer (see Figure 3 and Table 1).

d) Two independent PMU-based real-time situational awareness systems capable of performing a low-latency high-frequency state estimation of: (i) the 21kV grid and, (ii) the low-voltage microgrid.

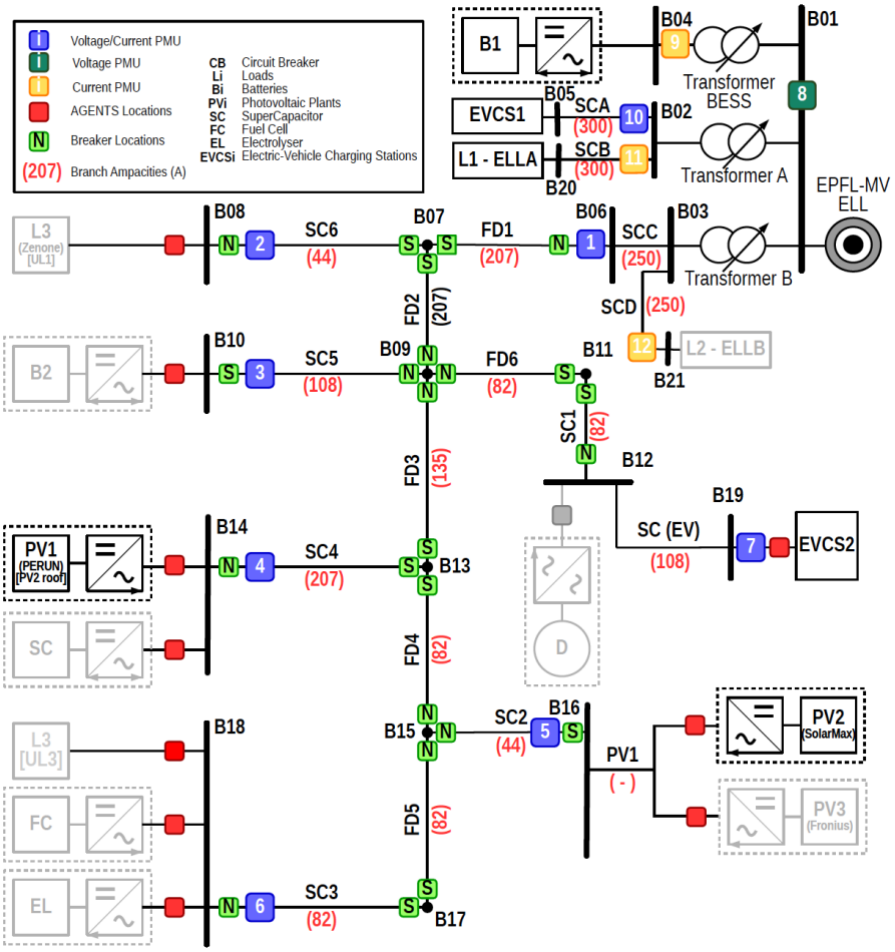

Figure 2: Configuration of the EPFL smart grid platform.

More details on some key pieces of infrastructure used for the project are presented below.

EV fast charging station

A GoFast fast-charging station infrastructure for private EV users is available on the EPFL smart grid platform. It is composed of an off-board Combined Charging System (CCS)/CHAdeMO EV chargers (EVC), with a power rate of up to 150 kW. A single transformer is used to supply this charging station from the 21 kV MV utility grid and from the same busbar where the BESS, as described below, is connected.

BESS

A 720 kW/560 kWh BESS connected to a 21 kV distribution feeder. It is based on the Lithium Titanate Oxide technology, which can perform up to 20.000 complete charge-discharge cycles at 4C discharge rate. Table 1 presents the main parameters of the EPFL BESS.

Figure 3: External view of the utility-scale BESS available at the EPFL smart grid platform and used for this project.

Table 1: Main parameters of the EPFL BESS

Parameter	Value
System parameters	
Nominal Energy Capacity	560 kWh
Maximum Power	720 kVA
Battery configuration	9p{15s{3p{20s}}}
Communication protocols (cycle time)	Modbus (>100 ms), Ethercat (10 ms)
Cell parameters	
Nominal capacity	30 Ah
Nominal voltage	2.3 V
Voltage range	1.7-2.7 V
Maximum current	120 A (4C)
Impedance	2 mOhm
Expected cycle life	20000 full cycles
Expected calendar life	20 years
Weight	1100 g
Dimensions (LxWxT)	287x179x12 mm
Inverter parameters	
Maximum AC-power	720 kVA
Rated AC-power	615 kVA
Rated grid voltage	300 V, three-phase
Maximum AC-current	1385 A
AC-current distortion (THD)	3%
Nominal DC Voltage	750 V
DC Voltage range	500-890 V
Efficiency	>97%
Transformer parameters	
Rated power	630 kVA
High voltage	3x21 kV
Low voltage	3x300 V
Group	Dd5

PMU-based grid sensing infrastructure

A cutting-edge sensing infrastructure for modern electrical distribution systems is available on the Aigle demonstrator site offering low-latency (<100ms) and high refresh rate (50 estimations per second) accurate awareness of the grid state. In particular, it is a commercial power grid monitoring and automation system based on time-and-phase aligned measurements of the grid voltage/current synchrophasors. Such a sensing system provides operators, and the foreseen controllers, with the real-time knowledge of the grid status and allows to locate and isolate faults enabling the restoration of power.

These devices provide measurements with a reporting rate of 50 frames-per-second (i.e., a reporting time 20 ms) and a total vector error in the order of 0.0X%[2]. The measurements provided by these devices are used for both the day-ahead dispatch plan construction (i.e., using historical data) as well as for the real-time control of the system (see Figure 4).

[2] The total vector error is the quantity used by the IEEE Standard C37.118 to quantify the accuracy of PMUs.

Figure 4: Image of a PMU toolkit installed in both demonstration sites.

Solar irradiation measurement units

A Global Irradiance and Temperature (GIT) measurements box has been installed at the EPFL smart grid platform in order to support a data-driven intra-day forecast of PV generation. The GIT box measures the global horizontal irradiance (GHI) and the PV cell temperature. The GHI is measured using a pyranometer Apogee SP-230 and the temperature using a Mouser 595-LMT87LP sensor. The acquisition system is based on a ruggedized National Instrument (NI) cRIO 9063. Measurements are sent to a central server using a 4G modem and saved at 1-second resolution in order to capture fast GHI dynamics (see Figure 5).

Figure 5: The GIT measurements box.

Figure 6: The EV fast charging station at the EPFL smart grid platform.

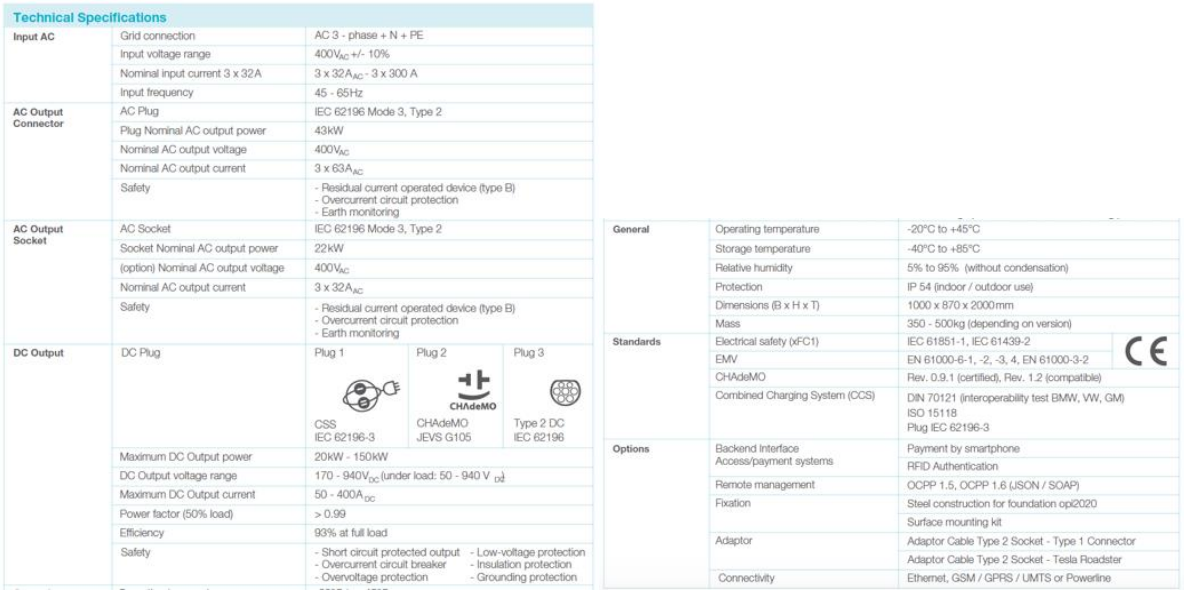

Technical Specifications				
Input AC	Grid connection	AC 3 - phase + N + PE		
	Input voltage range	$400V_{AC}$ +/- 10%		
	Nominal input current 3 x 32A	3 x $32A_{AC}$ - 3 x 300 A		
	Input frequency	45 - 65Hz		
AC Output Connector	AC Plug	IEC 62196 Mode 3, Type 2		
	Plug Nominal AC output power	43kW		
	Nominal AC output voltage	$400V_{AC}$		
	Nominal AC output current	3 x $63A_{AC}$		
	Safety	- Residual current operated device (type B) - Overcurrent circuit protection - Earth monitoring		
AC Output Socket	AC Socket	IEC 62196 Mode 3, Type 2		
	Socket Nominal AC output power	22kW		
	(option) Nominal AC output voltage	$400V_{AC}$		
	Nominal AC output current	3 x $32A_{AC}$		
	Safety	- Residual current operated device (type B) - Overcurrent circuit protection - Earth monitoring		
DC Output	DC Plug	Plug 1 CSS IEC 62196-3	Plug 2 CHAdeMO CHAdeMO JEVS G105	Plug 3 Type 2 DC IEC 62196
	Maximum DC Output power	20kW - 150kW		
	DC Output voltage range	170 - 940V_{DC} (under load: 50 - 940 V_{DC})		
	Maximum DC Output current	50 - 400A_{DC}		
	Power factor (50% load)	> 0.99		
	Efficiency	93% at full load		
	Safety	- Short circuit protected output - Overcurrent circuit breaker - Overvoltage protection	- Low-voltage protection - Insulation protection - Grounding protection	

General	Operating temperature	-20°C to +45°C
	Storage temperature	-40°C to +85°C
	Relative humidity	5% to 95% (without condensation)
	Protection	IP 54 (indoor / outdoor use)
	Dimensions (B x H x T)	1000 x 870 x 2000mm
	Mass	350 - 500kg (depending on version)
Standards	Electrical safety (xFC1)	IEC 61851-1, IEC 61439-2
	EMV	EN 61000-6-1, -2, -3, 4, EN 61000-3-2
	CHAdeMO	Rev. 0.9.1 (certified), Rev. 1.2 (compatible)
	Combined Charging System (CCS)	DIN 70121 (interoperability test BMW, VW, GM) ISO 15118 Plug IEC 62196-3
Options	Backend Interface Access/payment systems	Payment by smartphone
		RFID Authentication
	Remote management	OCPP 1.5, OCPP 1.6 (JSON / SOAP)
	Fixation	Steel construction for foundation opl2020
		Surface mounting kit
	Adaptor	Adaptor Cable Type 2 Socket - Type 1 Connector
		Adaptor Cable Type 2 Socket - Tesla Roadster
	Connectivity	Ethernet, GSM / GPRS / UMTS or Powerline

Figure 7: Technical specifications of the GoFast EV fast charging station at EPFL smart grid platform.

2.2. Demo site - Aigle

The demo site in Aigle is a field test facility already developed in the frame of the SFOE P&D REeL project and maintained as a permanent research infrastructure. It is located in a rural area, hence it embeds all the peculiarities of modern distribution networks: relatively long radial feeders, presence of distributed generators, and relatively large, concentrated load (e.g., the under-development EV fast charging station). More specifically, the feeder originates in Collombey (VS) and interfaces 68 independent producers (1790 kW, out of which 815 kW from small hydro power stations) and a large PV installation of 1.6 MW at the Migros-Carports. The power consumption reaches 4.3MW during the winter and 2.9MW during the summer. Therefore, it represents a unique field test site to carry out research in the domain of control and coordination of renewables-fed medium-voltage grids.

In the frame of the MESH4U project, this site was used for the assessment of the impact of the deployment of fast EVCSs on the power grid. This was achieved through simulations that consider all the specifications of the existing infrastructure and those of the EV fast charging station which is already foreseen to be developed on this site. The controllability of the available units, i.e., an MW-class BESS connected to a 20kV grid hosting the multi-MW PV and small hydropower plants, allows for the provision of several power system services, such as system frequency regulation, local voltage control, and lines congestion management, considering the actual status of the grid provided by an-already-deployed PMU-based situational awareness system. A dedicated setup for the measurement of meteorological quantities is also installed in the vicinity of the PV plants, to enable the accurate intra-day forecasting of the PV generation to support the formulation and implementation of predictive controls.

A schematic representation of the demonstration site is shown in Figure 8.

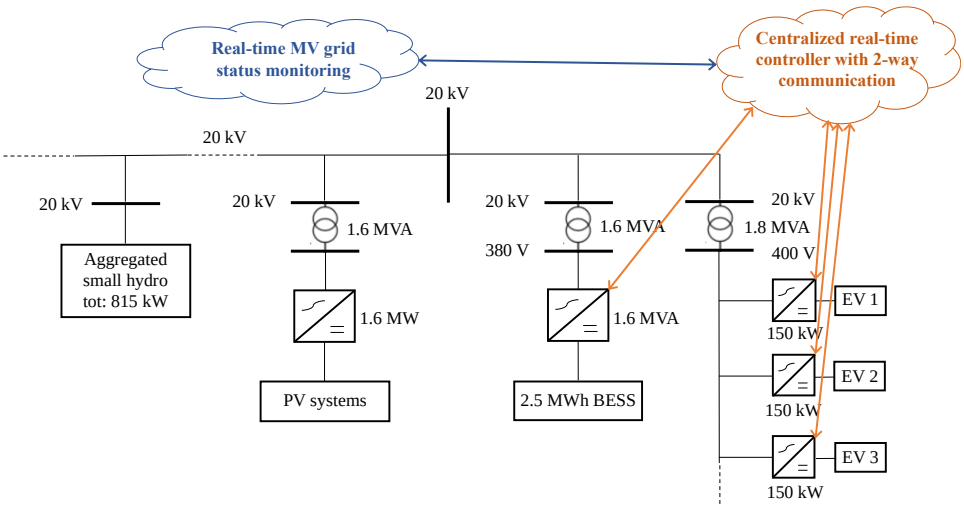

Figure 8: Schematic representation of the field demonstration site in Aigle.

As already mentioned, the site includes devices that have been installed in the frame of the SFOE P&D REeL project and were used in the frame of the MESH4U project too. Additional details about these devices are given below.

MW-class battery energy storage system

The MW-class BESS installed at the Aigle demonstration site is characterized by rated power and energy capacities of 1.6 MVA and 2.5 MWh, respectively. The BESS cells' electrochemistry is Lithium, Graphite / Nickel Manganese Cobalt. This specific type of cells' electrochemistry allows up to 4,500 complete charge-discharge cycles at 100% depth of discharge (DoD) at a 1C rate[3]. The BESS is equipped with a 1.6 MVA 4-quadrant converter that can operate in current source control mode (CSC, or grid-feeding) or in voltage source control mode (VSC, or grid-forming) with a seamless transition between the two operating modes. Furthermore, the BESS and its converter are characterized by a power ramping rate of several tens of MW/s (therefore, suitable to provide frequency containment reserve).

A 3-phase step-up transformer with a nominal power of 1.6 MVA connects the LV AC side of the BESS converter to the external medium voltage utility grid. The high-voltage side of the transformer has a delta connection with phase-to-phase rated voltage of 21 kV.

To achieve maximum flexibility and fast controllability of the system, a custom-made energy management system (EMS) is available to interact independently with the BESS power converter controller and the master string controller of the BESS cells. Such a design enables to send commands to the power converter via Ethercat with fast and low-latency communication (i.e., latency and refresh rate below 10 ms).

The technical parameters of the MW-class BESS, along with some insights on its controllability, are included in the Table 2.

[3] The C-rate is the unit to measure the speed at which a battery is fully charged or discharged. More specifically, the 1C rate of a battery cell represents the level of constant current charge or discharge that the cell can sustain for one hour of time.

Table 2: Technical parameters of the available MW-class BESS

Parameter	Value
BESS energy capacity	2.5 MWh
Expected battery cycle life	4.500 full cycles (100% DoD @ 1 C discharging rate). Remaining end of life capacity: 80%
Maximum AC apparent power	1.6 MVA
Rated AC grid voltage	21 kV
Rated grid frequency	50 Hz
DC voltage range	620 - 840 V
AC converter voltage	380 V ±10%
Operation on 4 AC P/Q quadrants	Capable
Distortion factor (THD) at the HV connection of the step-up transformer	< 3%
Efficiency	> 90% for all the operating conditions
Type of cooling	forced air convention
CSC operation mode	Capable
Refresh rate of CSC operation mode	10 ms
VSC operation mode	Capable
Refresh rate of VSC operation mode	10 ms

Level 3 EVCS

Initially, 4 EVCS, identical to the one installed on the EPFL smart grid platform, were foreseen to be installed at the Aigle demo site. Given the evolution of the EV market (see 1.1 Background information and current situation), the foreseen power rate of each of them was in the meantime increased to 300 kW for each of them. Since the authorization for their installation was postponed after the end of the project, simulations were undertaken based on the characteristics of the foreseen EVCS and data from other sites.

GIT meteo-boxes

Four Global Irradiance and Temperature (GIT) measurement boxes have been installed at the demo site in Aigle. These boxes are identical to the one installed at EPFL smart grid platform (see description above).

PMU measurements units

20 PMUs have been installed at the Aigle demo sites. These units present similar characteristics with those described above.

3. Procedures and methodology

To achieve the targets of this demonstration project, a set of activities have been defined. First, the project covers a **series of simulation studies** for the design and performance assessment of control solutions for optimal management of resources in converter-dominated modern power distribution grids. The simulation studies are based on realistic models of both Aigle the EPFL test facilities. Both models include insights of the resource's actual communication features (e.g., time latencies) and technical constraints (e.g., capability curves of the controllable converters). Then, a set of tests is undertaken on the real hardware available at the EPFL-DESL laboratory test facilities, which iteratively enables the implementation on a reduced-scale experimental environment before testing the proposed solutions on the larger experimental environment at the EPFL smart grid platform. Finally, the validated methodology is used for the Aigle site to simulate the foreseen integration of the EV fast charging station within the local power distribution grid. In particular, the same hardware for the EV fast charging station foreseen in Aigle is used in the laboratory environment, making it possible to test the control features of the available hardware as well as to enable real-time 2-way communication with the backend of the off-board EV charger. Information flow from the EVS is necessary for the centralized controller since it takes into consideration the status of the EV battery as well as the EV user's needs (e.g., desired departure time and desired EV State-of-Charge - SoC). This information is indeed used by the centralized controller to define the optimal and fair scheduling of the EVs charging processes.

The following list discusses the specific activities with associated detailed descriptions.

1. **EV users behavior analysis**

The first step is to grasp a behavioral assessment of EV users. In this respect, a survey was undertaken to know how flexibility can be harvested from charging sessions with minimal impact on customer satisfaction. The second step is to collect a large set of EV charging sessions data. This allows building statistical models to generate reliable scenarios of EV charging sessions.

2. **EV Charging station controllability**

In practice, controlling EV charging sessions is a complex task. Each EV, each plug type and each charging station have their own peculiarities, constraints, and capabilities and no one size fits all control frameworks in the context of controlling EV charging. Hence, the objective of this part is to assess the controllability of sessions in the context of a specific EV car, plugs and station.

3. **Dispatch plan and real-time control**

Providing day-ahead accurate prediction of the power profile of a whole subnetwork is a valuable information for aggregators and distribution systems operators (and even more so as intermittent renewable generation and stochastic EV charging consumption grows). Dispatching and real-time control to provide such service has been extensively researched by EPFL and Gridsteer partners of the project. Here the goal is to include highly stochastic, yet partially controllable EV charging stations, to the controllable assets of the targeted power distribution grid.

4. **Multi-service battery control**

This activity aims at undertaking a market assessment of economic and technical interest of an extensive list of services that BESSs can provide. Each service is listed in terms of economic interest but also complementary with other services provision. Then, a control framework is developed to allow multi-service provisioning from BESSs. Simulations and dedicated experimental campaign are performed in this respect. These activities valorize the involvement into the project of a variety of energy stakeholders, namely the DSO, local authorities and operators of EV charging stations.

4. Activities and results

4.1. EV user behavior analysis

4.1.1. Behavioral assessment

Context

Understanding the EV users' behavior, and willingness to provide flexibility during a charge, is crucial to developing a feasible EV charging station control scheme. A web-based system and a QR code have been placed on the parking spots of the EV fast-charging station installed at EPFL since end of January 2022. Once the customer scans the QR code, an on-line survey is made available. Although no reward scheme has been set, over 89 valid submissions have been recorded until April 2023. On top of these submissions, an additional 42 surveys have been given in person during experiments. A total of 131 participations have then been used for this analysis.

The goal of this survey is two-fold:

1. understand the willingness of the customers to participate in providing flexibility in their EV charge;
2. quantify the accuracy of the user to estimate their EV charge duration and energy needs.

Questions

The questions of the survey have been defined to be easy and fast to answer yet yield as much interesting information as possible. To this date, the average time spent on the survey is less than 3 minutes. The set of questions (from a mobile device) is reported in the screenshots here below.

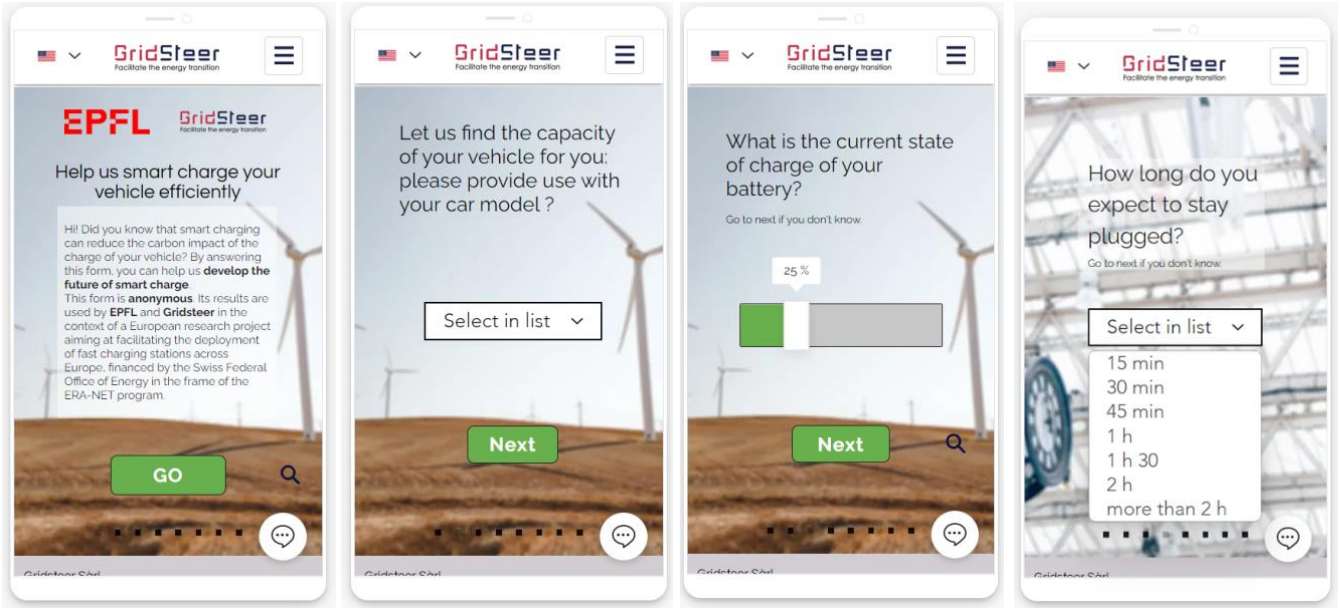

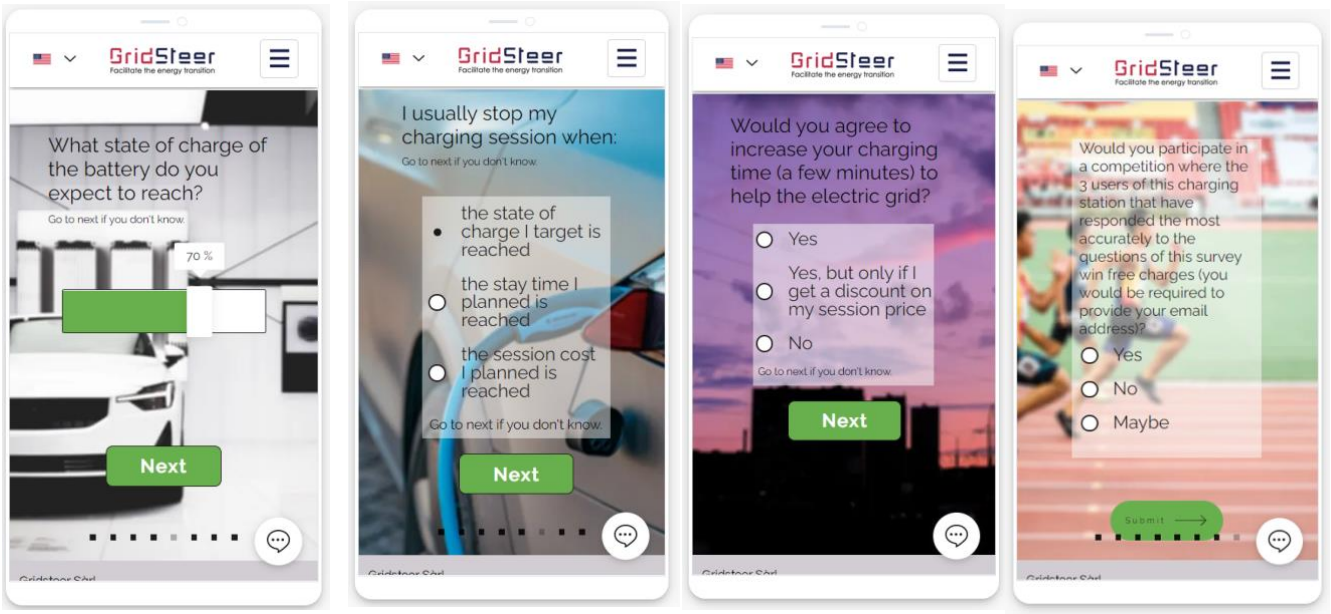

Results

With the submitted responses, the actual charging profile of each user has been compared to the (user's) predicted one. The set of questions and post-process analysis allowed to yield results on the following behavioral features:

a) deviation of energy delivered vs expected;
b) deviation of stay duration vs expected;
c) end of session decision factor;
d) tolerance for flexible charge;
e) gamification readiness.

Deviation of energy delivered vs expected

The energy delivered to the customer vs his prediction has been computed based on the customer's inputs on (a) the EV starting SoC; (b) the EV target SoC at the end of the session; and (c) the vehicle model (for retrieving the battery capacity).

The post-process analysis determined whether the delivered energy is higher, lower, or similar to the customer target. From 79 valid answers and charge profiles, it turns out that customers tend to charge in average about 4.3% more energy than the targeted value (see Figure 9) and that the spread of that deviation is quite large.

In general, users tend to leave with delivered energy close to their targeted one. Although not significant enough for a statistically strong conclusion, it seems some users may receive slightly less energy and still reach their target (and be satisfied by their charging session). Hence, some (limited) controllability could be applied with minimized customer dissatisfaction.

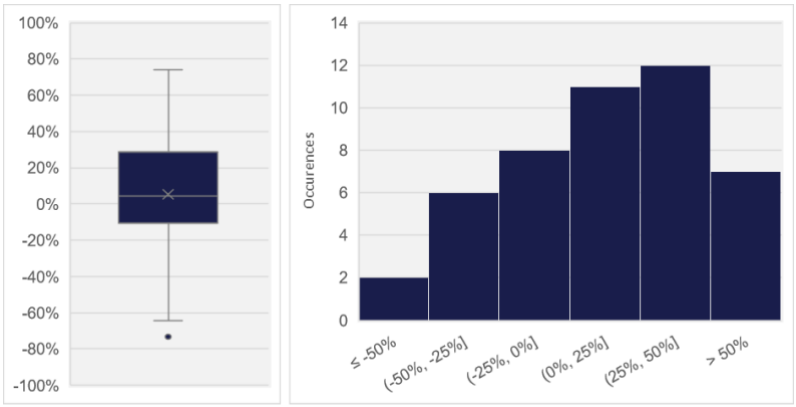

Figure 9: Energy delivered to customer vs his prediction.

Deviation of stay duration vs expected

Comparing the expected vs realized charge duration of 100 valid answers, we found that users tend to stay, in average, 10% longer than anticipated (see Figure 10). The overall answers are also quite precise between planned and actual stay duration. This is most probably due to the accurate prediction of the EV on-board computer to reach the target SoC.

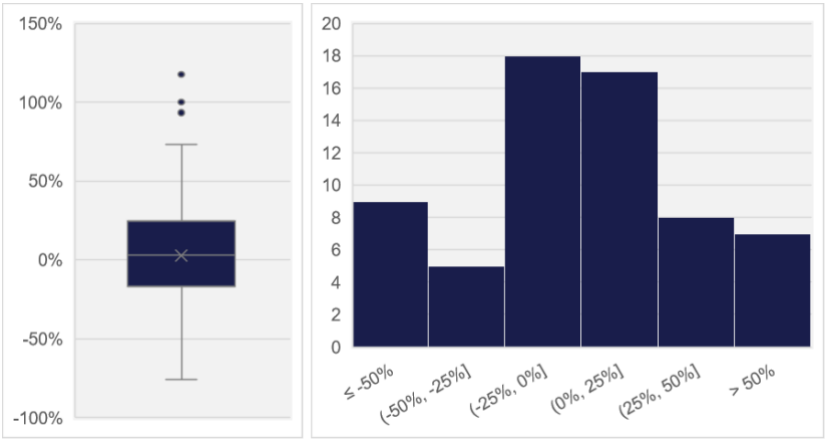

Figure 10 : Stay duration of customer vs his prediction.

End of session decision factor

Out of 101 valid answers, the decision factor to stop the charging session has been assessed. More than half of the participants decide to stop their session based on the EV battery SoC. About a third of them leave when their stay time is reached and, finally, 5% leave when a specific cost is reached (see Figure 11).

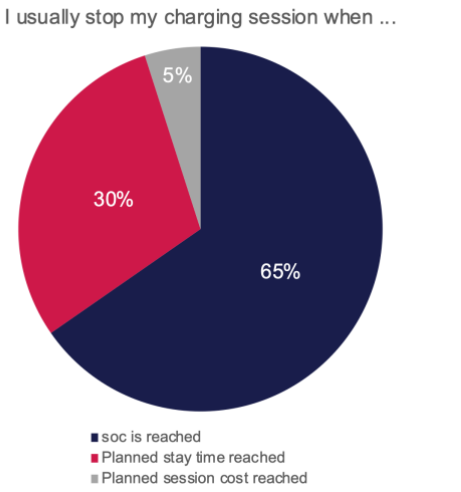

Figure 11 : Distribution of the end-of-session decision factor.

Tolerance for flexible charge

To assess the customers' readiness to allow for a slower charge if this helps the electrical grid, the following question was posed:

"Would you agree to increase your charging time (a few minutes) to help the electric grid? "

More than two thirds of 101 participants would accept to provide flexibility and half of them would do it even without a discount (see Figure 12). This shows a rejoicing number of customers ready to participate in grid flexibility. It is however possible that these participants could be considered as early adopters in the EV sector and as electric cars will gradually hit the common mass market, these results may change over time.

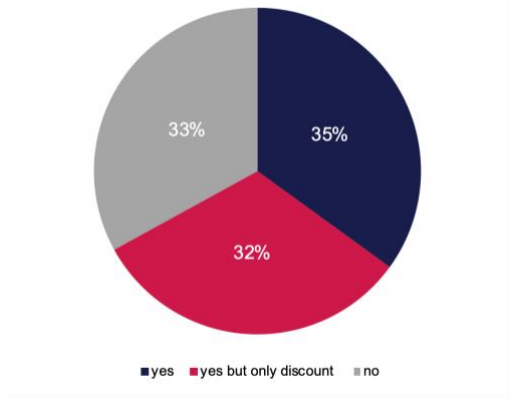

Figure 12 : EV customers tolerance for flexible charge.

Gamification readiness

Asking users to provide some information on their upcoming charge profile might be crucial to control their charge without significantly impacting the user's satisfaction. However, the user does not have any incentive to answer honestly. A competition between users for the most accurate answers could serve as such incentive. In this respect, the following question was formulated.

"Would you participate in a competition where the 3 users of this charging station that have responded the most accurately to the questions of this survey win free charges (you would be required to provide your email address)?"

Out of 60 valid answers, it appears that the reluctance to share one's email is still significant. 40% of users would rather not participate and an additional 27% are unsure (see Figure 13).

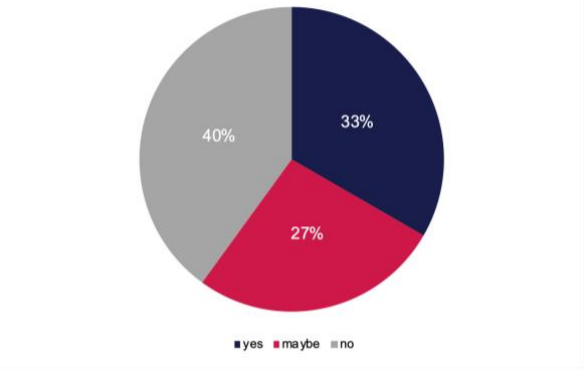

Figure 13 : EV customers gamification readiness.

Conclusions

Results show that slightly controlling the EV charging profile for the benefit of the grid without significantly changing their charging satisfaction, is a feasible control option. This conclusion can be derived in view of the following considerations:

1. customers tend to receive, in average, more energy than targeted (4% more);
2. customers leave, in average, later than anticipated (10% later);
3. customers are ready to extend their charge duration (by few minutes) to help the grid (35% against a discount and 32% even without a monetary discount).

Finally, it is worth observing that a control framework leveraging these flexibilities should consider that most users (65%) plan their EV charge based on a target SoC than a target stay duration or cost.

4.1.2. EV user statistical modelling[4]

Since EVCSs are considered as controllable entities, i.e., the active (and reactive) power injections of EVCSs are variables of the problem, there is the need to forecast EV users' behavior. More specifically, for a given EVCS, EV users behavior refer to: (i) the number of EV charging sessions per day, (ii) the EVs' arrival and departure times, (iii) the initial and final, i.e., target, SoCs of EVs' batteries, (iv) the EVs' battery capacities, and (v) the minimum and maximum active power injections (defined as, respectively, the maximum and minimum imposed by either the EVCSs' converters limits or by the EV on-board controller).

In view of the large number of quantities that define EV user behavior, a data-agnostic tool was developed that uses any amount of data with as many features as an input, and outputs the best Probability Density Functions (PDFs) that would model the data. As the input data is multi-variate, the output PDFs can be anything from several univariate distributions to a full Gaussian Mixture Model (GMM) that models all input variables (or features) simultaneously. The algorithm's idea is to fit the data with different functions then output the best-performing-probabilistic-model. The flowchart of the developed toolbox is depicted in Figure 14. As can be seen, the input data is first filtered then fitted to: (i) one multi-variate GMM (Multivariate GMM- approach, see Figure 14), (ii) *N*-univariate GMMs (Univariate GMM-approach, see Figure 14), with *N* being the number of input features, and (iii) a mix of multi- and uni-variate GMMs (Mixed GMM-approach, see Figure 14). Once all three fittings converge, they are compared using accuracy, bias and correlation metrics. Finally, the fitting with

[4] This section is adapted from the work presented in [14].

the overall best metrics is selected as the best-performing-probabilistic- model, where from the latter, EV user behaviors can be inferred based on the features – i.e., season and day-type – of the day we wish to forecast.

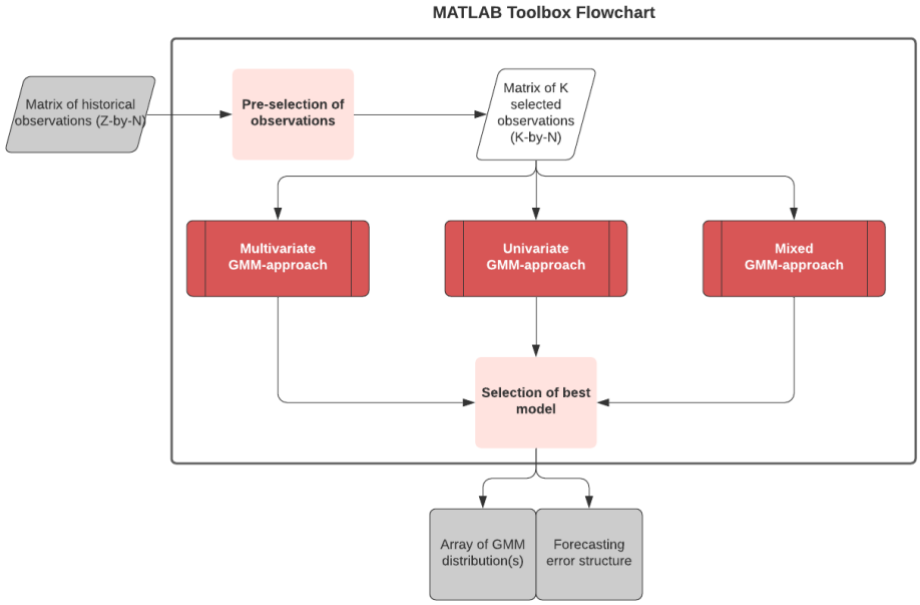

Figure 14: Flowchart of the data-agnostic EV user statistical modelling toolbox.

In the following, each sub-block of the flowchart in Figure 14 is explained.

Pre-selection of observations. The $Z \times N$ – where Z is the number of measurements and N is the number of features or variables – input matrix of measurement is automatically filtered based on a set of control parameters specified by the user. Namely the user chooses the season and the day-type (i.e., weekend or weekday). Indeed, this enables the user to create EV user behavior models that pertain to a specific season and day-type. The tool automatically provides the best model that statistically represents a subset of the historical data where only the desired season and day-type are included. The block outputs a reduced measurement matrix with a dimension of $K \times N$, where K_{meas} is the number of selected measurements.

Multi-variate GMM approach. In this block, the built-in MATLAB function `fitgmdist` is used together with `K-fold` cross-validation [15] to compute an optimal GMM[5] considering all filtered inputted variables simultaneously. The `fitgmdist` function has multiple parameters that can alter the outputted model. Therefore, in the proposed method, we loop over the number of components of the outputted GMM (from one to a user- defined maximum GMM order). For each GMM order, cross-validation is used to avoid over- fitting in cases where the GMM order gets too high (see Figure 16). Namely, for each GMM order, first, the filtered dataset is randomly divided into T groups (or folds) of the same size. Then, for each fold, the training and testing process is repeated T times. The training and testing process consists in fitting a GMM to the training data using the order of the current iteration, then, regenerate data using the GMM model and compute the mean absolute error between the newly generated data and the test set. Every fitted GMM-distribution is saved during the iterations. The model with the least mean absolute error at the loop exit is, then, chosen. The general scheme and details of the proposed method are shown in, respectively, Figure 15 and Figure 16.

[5] A Gaussian Mixture Model is a weighted sum of multivariate normal distributions. More information about GMMs can be found in [16].

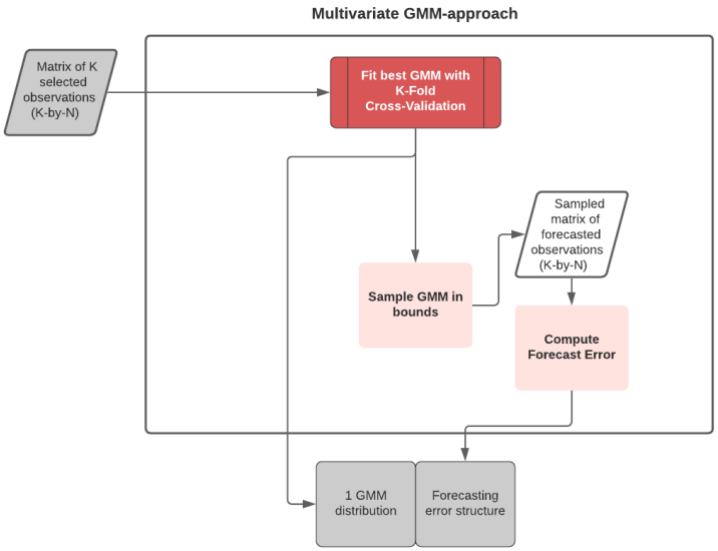

Figure 15: Flowchart of the multi-variate GMM approach block.

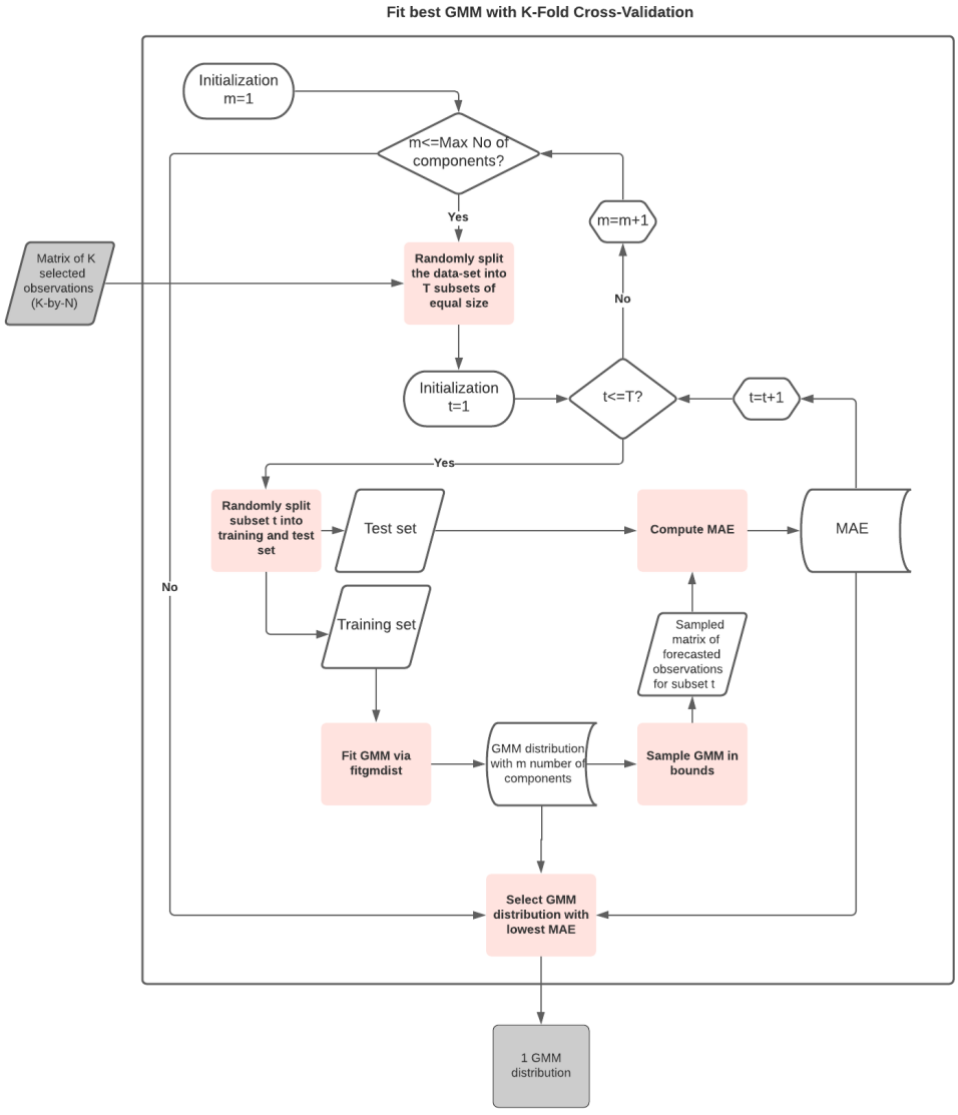

Figure 16: Flowchart of the mixed GMM-based process.

Uni-variate GMM approach. In this block, in contrast to the Multi-variate GMM approach that implicitly considers the input dataset variables or features to be correlated, the input data is modelled separately, i.e., each variable (column of the filtered data matrix) is considered independent of the others and, therefore, is fitted with its own GMM. Hence, the output of this block is a set of *N* GMMs. A schematic diagram of the block is shown in Figure 17.

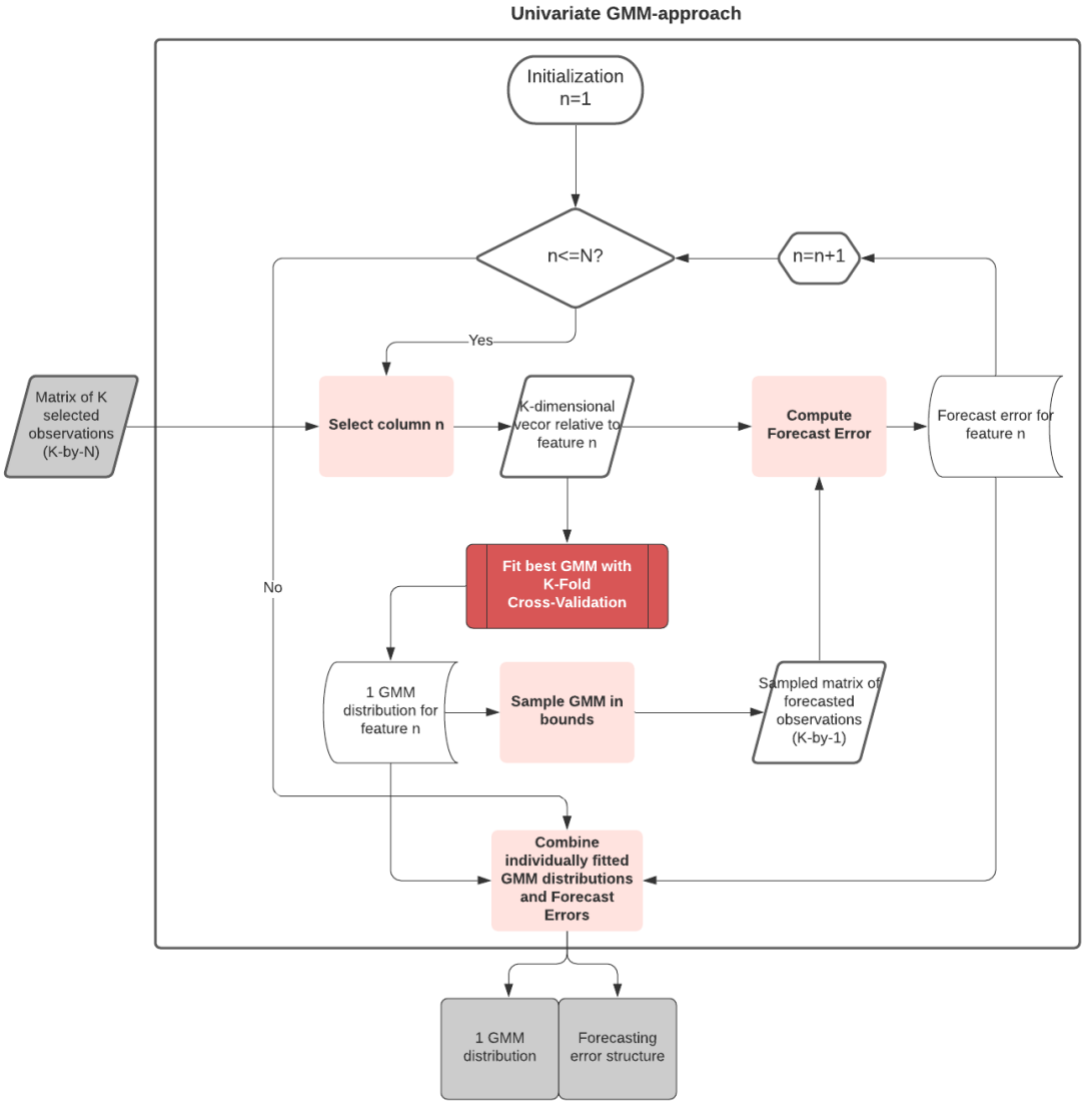

Figure 17: Flowchart of the univariate GMM approach block.

Mixed GMM approach. This block combines the functionalities of the two previous ones. Indeed, if the variables of the input dataset are split into correlated and uncorrelated datasets, it is optimal to fit the correlated variables with the multivariate-GMM approach. In contrast, the uncorrelated variables would be fit separately using the univariate-GMM approach (see Figure 18). In this approach, the correlation analysis block uses Pearson's Linear Correlation Coefficient (PLCC)[6]. The correlation tolerance is user-configurable, with a default value set at 0.5[7].

[6] The interested reader is referred to [17] for more information about the PLCC.
[7] Recall that PLCC values range from -1 to +1, where -1 corresponds to negative correlation while +1 corresponds to positive correlation.

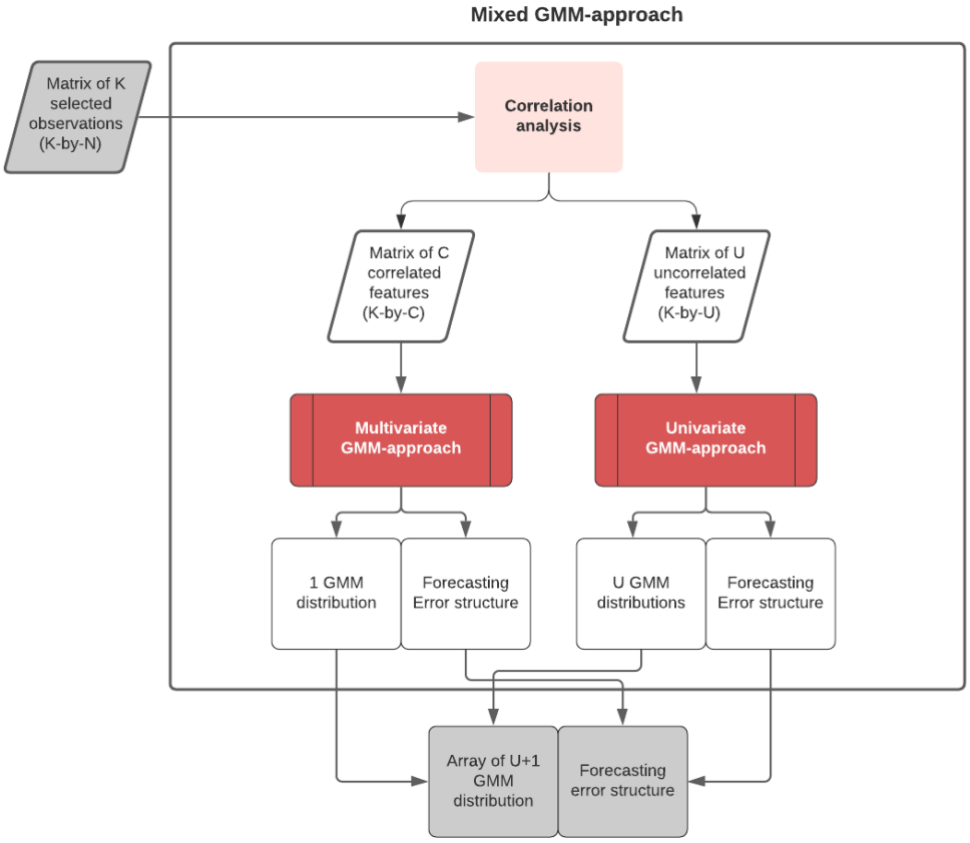

Figure 18: Flowchart of the mixed GMM approach block

Select best GMM approach. A set of metrics is used to select the *best-fitted* models between the three approaches. The metrics aim at evaluating the performance of each approach based on (i) *accuracy (A)*, i.e., the average discrepancy between individual pairs of observation and forecast, (ii) *bias (B)*, i.e., the mean deviation from average observation and average forecast, (iii) *correlation (R)*, i.e., PLCC correlation of observation and forecast vectors, and (iv) *goodness-of-fit*, i.e., the result of a P-value (two-sample Kolmogorov-Smirnow) test on the null hypothesis of having the same underlying distribution for the observation and forecast datasets. Table 3 enumerates all the metrics used to quantify *accuracy* (Table 3.a) and *bias* (Table 3.b), where $\epsilon_k = y_k - x_k$ is the forecast error and $Q_k = y_k / x_k$, with x and y being, respectively, the K-dimensional observation and forecast vectors. The final selection relies on the global forecasting error defined as a weighted sum of all the metrics. Formally, the forecasting error (FE) is defined as $FE = w_1 A + w_2 B + w_3 R$, where w_1, w_2, w_3 are user-defined weights, and A, B, R given by the following definitions.

$$A = \frac{1}{N}\sum_{n=1}^{N}\frac{|MAPE_n| + |sMAPE_n| + |MSA_n|}{3}$$
$$B = \frac{1}{N}\sum_{n=1}^{N}\frac{|MPE_n| + |SSPB_n|}{2},$$
$$R = \frac{1}{N}\sum_{n=1}^{N}|100(1 - R_n)| \qquad (1)$$

where each R_n corresponds to the PLCC correlation of the observation and forecast vectors for a given feature. The other metrics are defined in Table 3. The weights need to be assigned by the user based on the application requirement. In our case, based on the observed performance, it was observed that setting all the weights to 1 lead to the best results as the obtained models were not biased in favour of a specific metric. Note that in (1), the absolute value is used as the aim is not to evaluate the direction of the bias, i.e., under or over-estimation. Finally,

the *best-fit* is chosen as the set of models of the approach that leads to: i) the smallest FE, *and* (ii) a two-sample Kolmogorov-Smirnow test result that is lower than a user-defined critical value of 5% significance level[8].

Table 3: Metrics to compare different approaches and choose the best-fit.

(a) Accuracy metrics

Metric	Unit	Formula
Mean absolute percentage error (MAPE)	[%]	$\frac{100}{K}\sum_{k=1}^{K}\left\|\frac{\epsilon_k}{x_k}\right\|$
Symmetric mean absolute percentage error (sMAPE)	[%]	$\frac{100}{K}\sum_{k=1}^{K}\frac{\epsilon_k}{0.5(x_k+y_k)}$
Median symmetric accuracy (MSA)	[%]	$100\left(e^{\text{MEDIAN}(\lvert\log_e Q_k\rvert)}-1\right)$

(b) Bias metrics

Metric	Unit	Formula
Mean percentage error (MPE)	[%]	$\frac{100}{K}\sum_{k=1}^{K}\frac{\epsilon_k}{x_k}$
Median log accuracy ratio (MdLQ)	different	$\text{MEDIAN}(\log_e Q_k)$
Symmetric signed percentage bias (SSPB)	[%]	$100\text{sign}(MdlQ)\left(e^{\lvert MdlQ\rvert}-1\right)$

4.2. EV charging station controllability

There are different types of EVs being sold worldwide. In terms of charging, EVs present different plug-types based on their charging modes. Type-1 and type-2 charging plugs refer to single-phase and three-phase EV plugs for charging. As the electric connection of these plugs is AC, this requires the EV to have an on-board converter to convert AC to DC electricity supply. The IEC-61851 protocol used to communicate between a type-1 or type 2 AC plugs and an EVCS. The protocol is based on an analog square wave signal that dictates to an EV the maximum *per phase* RMS AC current it can absorb. DC charging plugs (e.g., CHAdeMO and CCS) refer to EV plugs that have a DC power supply (i.e., the AC-to-DC converter is outside the EV and installed into the EVCS). The ISO-15118 protocol used to communicate between the DC plug and the EVCS. This protocol is based on an TCP/IP layer protocol, that, in practice, can dictates to an EV its maximum allowable bidirectional active power exchange. In theory, the protocol also enables unidirectional (i.e., from the EV to the grid) reactive power control. However, in reality, the off-board AC-to-DC inverters in DC EVCS do not offer that possibility (this is also the case of the DC EVCS of this project).

Since different EV manufacturers produce vehicles with different components, EVCSs' controllability becomes dependent on both: (i) the EVCS (e.g., internal control mechanisms, different available plug types and front-end communication protocol), and (ii) the EV management system, converter ramping time for on-board chargers and charging limitations that are function of the battery SoC and its state (mainly temperature and cells balance).

As previously detailed, in the scope of the MESH4U project, a commercial GoFast (EVTec) charger was installed at the EPFL smart grid platform. As shown in Figure 7, the charger includes 6 plugs: 2 CCS, 1 CHAdeMO, 1 DC Tesla Plug, 1 AC Type 2 plug and 1 AC Type 2 socket. The idea of this section is to experimentally test the controllability of the GoFast charger. The aim is to compute EV charging power set-point at the centralized master multi-objective-controller level that will communicate, in real-time, with the single distributed units. The backend of all the EVC is accessible through the custom EMS, which continuously communicates with the external master controller. The EMS provides information about the connected EVs (e.g., SoCs, expected departure times, and total energy [kWh] needed to be charged within the available times) in order to offer an aggregated degree of flexibility that the main controller can consider and exploit in both the day-ahead dispatching and the real-time tracking phases of the proposed overall optimization problem (OP) (see Section 4.3 for more details). In the real-time phase, within the boundaries communicated by the EMS, optimal EV charging set-points are computed to set the charging power rates to be satisfied at best by the EV

[8] We refer the interested reader to [18] for more information about the Two-sample Kolmogorov-Smirnow test.

users' needs while satisfying the power grid constraints. With this IT configuration, only an external communication link from the main centralized controller to the EMS has to be established.

The manufacturers of the charging station (i.e., EVTec) gave access to the specifications of their proprietary communication protocol called DCMS. The DCMS protocol aims to exchange data packets containing: (i) monitoring information (packet sent from charger to our controller) and (ii) active power setpoints (packet sent from our controller to the charger). The protocol is based on a communication framework where setpoints can only be sent when a monitoring packet is issued/sent[9]. EVTec developed two versions of the DCMS protocol:

1. v0.9 enables a bidirectional communication with the EVCS allowing to exchange aggregate information. In other words, one can receive aggregate information (i.e., sum over all plugs) from the charger and can send setpoints only at the charger level (i.e., cannot control separate plugs).
2. v2.0 that extends v0.9 by allowing a *per-plug* control and data polling.

Both versions of the protocol have been integrated into a dedicated LabView code. This code streams the collected data to a dedicated database installed in a local server for logging purposes. A GUI of the logged data has also been developed on Grafana (see Figure 19 for an example of some of the recorded data of an *uncontrolled* EV charge).

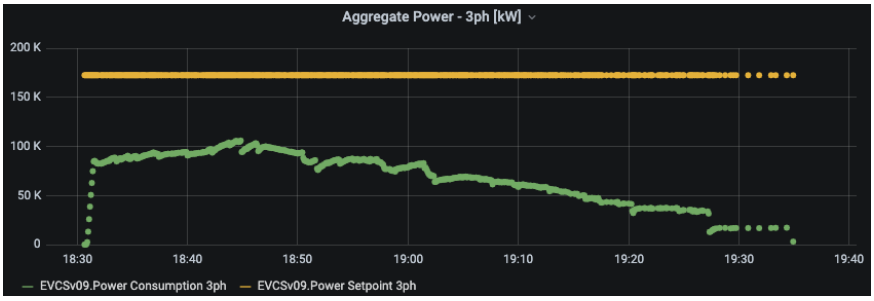

(a) Three-phase (Green) measured power and (Yellow) power setpoint

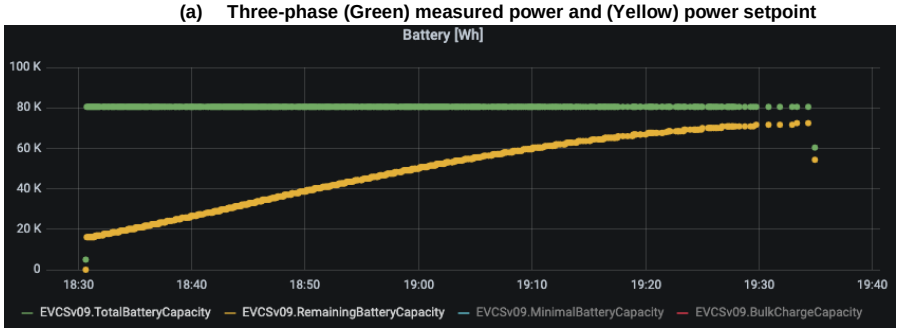

(b) (Green) Battery capacity and (Yellow) Measured SoC

Figure 19: GUI based on Grafana for the DCMS logged data from the EVTec EVCS installed at the EPFL.

The controllability assessment experiment was performed on the EVTec GoFast EVCS at EPFL using a Tesla Model S90D (the car was equipped with a dedicated adapter making it compatible with a CCS plug). The experiment consists in sending to the car subsequent step-like power setpoints in order to measure its response (i.e., ramp-up and ramp-down times) and the accuracy (i.e., error between the requested setpoint and implementation in steady state). The durations of the steps are long enough for the implementation to stably reach a steady state. Before and after the step-like setpoints requests, the requested power has been kept to 20kW. The results are shown in Figure 20 and Table 4. The measured ramp-up and ramp-down times are in the order of several seconds and are linearly increasing with the setpoint amplitude, meaning that the power ramping is constant (we measured values in the range of 3 – 5 kW/s).

The implementation error is characterized by a quadratic trend where for low and high setpoints the errors are the larger.

[9] In practice, we observed that monitoring packets are issued by the charger in an event-based fashion.

Figure 20: Results of GoFast station controllability experiment: Active power setpoint vs. implementation

Table 4: Results of GoFast station controllability experiment: rise times & implementation errors.

Setpoint [kW]	Rise Time [s]	Descent Time [s]	Maximum absolute steady state error [W]	Mean absolute steady state error [W]
100	17.6	7	2300	1366
80	11.95	6	600	270
60	9	3	997.5	1730
40	5	3	1412	4390
20	N/A	N/A	1722	1980

Furthermore, tests were carried on the non-commercial EV charging stations at the microgrid. Power-to-current lookup tables were characterized in order to enable explicit, active power control of Type-2 plugs[10]. As a result, power-to-current lookup tables were precomputed for every available Type-2-EV charging plug. The tables are shown in graphical format in Figure 21. These lookup tables are obtained for two cars: Renault Zoe and Tesla Model S 90D. From the plot for Renault Zoe, it can be observed that when the setpoint – i.e., per-phase current maximum allowable current – is lower than 7A, the car does not consume any active power. This, in practice, means that the EVCS controller could ask this car not to consume power while remaining plugged. This is not the case for the Tesla Model S as it consumes power even when the setpoint is set to the IEC-61851 standard's minimum allowable setpoint of 6A. As a result, a plugged Tesla Model S will always consume around 3kW[11].

[10] Note that Type-2 plugs are controlled through an analog pulsed signal that dictates to the EV the RMS value of the maximum per-phase current it can consume.

[11] Note that, in practice, the Tesla Model S's power could be reduced to zero if, as explained in the IEC-61851 standard, the duty-cycle of the control pilot signal is set to a value higher than 95%. However, through testing, it was observed that this created issues for the EV's on-board controller as the car was constantly locking and unlocking its plug. As a result, the look-up table was deliberately started from a minimum three-phase power of 3kW.

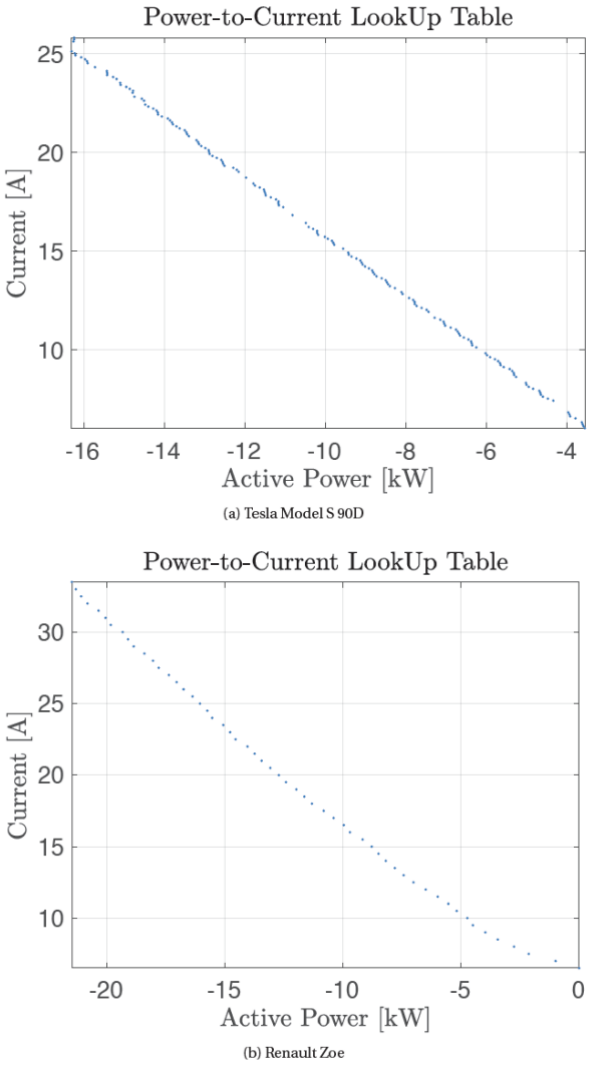

Figure 21: Power-to-current setpoint lookup tables.

4.3. Day-ahead and real-time control[12]

4.3.1. Introduction

As discussed in [9]: "*Day-ahead and intra-day scheduling of heterogeneous DERs has been advocated in the literature as a way to minimize the effect of uncertainties. It consists in determining an average power trajectory (dispatch plan – DP) at a certain resolution before operations, that is then followed during real-time operation.*". Even though the presented algorithms in [9] are aimed to work for heterogeneous resources, EVCSs' power and energy demands were not explicitly accounted for in the proposed problem formulation. Therefore, with adequate control, EVCS can be turned from given boundary conditions (i.e., demand) to controllable assets for the control of ADNs.

As a result, in the frame of the MESH4U project, the work in [9] was extended by accounting for EVCSs' power and energy demand flexibilities in both day-ahead and real-time stages. More specifically, in the scheduling phase on the day before operations, the stochastic OP computing an aggregated DP at the Point-of-Common-Coupling (PCC) is extended to account for EVCSs as controllable entities. We recall that the proposed day-ahead OP in [9], accounts for: (i) demand/generation forecasting errors using scenarios, (ii) resource

[12] This section has been readapted from the work presented in [14].

constraints, and (iii) grid operational constraints by leveraging the so-called grid sensitivity coefficients (SCs). In the real-time phase, the grid-aware model predictive control (MPC)-based control algorithm proposed in [9] is extended with an MPC-augmented-version of the EV-subproblem model presented in [19]. The real-time OP of [9] aims to securely – i.e., while accounting for resource and grid operational constraints – compute active and reactive power set-points for heterogeneous resources so that their aggregated contributions track the day-ahead optimally computed DP.

In summary, this activity enhances previous work of the EPFL-DESL by: i) extending the day-ahead OP of [9] to account for EVCSs as controllable entities by leveraging a developed EV user behavior forecasting tool, ii) extending the real-time control-algorithm of [10] with a MPC-augmented version of the EVCS GULC in [19], iii) numerically illustrating the merits of considering EVCSs as controllable entities in the day-ahead DP generation stage, and iv) experimentally validating on the EPFL smart grid platform the proposed real-time extension by safely tracking an optimally generated DP.

The rest of this section is organised as follows. In Sec. 4.3.2 the general assumptions, e.g., grid modelling, and problem formulation are presented. In Sec. 4.3.3 the day-ahead problem extension is presented. The latter also includes details on the developed EV user behaviour forecasting tool and illustrative numerical simulations to showcase the advantages of controlling EVCSs in the day-ahead stage. In Sec. 4.3.4 the real-time problem extension is presented. In Sec. 4.3.5 an experimental validation, performed on the EPFL-DESL microgrid, of all contributions of this chapter is shown. Finally, Sec. 4.3.6 concludes this section.

4.3.2. Problem Statement & Overview

The focus is on power grids whose states are evolving slowly enough such that they can be modelled by phasors. Specifically, ADNs are considered where the admittance matrix is known and whose power equilibrium is described by the standard AC power-flow equations. Furthermore, such grids shall contain uncontrollable and controllable resources. Hereinafter, controllable resources are considered to be interfaced through grid-following Controllable-Power-Converters (CPCs), that can receive active and reactive power setpoints[44]. This chapter focuses on the ADNs' dispatching at their PCC according to an optimally computed DP through a two-stages process as shown in Figure 22.

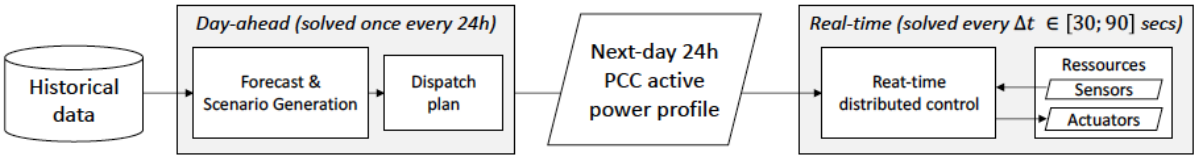

Figure 22: Schematic overview of the proposed two-stage ADN dispatch.

Day-ahead stage: in this stage, the operator computes a DP in the form of an active power profile to be followed at the PCC during the next-day operation. The DP is generated by accounting for ADNs and controllable resources operational constraints by leveraging proper forecasting of next-day grid status (i.e., injections of uncontrollable resources and EV user behaviours). As a result, this stage is split into two processes, named as forecasting and DP in Figure 22. During the forecasting process, historical data is input into statistical engines that output parametric probabilistic models. During the DP process, a security-constrained scenario-based OP, leveraging the models created in the last process, is solved to generate a 24h active power DP. Typically, the generated DPs are injection profiles with time resolutions of 30-600 seconds. The DP is operational starting at 00:00 of the next day.

Real-time stage: as explained in [9], in this stage, the ADN resources are controlled in real-time to compensate for power mismatches at the PCC between the optimal DP and actual realization. As in the day-ahead stage, the control problem accounts for ADNs and controllable resources operational constraints. Unlike the day-ahead stage, the resources' states are assumed to be known through accurate sensing. The problem is expressed by leveraging a MPC formulation to account for potential uncertainties along the optimization horizon. This stage's control algorithm starts and ends at, respectively, 00:00 and 23:59 of the day of operation.

As a final note, it is important to remind that, given the large uncertainties accompanying forecasting next-day grid statuses, the day-ahead stage considers ADNs to be balanced and, as a result, only the single-phase direct sequence equivalent of the ADN is considered.

4.3.3. Day-ahead stage

As previously mentioned, the main goal of the day-ahead stage is to compute the DP. Indeed, when proper forecasting tools are used, building a 24h active power profile at the PCC to be tracked by the next-day-real-time controller promotes optimal next-day usage of controllable resources. For instance, as the OP leverages a full-day MPC formulation, with proper next-day solar irradiance forecasting, the controller can anticipate the charge/discharge of a controllable BESS. Furthermore, as explained in [9], the grid operator can practically assume knowledge of the next-day PCC active power consumption since: (i) the DP is generated through stochastic scenario-based security-constrained optimization and (ii) the real-time controller steers the controllable resources to guarantee that the PCC injection realization matches the DP. As a result, the grid operator will have fewer potential risks of operational and financial costs related to real-time balancing or reserve activation needs [16].

This chapter's contribution extends the developed algorithms in [9] by accounting for EV user needs and considering EVCSs as controllable resources in both day-ahead and real-time stages. As EV user behaviours (e.g., arrival/departure times and energy needs), and associated Charging Profiles (CPs), exhibit high stochasticity, including EVCSs in the problem formulation increases the prediction and control complexities of the day-ahead stage. However, by adequately anticipating the latter, the whole bulk power-grid would need less secondary and tertiary power reserves.

In summary, the DP is the optimal result of a stochastic MPC-based OP. As in [9], the OP accounts for (i) next day-stochasticity of non-EV injections through scenarios, (ii) grid operational constraints by leveraging SCs and (iii) controllable resources' operational constraints (e.g., PQ capability and state-of-energy constraints). Unlike in [9], the OP (i) further accounts for next day-stochasticity of EV user behavior through scenarios, and (ii) is solved iteratively in order to alleviate the inaccuracies introduced by the linearization of the power-flow equations. In the following, first the details of the forecasting block of Figure 22 – i.e., the scenario generation block – are given, then the OP objective, constraints and solution algorithm are presented. Finally, the advantages of considering EVCSs as controllable resources in the day-ahead stage are showcased through numerical simulations.

Scenario Generation

Since the day-ahead OP is solved before the realizations of the next-day, proper forecasting is needed to predict different next-day quantities. The idea of the forecasting tool is to generate scenarios that can be used to formulate the OP of the day-ahead stage. In the following, first the techniques used to create probabilistic models for different stochastic quantities are described. Then, the ways those models were combined to generate scenarios are presented.

Non-EV injection models

For non-EV injections, a model can be in the form of a PDF created from historical data. Specifically, the PDFs are created using historical data in the form of active and reactive nodal injection profiles for every resource connected to a given node of the targeted ADN. For load resources, each of these profiles is first clustered into 4 seasons (i.e., winter, spring, summer and autumn), then, sub-clustered into day-type (i.e., working days, weekend or vacation days), then, finally sub-sub-clustered into the fixed time resolution of the control algorithm. For generation resources, assumed to be in the form of PV plants, each of these profiles is first clustered into 4 seasons (i.e., winter, spring, summer, and autumn), then, sub-clustered into sky-clearness (i.e., sunny, cloudy, and overcast), then, finally sub-sub-clustered into the fixed time resolution of the control algorithm. In both cases, for every sub-cluster, a Gaussian mixture model (i.e., a sum of multivariate Gaussian normal distributions) is fitted to the data using MATLAB's function `fitgmdist`. This is done to account for the time correlation between the different time-steps for each specific sub-cluster. In the end, we obtain multivariate PDFs (the random variables here are all the time-steps of a given day) for each nodal injection (i.e.,

uncontrollable generation or load) pertaining to a season and day-type or sky clearness. From those models, daily injection profiles can be inferred based on the features – i.e., season and day-type for loads and season and sky-clearness for generation – of the day we wish to forecast.

EV injection models

Refer to Sec. 4.1.

Combining non-EV injections and EV user models into scenarios

Following the non-EV injections and EV user models presented above, it is natural to define a non-EV injection scenario as a day-long power injection profile and, an EV user scenario as the set of all charging sessions for a specific day, where each charging session is described by: (i) the EV's arrival and departure times, (ii) initial and desired EV battery SoCs, (iii) the EV's battery capacity and (iv) minimum and maximum active power injection limits. Each uncontrollable resource would, therefore, have at least two associated non-EV injection scenarios (active and reactive power injections) and each EVCS would have one associated EV user scenario. The total number of scenarios would be the total combinations of all generated scenarios for all uncontrollable resources and EVCSs. This, clearly, can lead to a high complexity if the method of selecting the number of scenarios, presented in Rem. 3 of [14], is used without any assumptions. Therefore, first, we conservatively assume that the non-EV load and generation injection scenarios are *all* either at their 5 or 95% percentiles when inverse-sampling from the constructed models. Namely, this would lead to the four non-EV injection scenarios described in Table 5. With this assumption, the total number of scenarios would be four times the total number of considered EV user scenarios.

Table 5: Considered non-EV injection scenarios

Scenario number	Percentile of all uncontrollable loads [%]	Percentile of all uncontrollable generation (P-V plants) [%]
1	5	5
2	5	95
3	95	5
4	95	95

Since that reduced number still led to an OP with high complexity, a step further was undertaken to reduce the number of considered EV user scenarios. To do so, the k-means clustering algorithm [20] was leveraged together with the scenario number selection method explained in Rem. 3 of [14][13]. Namely, first the number of needed scenarios to achieve statistically meaningful results is computed. Then, after generating the needed EV user scenarios, the scenarios are partitioned and stored into a user-defined number of clusters (NUM_CLUSTERS) using the k-means clustering algorithm. Then, the medoid, i.e., the original scenario with the lowest probability distance from the centroid of a cluster, of each cluster is selected as a representative EV user scenario for the ones stored in that cluster. The reason the medoid is selected rather than the centroid, i.e., cluster analytical center, is that the centroid of a cluster is an artificial scenario that might not have any physical meaning. Finally, the output is the *representative* EV user scenarios, i.e., the cluster medoids. Naturally, this means that the reduced total number of considered EV user scenarios is equal to the user-defined number of desired clusters for the k-means algorithm (i.e., NUM_CLUSTERS).

It is important to note that, in their natural form, EV user scenarios are not easy to input into the k-means clustering algorithm. This is due to the complexity of their forecasting models, e.g., it is difficult to compare, for instance, a scenario that has 2 morning charging sessions w.r.t a scenario that has 3 evening charging sessions. As a result, *extra-features* needed to be defined to describe each EV user scenario. These features are listed in Table 6 and were used as input to the k-means clustering algorithm.

[13] For the interested reader, a similar yet more complex method of leveraging the k-means clustering algorithm to reduce the number of needed scenarios in a stochastic OP can be found in [21].

Table 6: Considered extra-features to describe an EV user scenario

Feature number	Description
1	Total number of charging sessions
2	Sum of all stay duration of all charging sessions
3	Sum of all energy demands of all charging sessions
4	Average maximum active power injection limits of all charging sessions
5	Occupancy rate* from 00:00 to 3:59
6	Occupancy rate* from 04:00 to 7:59
7	Occupancy rate* from 08:00 to 11:59
8	Occupancy rate* from 12:00 to 15:59
9	Occupancy rate* from 16:00 to 19:59
10	Occupancy rate* from 20:00 to 23:59

*For a given time interval, the occupancy rate is defined as the ratio of the number of control time-steps where a plug is used, over the total number of control time-steps.

Optimization Problem

As previously explained, the second process of the day-ahead stage is to solve a stochastic scenario- based security-constrained OP that outputs an optimal DP. Compared to the one in [9], the proposed OP (i) accounts for EVCSs[14] as controllable resources with specific objectives and constraints, (ii) does not include minimum PCC power factor hard-constraints but a minimization of the absolute reactive power flow at the PCC in the OP objective, and (iii) is solved iteratively in order to reduce potential power-flow linearization inaccuracies. In the following, the OP objective is first presented. Then, the constraints are listed. Finally, the full OP formulation is given together with its resolution algorithm.

Objective

The OP objective is threefold. The first aim consists in minimizing the deviation between the active power flow at the PCC for all scenarios $d = 1,\dots,D$ and the optimally computed DP $P_{s,t}^{Dispatch}$ where $t = 1,\dots,T$ is the timestep and $s \in S$ is the slack node index. Formally, this is given by,

$$\frac{1}{DT}\sum_{d=1}^{D}\sum_{t=1}^{T}\left|P_{s,t}^{d} - P_{s,t}^{\text{dispatch}}\right|, \tag{2}$$

where the norm-1 operator was used instead of the Euclidean norm to avoid quadratic terms and, consequently, decrease computation times. The second aim consists in minimizing the absolute reactive power flow at the PCC for all scenarios and timesteps. Formally, this is given by,

$$\frac{1}{DT}\sum_{d=1}^{D}\sum_{t=1}^{T}\left|Q_{s,t}^{d}\right|. \tag{3}$$

The third objective consists in minimizing all resource-specific cost functions that, as explained in [9], reflect the controllable resources' willingness to provide regulating power. Table 7 lists the different considered resources with their respective cost functions. For a BESS, the cost function tries to simply minimize its usage, i.e., absolute injections ($\left|P_{i,BESS,t}^{d}\right|$), to prevent its ageing due to cycling. On the other hand, for EVCSs the cost functions aim is twofold. First, they try to guarantee that each EV's departure SoC[15] ($SoC_{k,i}^{Leave^{d}}$ for a plug $k \in$

[14] In the following, all types of three-phase EVCSs are considered, i.e., Type-2 AC plugs and DC plugs.
[15] As explained in [14,15], K_i is the total number of plugs of the EVCS connected to node $i \in C$. Furthermore, at each node $i \in C$, there's an EV aggregator that can send active and reactive power setpoints to all CSs (or plugs).

K_i, node $i \in C$ and scenario d=1,…,D) is close to its desired SoC ($SoC_{k,i}^{Target^d}$ for a plug $k \in K_i$, node $i \in C$ and scenario d=1,…,D). The max function is used to penalize EVs only until they reach their target SoC without limiting extra charging/discharging when applicable (i.e., grid-secure). Second, they try to minimize EV battery wearing by avoiding large deviations of EV injections ($P_{t,k,i}^d$ for a plug $k \in K_i$, node $i \in C$ and scenario *d=1,…,D* at timestep *t=1,..T*) between subsequent time-steps [22]. All the factors scaling all presented cost functions, e.g., $\frac{3600}{\Delta t D K_i}$ where Δt is the DP time-resolution, are included in order to render all objective terms of the same nature (i.e., here, powers). The final OP objective is a weighted sum of all presented cost functions.

Table 7: Cost functions of all considered controllable resources

Resource	Objective
BESS connected at node $i \in \mathcal{K}$	$\frac{1}{DT}\sum_{d=1}^{D}\sum_{t=1}^{T}\left\lvert P_{i,\mathrm{BESS},t}^{d}\right\rvert$ (4)
EVCS connected at node $i \in \mathcal{C}$	$\frac{3600}{\Delta t D K_i}\sum_{d=1}^{D}\sum_{k=1}^{K_i}\max\left\{\mathrm{SoC}_{k,i}^{\mathrm{Target}\,d}-\mathrm{SoC}_{k,i}^{\mathrm{Leave}\,d},0\right\}+$ $\frac{1}{10(T-1)DK_i}\sum_{d=1}^{D}\sum_{k=1}^{K_i}\sum_{t=2}^{T}\left\lvert P_{t,k,i}^{d}-P_{t-1,k,i}^{d}\right\rvert$ (5)

Constraints

The OP constraints are twofold. The first set of constraints are the ADN operational constraints. As the ADN is assumed balanced in the day-ahead stage, the operational constraints are, formally, given by

$$\left|\bar{\boldsymbol{E}}_t\right|^d \in [E_{min}, E_{max}], \left|\bar{\boldsymbol{I}}_{ij,t}\right|^d \leq \boldsymbol{I}_{ij,max}, \left|\bar{\boldsymbol{S}}_{s,t}\right|^d \leq \boldsymbol{S}_{s,max} \quad (6)$$

where, *Emin* and *Emax* are, again, the allowed extremes of the nodal voltage magnitudes, $I_{ij,max}$, is the vector of branch ampacity limits, $S_{S,max}$ is the substation transformer apparent power limit and the superscript *d* refers to a given scenario. $|\bar{E}_t|$, $|\bar{I}_{ij,t}|$ and $|\bar{S}_{S,t}|$ are generically linearly approximated by,

$$\boldsymbol{\Gamma}_t^d \approx \tilde{\boldsymbol{\Gamma}}_t^d\left(\tilde{\bar{\boldsymbol{S}}}_t^d\right) + \left.\frac{\partial \boldsymbol{\Gamma}_t}{\partial \boldsymbol{P}_t}\right|_{\tilde{\bar{\boldsymbol{S}}}_t^d}{}^{53}\left(\boldsymbol{p}_{t,\mathrm{Control}}^{d\ \upsilon} - \boldsymbol{p}_{t,\mathrm{Control}}^{d\ \upsilon-1}\right) + \left.\frac{\partial \boldsymbol{\Gamma}_t}{\partial \boldsymbol{Q}_t}\right|_{\tilde{\bar{\boldsymbol{S}}}_t^d}{}^{53}\left(\boldsymbol{q}_{t,\mathrm{Control}}^{d\ \upsilon} - \boldsymbol{q}_{t,\mathrm{Control}}^{d\ \upsilon-1}\right) \quad (7)$$

Where, $\Gamma \in \{|\bar{E}_t|, |\bar{I}_{ij,t}|, |\bar{S}_{S,t}|\}$, $\tilde{\Gamma}_t^d(\tilde{\bar{s}}_t^d)$ is the electrical quantity resulting from the system-state obtained from a LF computation with nodal injections $\tilde{\bar{S}}_t^d = \tilde{\bar{s}}_t^d + \tilde{\bar{s}}_{t,Control}^{d\ \upsilon-1}$, where $\tilde{\bar{s}}_t^d$ are the sampled non-EV injection scenarios and $\tilde{\bar{s}}_{t,Control}^{d\ \upsilon-1} = \tilde{\bar{p}}_{t,Control}^{d\ \upsilon-1} + j\tilde{\bar{q}}_{t,Control}^{d\ \upsilon-1} = \bar{S}_{BESS,t}^{d\ \upsilon-1} + \bar{S}_{EV,t}^{d\ \upsilon-1}$ are the optimal injections of all controllable resources (i.e., $\bar{S}_{i,BESS,t}^d = P_{i,BESS,t}^d + jQ_{i,BESS,t}^d$ for a BESS connected to node $i \in K$ and $\bar{S}_{i,EV,t}^d = P_{i,EV,t}^d + jQ_{i,EV,t}^d$ for a BESS connected to node $i \in C$) at the previous resolution iteration $\upsilon - 1$. Finally, the partial derivative (or SCs) in (7) represent the partial derivatives of the electrical quantity Γ with respect to nodal active and reactive power injections, computed with the injections $\tilde{\bar{S}}_t^d$ using the method presented in [23].

The second set of constraints are the controllable resources operational constraints. Table 8 lists the different considered resources with their respective constraints. The BESS constraints consist in: (i) SoC energy bounds (c.f. (8)), where $E^{\max}$ is the BESS's maximum energy capacity, and (ii) apparent power limits (c.f. (9)). The

EVCS constraints consist in: (i) per EV SoC evolution constraints (c.f. (10)[16]), (ii) per EV SoC bounds (c.f. (11)), (iii) per EV definitions of the SoCs at departure $SoC_{k,i}^{Leave^d}$ (c.f. (12)[17]), (iv) per plug maximum/minimum active[18] (c.f. (13)), reactive[19] (c.f. (14)) and apparent (c.f. (15)) power constraints, and (v) constraints linking the per plug variables to the per node aggregate EVCSs injections (c.f. (16)).

It should be pointed out that in the SoC constraints (i.e., (8) and (10)) the efficiency is assumed unitary. However, since in practice this is not true for both BESSs and EVs, power losses are accounted by integrating the latter's equivalent series resistance into the network admittance matrix as explained in [9].

Table 8: Constraints of all considered controllable resources.

Resource	Constraint
BESS connected at node $i \in \mathcal{K}$	$\text{SoC}_{i,\min} \le \text{SoC}_{t-1,i}^{d} - \frac{P_{i,\text{BESS},t}^{d}\Delta t}{E_i^{\max}} \le \text{SoC}_{i,\max}$ (7.8) $\left(P_{i,\text{BESS},t}^{d}\right)^2 + \left(Q_{i,\text{BESS},t}^{d}\right)^2 \le S_{i,max}$ (9)
EVCS connected at node $i \in \mathcal{C}$	$\text{SoC}_{t,k,i}^{d} = \begin{cases} \text{SoC}_{t_{0,k,i}^{d},k,i}^{d} & \text{if } t = t_{0,k,i}^{d} \\ \text{SoC}_{t-1,k,i}^{d} - \frac{P_{t,k,i}^{d}\Delta t}{E_{k,i}^{d,\max}} & \text{otherwise} \end{cases}$ (10) $0 \le \text{SoC}_{t,k,i}^{d} \le 1$ (11) $\text{SoC}_{k,i}^{\text{Leave}\,d} = \text{SoC}_{t_{f,k,i}^{d},k,i}^{d}$ (12) $-\omega_{t,k,i}^{d} P_{k,i}^{d,\min} \ge P_{t,k,i}^{d} \ge -\omega_{t,k,i}^{d} P_{k,i}^{d,\max}$ (13) $-\omega_{t,k,i}^{d} Q_{k,i}^{d,\min} \ge Q_{t,k,i}^{d} \ge -\omega_{t,k,i}^{d} Q_{k,i}^{d,\max}$ (14) $\left(P_{t,k,i}^{d}\right)^2 + \left(Q_{t,k,i}^{d}\right)^2 \le \left(S_{k,i}^{d,\max}\right)^2$ (15) $\bar{S}_{i,\text{EV},t}^{d} = \sum_{k=1}^{K_i} P_{t,k,i}^{d} + jQ_{t,k,i}^{d}$ (16)

Recap and Problem Resolution

The final OP of the day-ahead stage is given by (17). The variables of the OP are all the apparent power injections of all controllable resources together with the optimal DP ($P_s^{dispatch}$). The different $\alpha_\bullet$ are user-tunable weights. Finally, for clarity and completeness, Alg. 1 summarizes all the needed steps for both processes of the day-ahead stage, where tp and tc are, respectively, maximum tolerances for control variable and cost function variations between consecutive OP resolutions.

$$\boldsymbol{P}_s^{\text{dispatch}} = \text{argmin}\left\{ \alpha_{\text{Disp}}(2) + \alpha_{\text{PF}}(3) + \sum_{\substack{i\in\mathcal{K} \\ \text{where BESS is connected}}} \alpha_{i,\text{BESS}}(4) + \sum_{i\in\mathcal{C}} \alpha_{i,\text{EV}}(5) \right\}$$

s.t. (17)

$(6), \forall d = 1,\ldots,D, \forall t = 1,\ldots,T$

$(8)-(9), d = 1,\ldots,D, \forall t = 1,\ldots,T, \forall i \in \mathcal{K}$ where a BESS is connected

$(10)-(16), \forall d = 1,\ldots,D, \forall t = 1,\ldots,T, \forall i \in \mathcal{C}, \forall k = 1,\ldots,K(i)$

[16] As explained in [19], $t_{0,k,i}^{d}$ is the arrival time of an EV at plug $k=1,\ldots,K_i$ and node $i \in C$ for scenario $d = 1,\ldots,D$. Also, $E_{k,i}^{d,max}$ is the battery capacity of the EV connected to plug $k=1,\ldots,Ki$ and node $i \in C$ for scenario $d = 1,\ldots,D$. In the day-ahead stage, both quantities are forecasted (i.e., are part of the EV user behaviour scenario).

[17] As explained in [19], $t_{f,k,i}^{d}$ is the departure time of an EV at plug $k=1,\ldots,K_i$ and node $i \in C$ for scenario $d = 1,\ldots,D$. In the day-ahead stage, the latter quantity is forecasted (i.e., are part of the EV user behavior scenario).

[18] As explained in [19], $\omega_{t,k,i}^{d}$ is a known Boolean expressing whether, or not, an EV is connected to plug $k=1,\ldots,Ki$.

[19] As previously mentioned, reactive power limits depend on the plug type. Namely, if the EV plugs are DC-Typed plugs, the reactive power injections are non-null and are only limited by the plug's apparent power bound, otherwise, they are null.

Algorithm 1 Day-ahead stage

1. Create forecasting models using historical data;
2. Generate next-day scenarios;
3 **Do:** starting from $v = 1$, with ${\boldsymbol{p}^{d}_{t,\text{Control}}}^{0} = {\boldsymbol{q}^{d}_{t,\text{Control}}}^{0} = \mathbf{0}$;
3.a Solve (17);
3.b Store ${\boldsymbol{p}^{d}_{t,\text{Control}}}^{v}$ and Final objective^{v} = Objective of (7.17);
Until: $\max\left\{\left|\frac{{\boldsymbol{p}^{d}_{t,\text{Control}}}^{v}-{\boldsymbol{p}^{d}_{t,\text{Control}}}^{v-1}}{{\boldsymbol{p}^{d}_{t,\text{Control}}}^{v-1}}\right|\right\} \leq t_p$ and $\max\left\{\left|\frac{\text{Final objective}^{v}-\text{Final objective}^{v-1}}{\text{Final objective}^{v-1}}\right|\right\} \leq t_c$;
4. Store final iteration optimal DP ($\boldsymbol{P}_s^{\text{dispatch}}$).

4.3.4. Numerical Simulations

To showcase the advantages of considering EVCSs as controllable resources in the day-ahead stage, two sets of numerical simulations are performed. All simulations were performed on MATLAB using the same electrical grid that contains one BESS and two EVCSs aggregators. The main difference between the two sets of simulations is that the second set of simulations performs a sensitivity analysis w.r.t. to the BESS's energy and apparent power capacities. In the following, first the simulation setup is described, then, both sets of simulations are presented. Note that, in the appendix the reader can find further simulations that were performed on the EPFL-DESL microgrid.

Simulation setup: the EPFL smart grid platform

All simulations were performed using a virtual twin (single-phase equivalent) of the low-voltage electrical-grid of the EPFL smart grid platform. A schematic of the grid is depicted in Figure 2 where the greyed-out resources were not used for the simulations and node B01 corresponds to the unique slack node. EVCS2 corresponds to the CS described in Table 9. EVCS1 is the commercial GoFast EV fast-charger whose photographic depiction and technical specifications can be found in Figure 6 and Figure 7. B1 is a commercial utility-scale BESS whose external view and technical specifications can be found in Figure 3 and Table 1. Table 10, Table 11 and Table 12 give, respectively, the branch, nodes, and transformers parameters of the network. The latter parameters were used as is in all the simulations of this section. Table 13 lists the used resource parameters. Table 14 lay-out the used simulation parameters. Finally, Table 15 describes the origin of the historical data used for every resource in the *forecast & scenario generation* block of Figure 22.

Table 9: EV Charging station protocols, protection and rating

	Plug 1 - Type-2	Plug 2 - Type-2	Plug 3 - CHAdeMO
Protocol	IEC-61851	IEC-61851	DCMS - proprietary protocol of EvTec
Protocol Notes	• Based on an analog pulsed *control pilot* signal • Logic implemented using NI CompactRio and AI/AO Modules • The maximum per-phase current that the car can consume is set by modulating the control pilot's duty cycle	• Based on an analog pulsed *control pilot* signal • Logic implemented using NI CompactRio and AI/AO Modules • The maximum per-phase current that the car can consume is set by modulating the control pilot's duty cycle	• Based on a TCP/IP-based websockets communication • Explicit active power setpoint control
Protection	• Circuit breaker - A9F84432 - 32A • Differential breaker with earth-leakage Type B protection - A9Z61440	• Circuit breaker - A9F84432 - 32A • Differential breaker with earth-leakage Type B protection - A9Z61440	• Circuit breaker - A9F84432 - 32A • Differential breaker with earth-leakage Type B protection - A9Z61440
Rating	• IEC-61851 protocol limited 80A per phase • EPFL-DESL Microgrid branch amapcity is 82A • A9F84432 circuit breaker trips at 32A	• IEC-61851 protocol limited 80A per phase • EPFL-DESL Microgrid branch amapcity is 82A • A9F84432 circuit breaker trips at 32A	10kVA

Table 10: Day-ahead numerical simulation: branch parameters.

(a) Branches parameters: line data

From	To	Length [km]	Configuration	Ampacity (from-to) [A]	Ampacity (to-from) [A]
B01	B02	1.000	10	17.32	866.03
B01	B03	1.000	9	17.32	866.03
B01	B04	1.000	8	17.32	1212.44
B02	B05	0.037	6	300.00	300.00
B03	B06	0.037	7	250.00	250.00
B06	B07	0.070	5	207.00	207.00
B07	B08	0.030	1	44.00	44.00
B07	B09	0.035	5	207.00	207.00
B09	B10	0.030	3	108.00	108.00
B09	B11	0.105	2	82.00	82.00
B11	B12	0.030	2	82.00	82.00
B09	B13	0.070	4	135.00	135.00
B13	B14	0.030	5	207.00	207.00
B13	B15	0.105	2	82.00	82.00
B15	B16	0.030	1	44.00	44.00
B15	B17	0.035	2	82.00	82.00
B17	B18	0.030	2	82.00	82.00
B12	B19	0.038	3	108.00	108.00
B02	B20	0.010	6	300.00	300.00
B03	B21	0.010	7	250.00	250.00

(b) Branches parameters: configurations

Configuration	Longitudinal impedance $[\Omega/km]$	Shunt admittance (from-to) $[\mu S/km]$	Shunt admittance admittance (to-from) $[\mu S/km]$
1	$3.300 + j0.141$	$0.000 + j23.562$	$0.000 + j23.562$
2	$1.210 + j0.132$	$0.000 + j36.128$	$0.000 + j36.128$
3	$0.780 + j0.126$	$0.000 + j32.987$	$0.000 + j32.987$
4	$0.554 + j0.123$	$0.000 + j40.841$	$0.000 + j40.841$
5	$0.272 + j0.119$	$0.000 + j50.266$	$0.000 + j50.266$
6	$0.225 + j0.070$	$0.000 + j27.332$	$0.000 + j27.332$
7	$0.146 + j0.070$	$0.000 + j27.332$	$0.000 + j27.332$
8	$7.944 + j43.877$	$3.923 + j5.884$	$0.000 + j0.000$
9	$5.027 + j40.358$	$1.383 + j1.445$	$0.000 + j0.000$
10	$5.004 + j40.290$	$1.365 + j1.652$	$0.000 + j0.000$

Table 11: Day-ahead numerical simulation: node parameters.

Node	Base Voltage [V]	Base Power [MVA]
B01	21000	1
B02	420	1
B03	420	1
B04	300	1
B05	420	1
B06	420	1
B07	420	1
B08	420	1
B09	420	1
B10	420	1
B11	420	1
B12	420	1
B13	420	1
B14	420	1
B15	420	1
B16	420	1
B17	420	1
B18	420	1
B19	420	1
B20	420	1
B20	420	1

Table 12: Day-ahead numerical simulation: transformer parameters.

	Transformer A	Transformer B	Transformer BESS
MV rated Voltage [kV]	21	21	21
LV rated Voltage [V]	420	420	300
Rated power [kVA]	630	630	630
Short-circuit voltage [% of MV rated voltage]	5.8	5.81	6.37
Winding losses [W]	4504	4524	7150
Core losses [W]	602	610	1730
Zero-load current [% of MV nominal current]	0.15	0.14	0.495

Table 13: Day-ahead numerical simulation: controllable resources parameters.

Name	Parameters
B1	$S_{4,max} = 200$ kVA, $\text{SoC}_{4,min} = 0.1$, $\text{SoC}_{4,max} = 0.9$, $E_4^{max} = 200$kWh
EVCS1	$K_5 = 6$ (2 AC-Type-2 and 4 DC [unidirectional])
EVCS2	$K_3 = 3$ (2 AC-Type-2 and 1 DC [bidirectional])

Table 14: Day-ahead numerical simulation: simulation parameters.

Parameter	Value	Unit
Objective weights:		
α_{Disp}	100	-
α_{PF}	1	-
$\alpha_{4,\text{BESS}}$	0.01	-
$\alpha_{5,\text{EV}}$	1	-
$\alpha_{19,\text{EV}}$	1	-
Timing:		
Δt	5	minutes
Scenarios:		
Number of EV scenarios	20	-
Total number of scenarios D	80	-
ADN tolerances:		
E_{min}	0.9	p.u.
E_{max}	1.1	p.u.
$S_{s,max}$	1	p.u.
Alg. 7 tolerances:		
t_p	1	%
t_c	1	%

Table 15: Day-ahead numerical simulation: inputted historical data.

Resource	Description
PV1 & PV2	Same as data used in [6].
L1 - ELLA	Measured data coming from PMU 11 of Fig. 7.7.
EVCS1 & EVCS2	Combination of measured and public data coming from (i) Local back-end logger of EVCS1, and (ii) a confidential dataset provided by GoFAST [119] that contains information about many EV plugs situated in different parts of Switzerland.

Simulation 1: EVCSs as the only day-ahead controllable entities

The first set of simulations considers the case where the BESS is not connected to the grid of Figure 2 (i.e., B1). Namely, the only controllable entities in the day-ahead stage are EVCS1 and EVCS2. Using the same scenarios, the idea of these simulations is to compare the obtained DPs when (i) EVCSs are not controlled and plugged EVs simply charge at their maximum rated power, and (ii) EVCSs are considered controllable. Since there are no controllable entities in the latter case (i), the resulting DP is nothing more than the average of all scenarios of the active power injections at the PCC. In order to compare DPs, a set of metrics is defined that are given in Table 16. As defined in [25], the UEE^{+} and UEE^{-} represent the cumulative *worst-case*, respectively upper- and lower- bound of the energy discrepancy needed to merge all PCC nodal active power into the unique DP (i.e., for the PCC active power injections for all scenarios to be equal to the DP). The MAE quantifies the maximum absolute error, in terms of power, between the DP and the PCC active power injection realizations. The MPP is equal to the maximum absolute PCC active power injection realizations. The MEVUS metric represents the worst ratio, over all charging sessions of all scenarios, of received over best *feasible* energies, where the best *feasible* energy is the minimum between what the EV user requested, i.e., the forecasted quantity given by

$$E_{k,i}^{\text{desired}\,d} = E_{k,i}^{d,\max}\left(\text{SoC}_{k,i}^{\text{Target}\,d} - \text{SoC}_{t_{0,k,i}^{d},k,i}^{d}\right) \text{ for } i \in \mathscr{C},\ k = 1,..,K_i \text{ and } d = 1,...D, \tag{17a}$$

And the maximum energy an EV can receive if it was charging at its maximum power – i.e., no control – for its whole plugged duration, i.e., the forecasted quantity given by

$$E_{k,i}^{\text{best}\,d} = P_{k,i}^{d,\max}(t_{f,k,i}^{d} - t_{0,k,i}^{d}) \tag{17b}$$

Table 16: Metrics used to quantify the performance of the result of Alg. 1.

Metric	Formula
Uncovered Energy Error (UEE^{+}) [kWh]	$\text{UEE}^{+}(t) = \frac{\Delta T}{3600}\sum_{\tau=1}^{t}\max_{d}\left\{P_{s,\tau}^{d}\right\} - \boldsymbol{P}_{s,\tau}^{\text{dispatch}}$
Uncovered Energy Error (UEE^{-}) [kWh]	$\text{UEE}^{-}(t) = \frac{\Delta T}{3600}\sum_{\tau=1}^{t}\min_{d}\left\{P_{s,\tau}^{d}\right\} - \boldsymbol{P}_{s,\tau}^{\text{dispatch}}$
Maximum Absolute Error (MAE) [kW]	$MAE = \max_{d,t}\left\{\left\lvert \boldsymbol{P}_{s,t}^{\text{dispatch}} - P_{s,t}^{d}\right\rvert\right\}$
Maximum PCC Power (MPP) [kW]	$MPP = \max_{d,t}\left\lvert P_{s,t}^{d}\right\rvert$
Minimum EV User Satisfaction (MEVUS) [%]	$MEVUS = 100\min_{k,i,d}\left\{\frac{E_{k,i}^{\text{received}\,d}}{\min(E_{k,i}^{\text{best}\,d}, E_{k,i}^{\text{desired}\,d})}\right\}$

The results of the simulations are depicted in Figure 23, Figure 24 and Table 17. Figure 23 *a* and *b* show, respectively, the active and reactive nodal power injections at the PCC. Figure 24 shows the time evolution of the UEE.

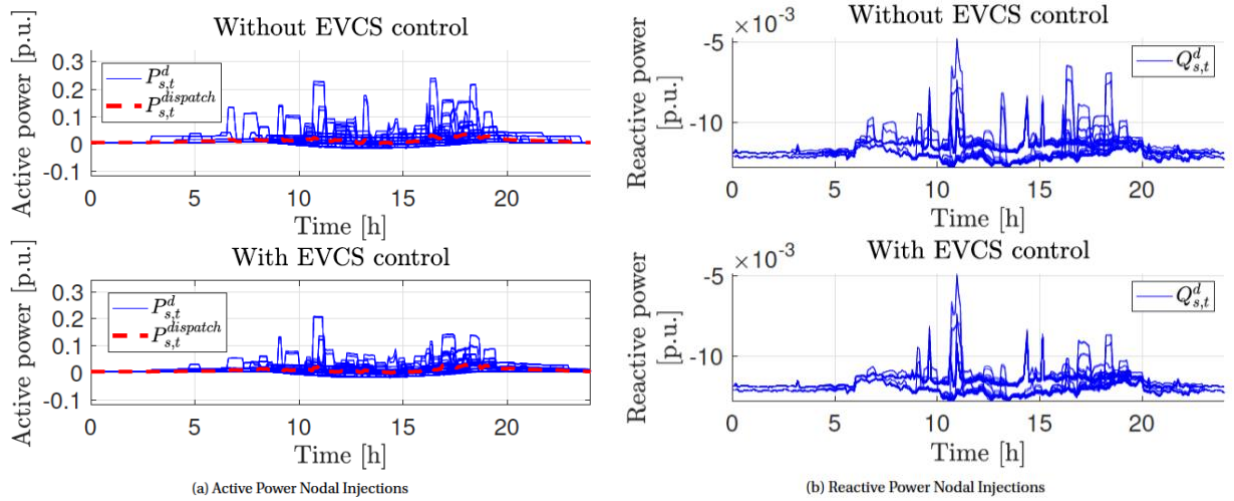

(a) Active Power Nodal Injections

(b) Reactive Power Nodal Injections

Figure 23: PCC nodal power injections.

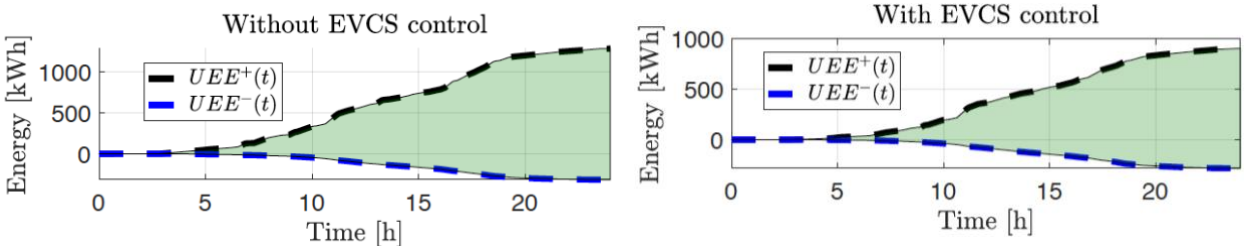

Figure 24: UEE time evolution.

Table 17: Simulation 1 – results

Metric	without control	with EVCSs control
$\mathrm{UEE}^{+}(t=T)$ [kWh]	1280.93	860.32
$\mathrm{UEE}^{-}(t=T)$ [kWh]	-316.10	-284.26
MAE [kW]	214.09	188.59
MPP [kW]	240.64	208.94
MEVUS [%]	100	100

All results lead to the same conclusion: controlling EVCSs in the day-ahead stage (i) improves the merger of all PCC active power scenario realizations into a unique DP, (ii) reduces the untracked energy error and (iii) shaves the peak PCC injections, without penalizing EV users' satisfaction. However, in practice, having *only* EVCSs as controllable entities in the day-ahead stage is not enough to fully merge the PCC active power realizations into the DP as they do not have enough *bidirectional energy storage* capabilities[20]. Finally, note that no voltage, branch current, or slack power plots are shown as there were no grid operational constraint violations for any scenario in both simulations, i.e., with and without EVCSs control. Indeed, as the grid awareness of the developed method was already showcased in [9], our goal was not to stress-test Alg. 1 by tightening the grid operational constraints tolerances, but to illustrate how EVCS can help merge the PCC active power realizations into a unique DP.

Simulation 2: EVCSs and BESSs as day-ahead controllable entities

In the second set of simulations, the BESS is considered connected to the grid of Figure 2 (i.e., B1). Namely, the controllable entities in the day-ahead stage are the BESS, EVCS1 and EVCS2. As in the previous simulations, the same scenarios are used and the idea is to compare the obtained DPs when (i) neither EVCSs nor the BESS are controlled, (ii) only the EVCSs are controlled and (iii) both EVCSs and the BESS are controlled. The novelty, w.r.t Simulation 1, is that the comparison is done for different sizes – in terms of maximum apparent power *and* energy capacity – of the BESS. All simulations assume that for all scenarios the BESS's beginning of day SoC is 0.5. Since the BESS is considered, two extra metrics are introduced: the *maximum BESS usage (MBU)* and the *Maximum absolute BESS injections (MABI)*. The MBU is defined as the ratio of (i) the largest energy usage of the BESS over all scenarios, and, (ii) the total usable capacity of the BESS. It is given by:

$$100\frac{\max\limits_{d}\left\{\max\limits_{t}\mathrm{SoC}_{t,4}^{d}-\min\limits_{t}\mathrm{SoC}_{t,4}^{d}\right\}}{\left(\mathrm{SoC}_{4,\max}-\mathrm{SoC}_{4,\min}\right)E_{4}^{\max}} \quad (17c)$$

The MABI is defined as the absolute maximum BESS active power injections over all scenarios and timesteps. The results of all simulations are summarized in Table 18 and Table 19. In terms of merging the PCC active power realizations into a unique DP, Table 18 a, b & c confirm that (i) the BESS decreases the UEE more than EVCSs, (ii) increasing the BESS size decreases the UEE, (iii) controlling EVCSs always further decreases the UEE, and (iv) the PCC active power realizations are only *perfectly* merged when the BESS is sufficiently large *and* the EVCSs are controlled. As in the previous simulation, there were no grid operational constraints' violations. As a result, all simulations lead to perfect EV user satisfaction (c.f. Table 19a). Table 19b shows the BESS's MBU for different BESS sizes and simulation configurations. Increasing the BESS's apparent power limit had little-to-no influence as the maximum active power injections were practically all equal. This behavior is due to: (i) the scenarios used for the simulations that did not require extra BESS injections, and (ii) the lack of ADN operational constraints violations. Finally, Table 18c proves again the advantages of controlling EVCSs as it always led to less utilization of the BESS for the same EV user satisfaction (c.f. Table 19a).

[20] Indeed, this could change in the future with the potential penetration of large quantities of bidirectional public chargers which would render the aggregate usable storage of plugged EVs comparable to BESSs used in grid-applications.

Table 18: Simulation 2 – results.

(a) $UEE^{-}(t = T)$ - kWh

Controllable Entities \ $S_{4,max}$ [kVA] & $E_4^{\max}$ [kWh]	200 & 200	300 & 300	500 & 500	1000 & 1000
None	-316.10	-316.10	-316.10	-316.10
EVCSs	-284.26	-284.26	-284.26	-284.26
BESS	-178.93	-145.35	-74.37	-5.73
EVCSs+BESS	-136.48	-97.51	-20.95	-0.02

(b) $UEE^{+}(t = T)$ - kWh

Controllable Entities \ $S_{4,max}$ [kVA] & $E_4^{\max}$ [kWh]	200 & 200	300 & 300	500 & 500	1000 & 1000
None	1280.93	1280.93	1280.93	1280.93
EVCSs	860.32	860.32	860.32	860.32
BESS	222.46	154.00	66.88	13.92
EVCSs+BESS	165.45	110.77	14.12	0.03

(c) MAE - kW

Controllable Entities \ $S_{4,max}$ [kVA] & $E_4^{\max}$ [kWh]	200 & 200	300 & 300	500 & 500	1000 & 1000
None	214.09	214.09	214.09	214.09
EVCSs	188.59	188.59	188.59	188.59
BESS	58.13	48.19	38.71	38.62
EVCSs+BESS	8.39	5.09	0.93	0.02

(d) MPP - kW

Controllable Entities \ $S_{4,max}$ [kVA] & $E_4^{\max}$ [kWh]	200 & 200	300 & 300	500 & 500	1000 & 1000
None	240.64	240.64	240.64	240.64
EVCSs	208.94	208.94	208.94	208.94
BESS	117.27	119.12	115.55	109.64
EVCSs+BESS	57.24	50.83	48.59	50.26

Table 19: Simulation 2 – results – continued.

(a) MEVUS - %

Controllable Entities \ $S_{4,max}$ [kVA] & E_4^{max} [kWh]	200 & 200	300 & 300	500 & 500	1000 & 1000
None	100	100	100	100
EVCSs	100	100	100	100
BESS	100	100	100	100
EVCSs+BESS	100	100	100	100

(b) MBU - %

Controllable Entities \ $S_{4,max}$ [kVA] & E_4^{max} [kWh]	200 & 200	300 & 300	500 & 500	1000 & 1000
None	N/A	N/A	N/A	N/A
EVCSs	N/A	N/A	N/A	N/A
BESS	100	99.60	92.71	67.57
EVCSs+BESS	98.73	76.22	84.06	43.69

(c) MABI - kW

Controllable Entities \ $S_{4,max}$ [kVA] & E_4^{max} [kWh]	200 & 200	300 & 300	500 & 500	1000 & 1000
None	N/A	N/A	N/A	N/A
EVCSs	N/A	N/A	N/A	N/A
BESS	178.72	178.07	172.45	164.05
EVCSs+BESS	198.88	206.42	197.50	198.14

Simulation setup: the Aigle demo site

Although the installation of the four charging stations on the Aigle demo site have been delayed beyond the scope of the project, the simulation of a dispatch plan with the existing infrastructure with the anticipated stations has been performed.

Grid topology

As shown in Figure 25, the grid topology features a similar number of nodes than the EPFL setup. However, the complexity and global prosumption of the network are significantly larger. At the PCC, the power fluctuates between -2MW and +1MW whereas on EPFL setup, it fluctuates between 0 and 200kW. The Aigle demo site thus has a PCC overall amplitude variation fifteen times larger than the one of the EPFL setup. It is planned to install four charging stations similar to the one installed on the EPFL smart grid platform (described in Figure 7), however with 300kW peak power each instead of 150kW. The BESS has a rated apparent power of 1.6MVA and a rated capacity of 2.5MWh. More technical specifications can be found in *Section 2*.

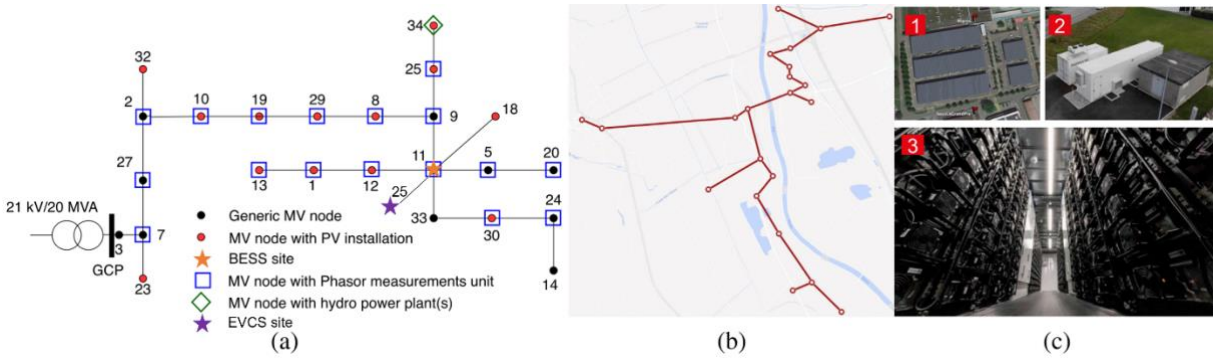

Figure 25 : Figure from source [31] - (a) Topology with locations of the PMUs, PV plants, hydro-power plants, (b) Location of the substations and lines on the map, and (c) BESS and PV infrastructure: (1) Satellite view of the centralized PV plant of capacity 1.8 MWp, (2) battery container and (3) interior of the battery.

Results

Simulation 1: four charging stations

20 scenarios of prosumption on every node has been generated based on historical data. For each scenario an additional anticipated scenario for the four EVCS has been added. The PCC power for each scenario is shown in blue in Figure 26. We notice how the dispatching squeezes the profiles thanks to the control of both the battery and four charging stations. The profiles don't overlap perfectly because the variance is too high with respect to the size of the battery and charging stations.

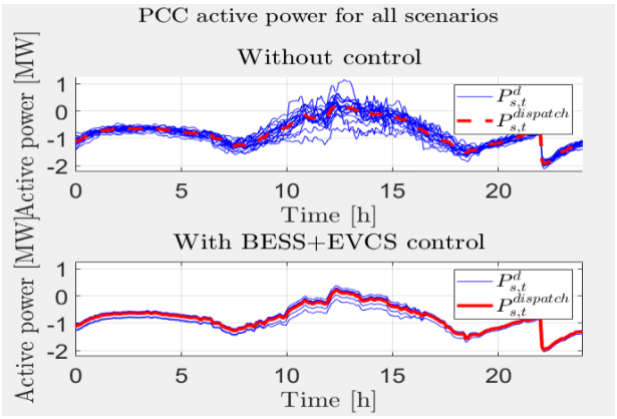

Figure 26 - PCC active power for all scenarios (4 EVCS)

The uncovered energy error reduced from 16.39MWh without control down to 6.88MWh with BESS+EVCS control as shown in Figure 27.

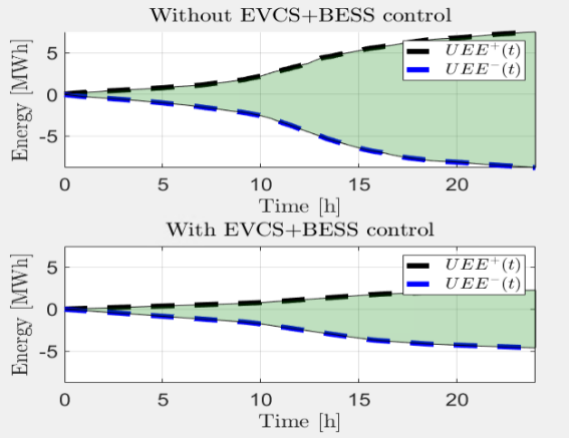

Figure 27 - Uncovered energy error (4 EVCS)

Using the metrics presented in Table 16, we notice the strong contribution of controlling the battery. Adding the four charging stations control does improve the metrics yet only in a small manner as the flexibility provided is very small with respect to the PCC volatility.

Table 20: Aigle simulations metrics (4 EVCS)

Metric	no control	BESS control	BESS + EVCS control
UEE^{+} [MWh]	7.52	2.39	2.26
UEE^{-} [MWh]	-8.87	-4.61	-4.62
MAE [MW]	1.05	0.37	0.34
MPP [MW]	2.12	2.06	2.06
MEVUS [%]	100	100	100

Simulation 2: forty charging stations

GoFast anticipates increasing the number of charging stations at this location as demand increases. Let's suppose that not four but forty charging stations are installed. The total uncovered energy error without control rises from 16.39MWh up to 17.5MWh brought by the additional stochasticity of the stations. However, as they are controllable, they bring additional flexibility to the whole system reducing the uncovered energy error with control from 6.88MWh down to 4.81MWh. This shows that adding new highly stochastic charging stations can have a positive impact on the overall consumption predictability if they are adequately controlled. And this without significantly impacting the customer satisfaction as seen in the MEVUS metric.

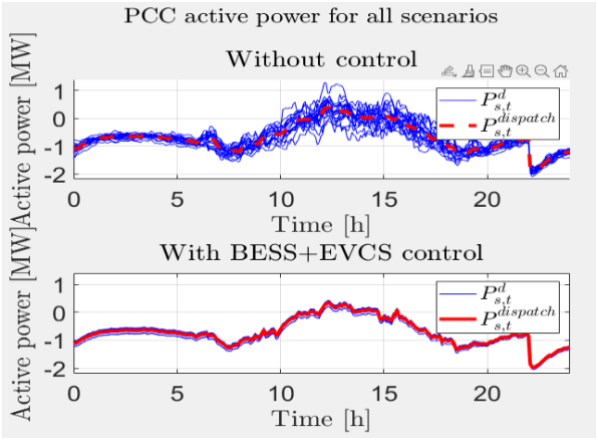

Figure 28 - PCC active power for all scenarios (40 EVCS)

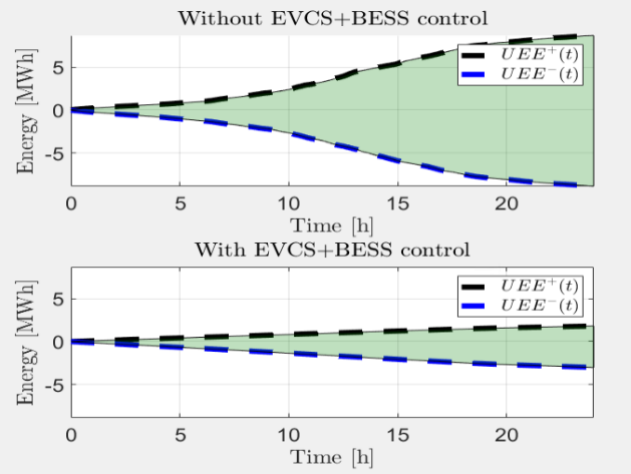

Figure 29 - Uncovered energy error (40 EVCS)

Table 21: Aigle simulation metrics (40EVCS)

Metric	no control	BESS control	BESS + EVCS control
UEE^+ [MWh]	8.65	2.32	1.8
UEE^- [MWh]	-8.85	-3.71	-3.01
MAE [MW]	1.04	0.18	0.14
MPP [MW]	2.09	2.03	2.05
MEVUS [%]	100	100	98.9

Discussion

The comparison between simulation 1 (4 stations) and simulation 2 (40 stations) highlights a key takeaway message for planners. It is ubiquitous that adding fast charging stations is inevitable to promote the transition towards electric mobility. It is also known that their deployments are viewed as a risk for the grid from the added stochasticity and peak power demands. However, with an adequate control of the stations, not only lower their impact on the grid can be lowered but they can also provide grid support by increasing the overall day-ahead predictability. Public fast charging stations can therefore help the electric mobility transition while providing grid flexibility under the condition that they are both controllable and controlled. It is thus important to consider this aspect in the selection process of future charging station providers.

Simulation setup: the EPFL case with commercial fleet versus public fast charging station (international cooperation within the MES4U project)

Context

As EPFL, the group of Prof. Mulone at the University of Rome Tor Vergata, Italy, is a partner of the MESH4U consortium. Prof. Mulone's group has worked extensively on optimal sizing and scheduling of commercial fleet charging stations specifically for grid support. More information on results can be found in [32]. On the EPFL side, the dispatch plan and real-time control has the objective of providing a reliable day-ahead prediction of power profiles to also enhance grid support. Within the MESH4U project, this dispatching has been extended to include public fast charging stations reflecting the physical setup on the EPFL smart grid platform and, eventually, in Aigle. However, the larger control and flexibility of a commercial fleet charging station is an interesting topic to include in our optimization problem. The collaboration with Prof. Mulone's group has enabled the consideration of such commercial fleets. Data generated by his group allowed the comparison of the dispatchability performance between public fast charging stations (PFCS) with respect to a commercial fleet charging station (CFCS).

Model and objective

Providing a perfectly predictable power profile at the PCC with the inclusion of loads, solar power and charging stations is not achievable with the control of the charging stations alone. An adequately sized battery is necessary. The size of the battery grows with the stochasticity of the power generated/absorbed by the non-controllable resources. A larger battery is required for PFCSs compared to CFCS as costumers' arrival and departure time is not scheduled and the charging power delivered must remain high to ensure customer satisfaction. The objective is to assess the battery size difference in both cases.

The grid topology considered in this assessment is the same presented in section *4.3.4 Numerical Simulations*. For the case of CFCS, the GoFast EVCS has been replaced by a station with ten 22kW slots, one per vehicle. The shift schedule and energy demand per vehicle for each day of the week is given by the optimization problem of the University of Rome Tor Vergata. For our comparative analysis we will use the scheduling of the first working day of a generic week (i.e. Monday), as show in Table 22.

Table 22: Monday optimal shift schedule and energy demand

EV id	Shift start	Shift end	Energy demand [kWh]
1	7h	14h18	22.3
2	7h	13h54	23.1
3	7h	14h42	23.6
4	7h	14h12	22.4
5	7h	14h30	23.1
6	7h	15h54	25.7
7	7h	15h06	23.6
8	7h15	13h24	21.5
9	7h	15h06	23.3
10	8h30	15h48	22.5

This data input is then slightly different to the data generated by the forecasting method presented in section *4.1.2 EV user statistical modelling*. For PFCSs, several scenarios are generated including session start and end time as well as the energy demand. The optimization problem for the commercial fleet must then be readjusted.

Hypotheses:

1. Each commercial vehicle is assigned to a plug.
2. Each commercial vehicle is constantly plugged except during its shift.
3. The real-time demand is equivalent to the scheduled scenario.
4. For each day, all the sessions start at midnight and last 24h. A single session is considered per vehicle with an interruption of charge during the shift.

Cost function modifications:

The same cost function as in section *Objective* in *4.3.3 Day-ahead stage* is used with the additional objective of reaching the SoC target upon start of shift. The additional piecewise cost element is shown in blue.

$$\min_{\mathbf{P}}[\alpha_1 \frac{3600}{\Delta t D K} \sum_{d=1}^{D}\sum_{k=1}^{K} \max\left\{\mathrm{SoC}_k^{d,\mathrm{target}} - \mathrm{SoC}_k^{d,\mathrm{leave}}, 0\right\} +$$
$$\alpha_2 \frac{3600}{\Delta t D K} \sum_{d=1}^{D}\sum_{k=1}^{K} \max\left\{\mathrm{SoC}_k^{d,\mathrm{target}} - \mathrm{SoC}_k^{d,\mathrm{shift\ start}}, 0\right\}$$
$$\alpha_3 \frac{1}{(T-1)DK} \sum_{t=2}^{T}\sum_{d=1}^{D}\sum_{k=1}^{K} |P_{t,k}^{d} - P_{t-1,k}^{d}|]$$

for timestep $t=1,\ldots,T$, plug $k=1,\ldots,K$, node $i \in C$ and scenario $d = 1,\ldots,D$

Constraints modifications:

The same constraints as in section *Constraints* in *4.3.3 Day-ahead stage* are used with a few modifications. The first is that SoC dynamics need to account for the energy consumption during the shift. The second is a limitation on the overall active power consumption as the grid topology is not dimensioned for ten EVs charging at 22kW at the same time. Only up to a total of 150kW is possible without exceeding the ampacity limit of the line following the charging station node. Third, all power limits are only in active power as we cannot control the reactive power on type-2 AC chargers. Finally, the node index i has been removed as all the plugs are supposed to be on the same charging station node. Note that even if we have a single scheduled scenario for the EVs, we have several scenarios to reflect the uncertainty of load consumption and solar production. Hence the charging behavior will differ from one scenario to the next even if they all share the same schedule. Changes in the constraints are shown in blue.

Additional constraints:

$$\begin{cases} \mathrm{SoC}^d_{t,k} = \mathrm{SoC}^d_{t^d_{0,k},k} & \text{if } t = t^d_{0,k} \\ \mathrm{SoC}^d_{t,k} = \mathrm{SoC}^d_{t-1,k} - \dfrac{P^d_{t,k}\Delta t - E^{d,\text{shift}}_k}{E^{d,\max}_k} & \text{if } t = t^{d,\text{shift end}}_k \\ \mathrm{SoC}^d_{t,k} = \mathrm{SoC}^d_{t-1,k} - \dfrac{P^d_{t,k}\Delta t}{E^{d,\max}_k} & \text{otherwise} \end{cases}$$

$$0 \le \mathrm{SoC}^d_{t,k} \le 1$$

$$\mathrm{SoC}^{d,\text{leave}}_k = \mathrm{SoC}^d_{t^d_{f,k},k}$$

$$\mathrm{SoC}^{d,\text{shift start}}_k = \mathrm{SoC}^d_{t^{d,\text{shift start}_k},k}$$

$$\omega^d_{t,k} P^{d,\min}_k \le P^d_{t,k} \le \omega^d_{t,k} P^{d,\max}_k$$

$$0 \le P^d_{t,k} \le P^{\max,\text{plug}}_k$$

$$\sum_{k=1}^{K} P^d_{t,k} \le P^{d,\max,\text{node}}$$

for timestep $t=1,\dots,T$, plug $k=1,\dots,K$ and scenario $d = 1,\dots,D$. As explained in [19], $\omega^d_{t,k,i}$ is a known Boolean expressing whether, or not and EV is plugged.

Results

The physical battery on EPFL smart grid platform is large enough to remove all the uncovered energy errors in both public fast charging and industrial fleet. However, even if the daily energy throughput is the same for both CFCS and PFCS, the BESS energy throughput and maximum active power is approximately ten times larger to remove the UEE for PFCSs with respect to industrial fleet. These results can be seen in the three last rows of Table 23. Two reasons account for this significant difference.

The main is that the battery needs to compensate for the high uncertainty of arrival, departure, and energy demand of PFCS customers. Figure 30 (a) shows the PCC power volatility between scenarios. In Figure 30 (b) the differences between scenarios are only due to the load and PV uncertainties which with a good forecast can be fairly small. Indeed, the scheduling of the fleet EVs allows a perfect knowledge of arrival, departure, and energy demand which the battery doesn't need to compensate for.

The second reason is that the EV fleet are plugged in much longer and have no rush to differ their charge whereas public fast charging stations have a high demand and small flexibility. The last point can also be grasped by focusing on the contribution of EVCS control. The BESS throughput is reduced by about 20% for the PFCS and 50% for the CFCS when EVCS control is applied.

Figure 30 (b) also displays the effect of the following piecewise cost element:

$$\alpha_3 \frac{1}{(T-1)DK} \sum_{t=2}^{T} \sum_{d=1}^{D} \sum_{k=1}^{K} \left| P^d_{t,k} - P^d_{t-1,k} \right|]$$

The goal of this cost function is to minimize the EVCS battery damage by gradually changing the power setpoint. With EVCS control, the charging profiles are less abrupt.

Table 23: Dispatching public and fleet charging stations

Metric	No control		BESS control		BESS + EVCS control	
	Public	Fleet	Public	Fleet	Public	Fleet
UEE^{+} [MWh]	1762.4	105	1.8	0.1	1.2	0.1
UEE^{-} [MWh]	-587.5	-105	-1.3	-0.1	-0.9	-0.1
MAE [MW]	219.5	11.3	0.3	0.01	0.3	0.03
MPP [MW]	264	224.9	98	218.3	95.7	210.6
MEVUS [%]	100	100	100	100	100	100
CS throughput [kWh]	454.9	554.2	454.9	554.2	391	403.4
BESS throughput [kWh]	-	-	561.9	83.3	450.2	42.4
BESS $P_{\max}$ [kW]	-	-	219.5	11.4	173.8	11.4

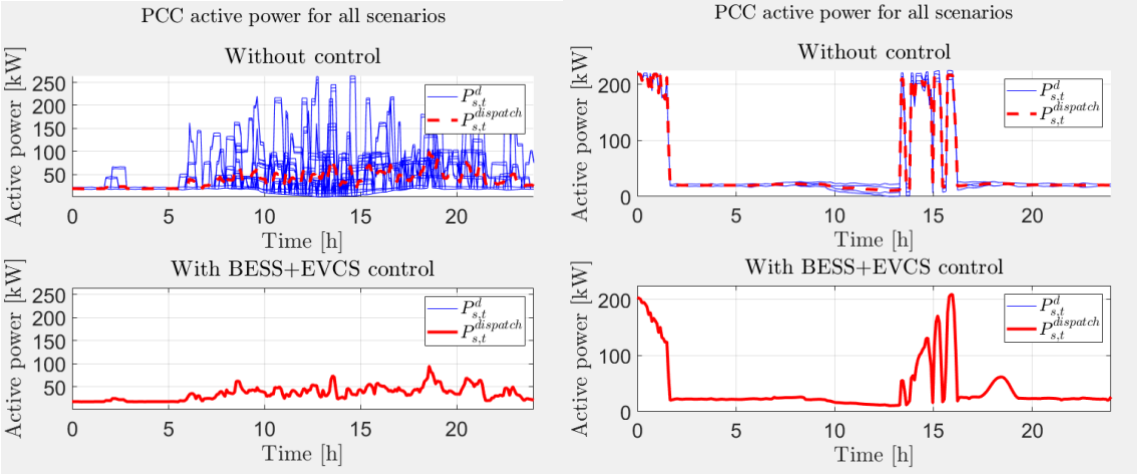

Figure 30 - PCC active power for all scenarios with and without control for (a) a public fast charging station and (b) an industrial fleet charging station

Discussion

The key takeaway of this collaboration is that, for the same charging station energy demand, the required battery size to track the dispatch plan is ten times smaller for a CFCS.

In terms of required infrastructure and investments, one can achieve more grid predictability and flexibility with lower investments by implementing dispatch plans on nodes encapsulating schedulable and controllable commercial fleet charging stations. Due to the significantly higher stationary battery investment costs, when truly necessary for the grid, tracking a PCC node encapsulating highly stochastic PFCSs can be achieved.

The qualitative plot below shows the grid support versus cost analysis between different levels of prediction/scheduling and control for both PFCS and CFCS:

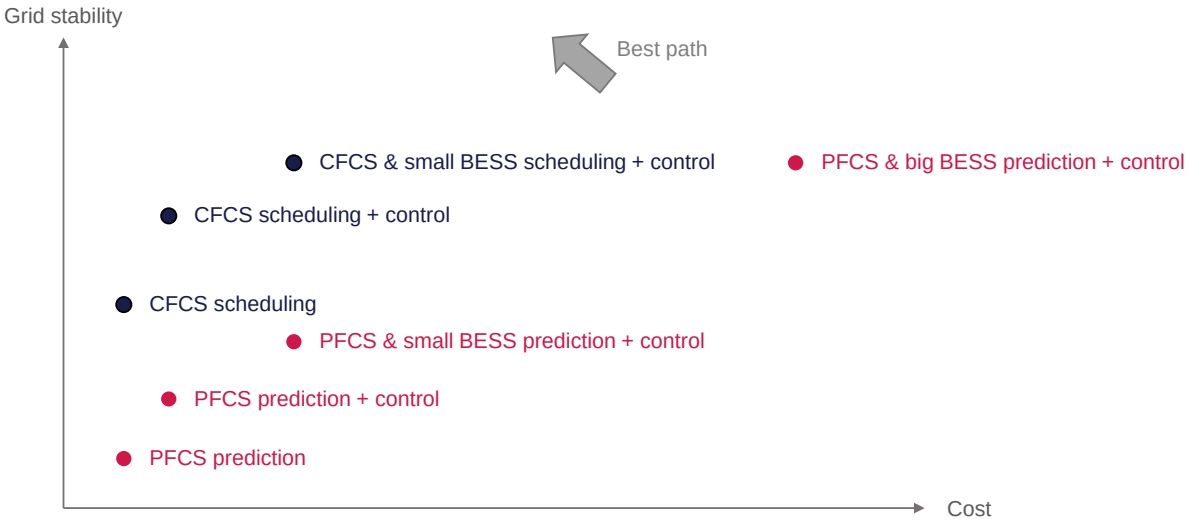

Figure 31 - CFCS vs PFCS measures analysis in grid stability and cost.

4.3.5. Real-time stage

As previously mentioned, the main goal of the real-time stage is to track the optimal DP determined by the day-ahead stage. To do so the same problem formulation is used and distributed solution method described in [9]. However, since we consider EVCSs as controllable entities, extra objectives and constraints are added to the centralized OPF (11) of [9]. Indeed, we leverage the EV-subproblem objectives and constraints presented in [19]. However, as the OP in [9] is expressed as an MPC problem, the latter are expanded for a given time horizon (denoted by tH as in [9]). Furthermore, as the real-time controller developed in [9] assumes balanced operation for the ADN, the unbalanced constraints are here omitted. This leads to the objectives and constraints described in Table 24. As previously explained, the objective is twofold. The first one tries to reach the target EVs SoCs as soon as possible (c.f. (18)). The second minimizes the EV battery wearing by penalizing large setpoint variations (c.f. (19)). All objectives are weighted[21] in a way to favor plugged EVs with shorter remaining connection times and higher remaining energy demands. In terms of constraints, the first set of constraints guarantees that an EVs' SoCs do not surpass users requested target (c.f. (20)). The second set of constraints guarantees that the computed setpoints are within the EVCS and plugged EVs operational constraints (c.f. (21)). Additionally, the maximum and minimum EV power limitations are considered as time-dependent and known at time t. Finally, the last set of constraints (c.f. (22)) was added to guarantee the knowledge of the inputted data at time t over the MPC time horizon (i.e., from t to tH). Indeed, as the problem is formulated using MPC, proper forecasting is required to predict the evolution of the inputted EV user behavior, e.g. the Boolean $\omega t,k,I$ expressing whether, or not, an EV is plugged to plug $k = 1,..., Ki$ of node $i \in C$ at timestep t. As a result, the constraints impose persistent forecast of the latter over the considered horizon. This is acceptable as the horizon is usually selected to be in the order of minutes and the EV user behavior usually does not drastically change during these timescales.

[21] The details of how the weights are defined can be found in [19].

Table 24: Real-time stage objectives and constraints of an EVCS aggregator connected to node $i \in C$.

(a) Objectives

Description	Equation
Reach Target SoC	$\sum_{\tau=t}^{t_H} \sum_{k=1}^{K_i} \kappa_{\tau,k,i} \left(\mathrm{SoC}_{t_{f,k,i},k,i} - \mathrm{SoC}_{\tau,k,i} + \frac{\eta_{k,i} P_{\tau,k,i} \Delta t}{E_{k,i}^{\max}} \right)$ (18)
Minimize EV battery wearing	$\sum_{\tau=t}^{t_H} \sum_{k=1}^{K_i} \lambda_{\tau,k,i} \kappa_{\tau,k,i} \left\| P_{\tau,k,i} - P_{\tau-1,k,i} \right\| \frac{\Delta t}{E_{k,i}^{\max}}$ (19)

(b) Constraints

Description	Equation
SoC Limitations	$\mathrm{SoC}_{\tau,k,i} - \frac{\eta_{k,i} P_{\tau,k,i} \Delta t}{E_{k,i}^{\max}} \leq \mathrm{SoC}_{t_{f,k,i},k,i} \forall \tau = t, \ldots, t_H$ (20)
Power Limitations	$(P_{\tau,k,i}, Q_{\tau,k,i}) \in \begin{cases} \{(P,Q) \mid P^2 + Q^2 < \left(S_{k,i}^{\max}\right)^2, -P_{\tau,k,i}^{\min} \geq P \geq -P_{\tau,k,i}^{\max}\} & \omega_{\tau,k,i} = 1 \\ \{(0,0)\} & \omega_{\tau,k,i} = 0 \end{cases}, \forall \tau = t, \ldots, t_H$ (21)
Persistent Forecasting	$\begin{cases} \omega_{\tau,k,i} = \omega_{\tau-1,k,i} \\ \kappa_{\tau,k,i} = \kappa_{\tau-1,k,i} \\ \lambda_{\tau,k,i} = \lambda_{\tau-1,k,i} \\ P_{\tau,k,i}^{\max} = P_{\tau-1,k,i}^{\max} \\ P_{\tau,k,i}^{\min} = P_{\tau-1,k,i}^{\min} \end{cases}, \forall \tau = t+1, \ldots, t_H$ (22)

4.3.6. Experimental validation

This section presents an experimental validation of both the day-ahead and real-time stages. First an optimal day-ahead DP is calculated and then, the real-time controller is used in order to track the DP while accounting for ADN and resources operational constraints. The goal of the experiment is twofold. First, we show that the integration of EVCSs in both the day-ahead and real time stages improves the tracking of an optimally computed DP. Second, we experimentally prove the aptness of the proposed real-time EVCS controller to best satisfy EV user demands. In the following, first the experimental setup is described. Then, some notes on the experiment are given. Finally, the results of the experiment are shown.

Experimental setup: the EPFL low voltage microgrid

The experimental validation of the proposed algorithms is performed on the EPFL smart grid platform as shown in Figure 7. The experiment uses: (i) the IT infrastructure described in [26], (ii) the branch and node parameters listed, respectively, in Table 10 and Table 11, and (iii) the PMU-aided monitoring infrastructure shown in Figure 25. While the grid interfaces several resources, for the purpose of this experiment, only a subset is considered, namely the three uncontrollable PV plants (PV1 (Perun), PV2 (Solarmax) and PV3 (Solis-Facade), controllable EVCS (EVCS1 and EVCS2) and a battery (BESS1). The loads at nodes B20, B21 are assumed to be uncontrollable. The resource parameters are summarized in Table 25.

Table 25: Specification of resources for the real-time experiment.

Resources	Nominal Rating	Units
PV1 (Perun)		
Rate power of PV cells Apparent power Controllability	13 13 Uncontrollable	kWp kVA -
PV2 (Solarmax)		
Rated power of PV cells Apparent Power Controllability	16 16 Uncontrollable	kWp kVA -
PV3 (Solis-Facade)		
Rated power of PV cells Apparent Power Controllability	15 15 Uncontrollable	kWp kVA -
BESS1		
Ratings Controllability	See Figure 23 Active and reactive power controllable	
EVCS1		
Ratings Controllability	See Table 12 Active power controllable	
EVCS2		
Ratings Controllability	See Table 12 Active power controllable	

Experimental notes: As the goal of the experiment was not to stress test the algorithms in terms of ADN and resources operational constraints, all resources were used at full capacity and the ADN operational limits were set to the values in the EN-50160 standard. However, for the battery available at the microgrid, the maximum and minimum allowable SoCs for the BESS are limited to 0.9 and 0.2, respectively.

Figure 37 shows the sequence of the operations and communications flows during the real-time operation. At 00.00 local time, the real-time operation starts. It takes as input the dispatch plan computed at the day ahead-stage based on the forecasts of the uncontrollable injection and flexibility offered by the controllable resources. The real-time controller runs every 30 seconds with updated short-term forecasts of the load, generation, and EVCS demand. It computes the active and reactive power setpoints and sends them to the resources for actuation. This cycle is repeated each 30 second till the day's end.

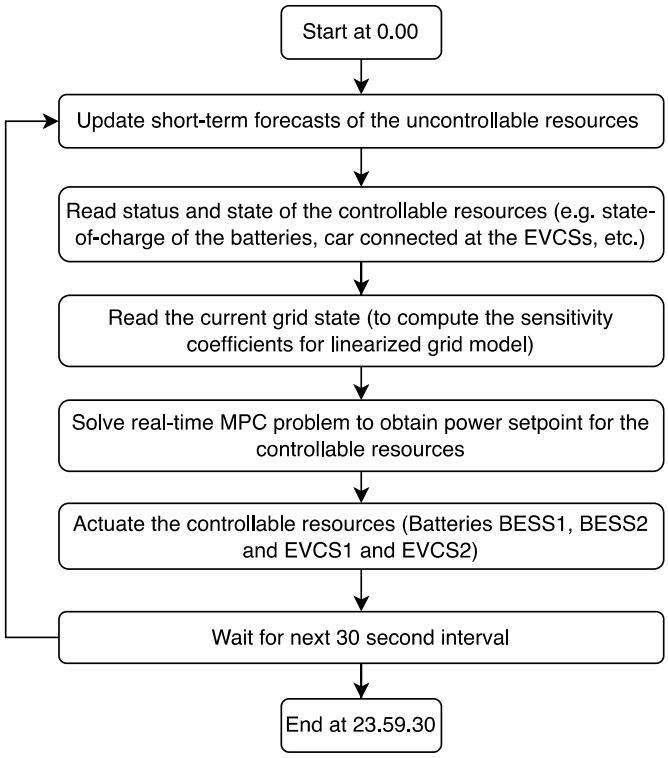

Figure 32: Sequence of operations during real-time control

Results

The experimental validation was performed for several days, exhibiting different day types and irradiance conditions. For the sake of brevity, the results of two distinct days are presented. Day 1 is a weekday and a cloudy day, whereas day 2 is a weekend day and rainy. Results for multiday experiments are shown, demonstrating that the dispatching framework can run successfully for multiple contiguous days. The experimental results are described below.

Day 1 (17-April-2023)

It corresponds to a weekday (Wednesday) and is characterized by a day with cloudy irradiance patterns. The source of uncertainty is the generation from the photovoltaic plants and the EVCS power demand.

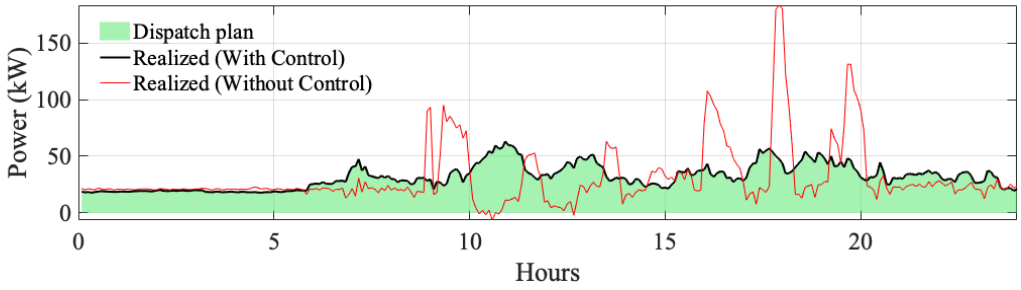

Figure 33: Dispatch plan, and power at the GCP with and without control.

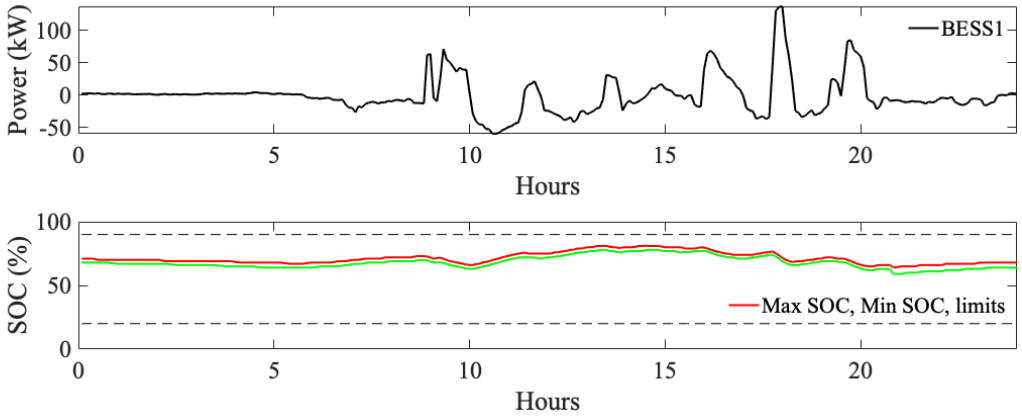

Figure 34: Active power regulation from the BESS1, and lower panel: minimum and maximum state-of-charge (SoC).

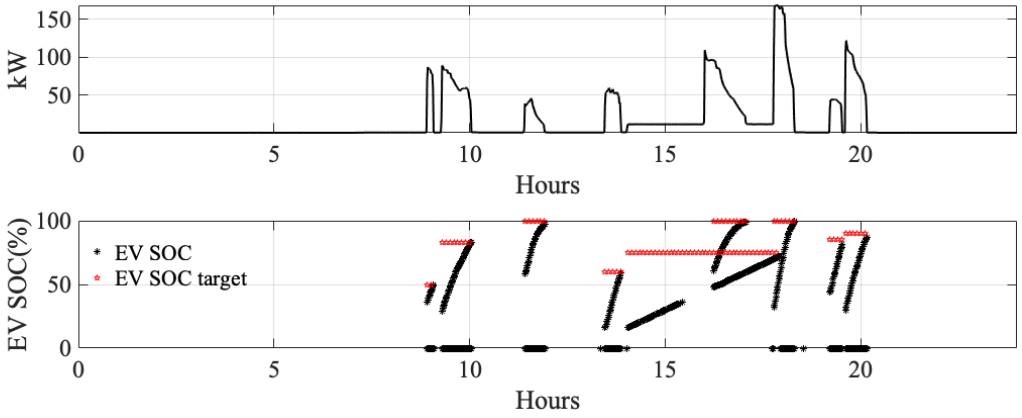

Figure 35: Upper: Controlled active power consumption by EVCS1, lower: EV SoC during the day along with the SoC target.

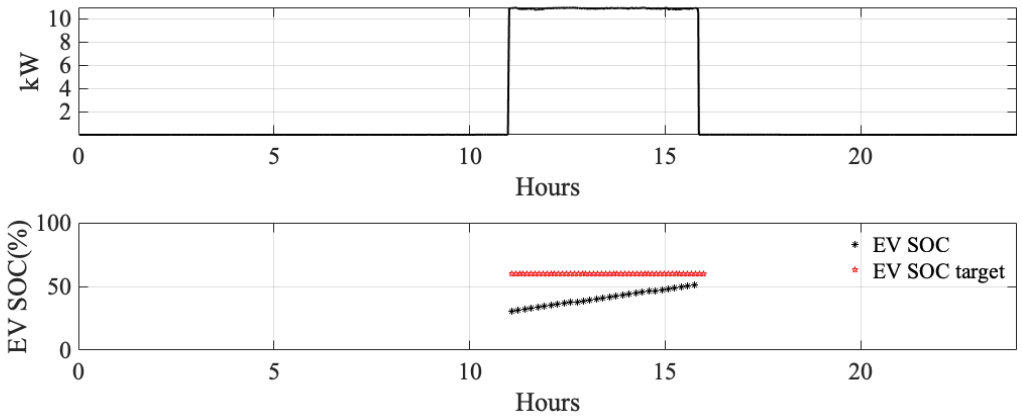

Figure 36: Upper: Active power consumption by EVCS2, and lower: EV SoC during the day along with the SoC target.

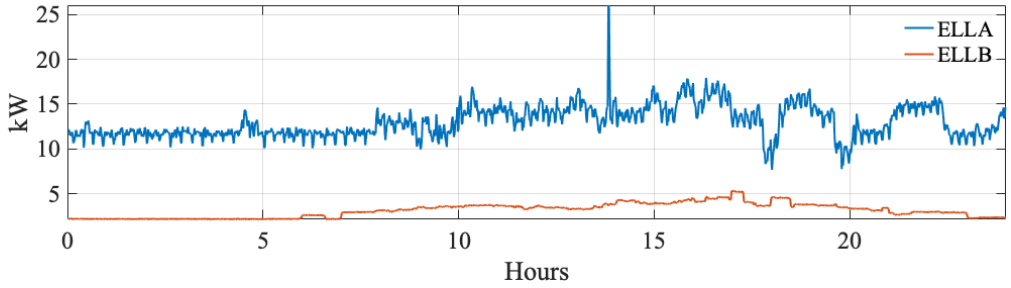

Figure 37: Demand profiles: ELLA and ELLB represents the aggregated loads of the ELL building of the EPFL smart grid platform, at nodes B20, and B21.

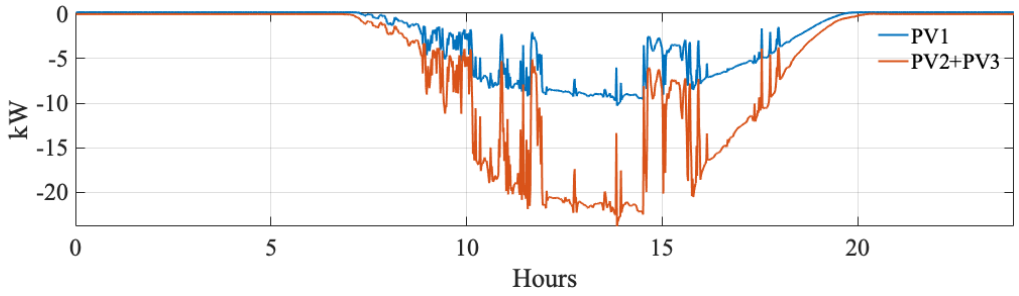

Figure 38: PV generation at nodes B14 and B16.

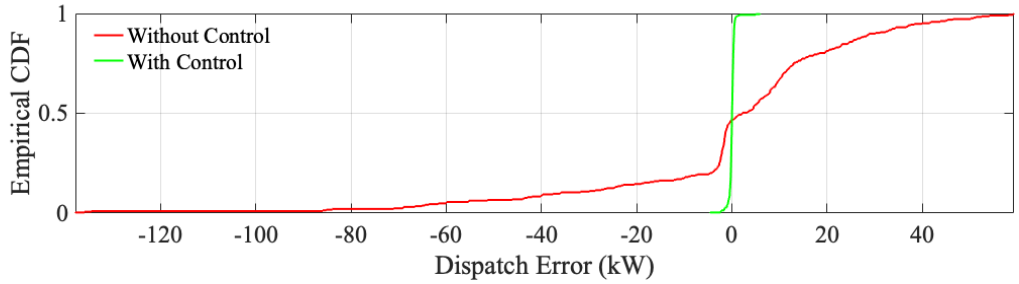

Figure 39: Cumulative distribution function (CDF) of Dispatch error with and without control.

Figure 33-39 shows the experimental results obtained on day 1.

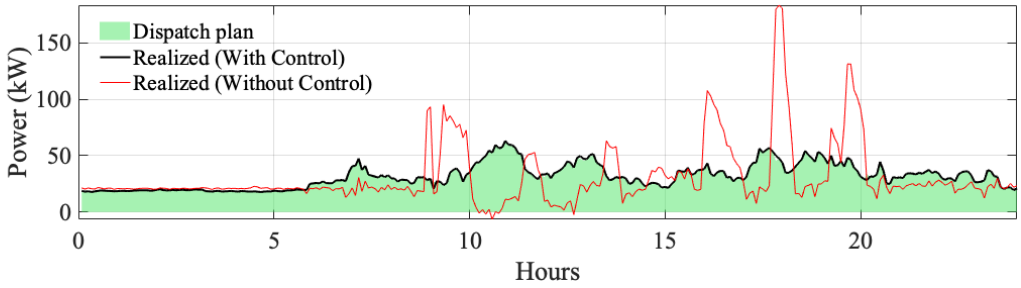

Figure 33 shows the dispatch plan in shaded green and realized power at the GCP with and without control is shown in black and red color, respectively. Since each experiment day is unique with respect to the solar irradiance, number and energy demand of EV charging sessions, it is impossible to redo the same experiments in “without control” mode. Therefore, we obtain the plot “without control” by removing the contribution of the BESS and re-running the AC load flow with the rest of the injections.

Figure 34 shows the power injections and the SoC from the controllable battery BESS1. Figure 35 and Figure 36 show the EV demand (with control) and the EV SoC of the connected cars at the EVCS1 and EVCS2, respectively. In these figures, the target SoC is shown in red, and the SoC is shown in black. Figure 37 and

Figure 38 show the uncontrollable demand (at nodes B20 and B21) and PV generation (at nodes B14 and B16). Figure 39 shows the cumulative distribution function (CDF) of the error in power (averaged over the dispatch period of 5 minutes) with and without real-time control.

The dispatch plan is tracked with high fidelity (

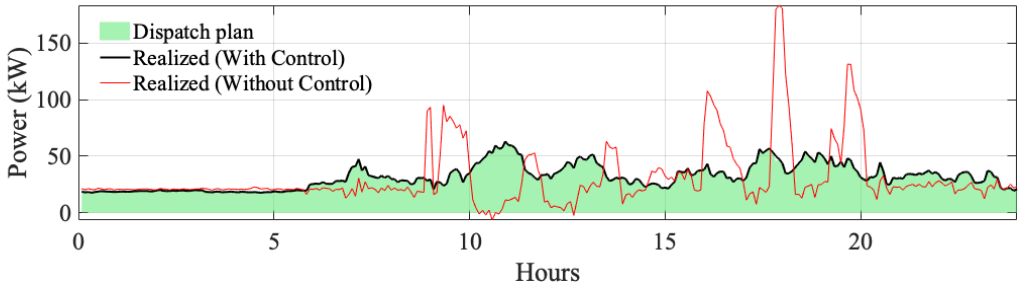

Figure 33), thanks to the power injected from the controllable BESS and curtailments actions from EVCS(s). From the plot, it can also be observed that the variation in the generation at the PV plants is well compensated by the battery storage. In Figure 34, the BESS SoC is respected within the imposed constraint of 20 to 90 %. Figure 35-Figure 36 shows the target SoC of the EVs, and in most of cases, EV users meet their target SoC.

Table 26 shows different metrics to quantify the dispatch error with and without control. It shows the RMSE error, max absolute error (MAE), and Absolute Energy Error (AEE) of the dispatch over the day. AEE is absolute sum of the dispatch tracking error over the whole day. From the comparison, it is pointed out that the RT control manages to track with high accuracy exhibiting low RMSE and MAE. The real-time control manages to reduce error metrics by more than tenfold.

Table 26: Performance Metrics for Real-time Operation

Metrics	Day 1		Day 2	
	Without Control	**With Control**	**Without Control**	**With Control**
RMSE (kW)	28.7	0.7	19.1	0.5
MAE (kW)	137.9	5.9	91.9	2.9
Absolute Energy Error (kWh)	441.7	8.5	327.4	1.5

Day 2 (15-April-2023)

It corresponds to a weekend (Saturday) and is characterized by a rainy day, so it exhibits low irradiance day leading to low PV generation and relatively low demand compared to the weekday.

Again, we show the active power realization at the GCP with and without control. It is shown in Figure 40; it can be observed that the dispatch plan is again tracked well, thanks to the power regulation provided by the controllable batteries, as shown in the Figure 41 and curtailment action of EVCS1 as shown in Figure 42.

As this day corresponds to a rainy day, the peak power of the dispatch plan is higher than in the case of day 1. On this day, there are no sessions on the EVCS2, as it belongs to the office's private space, which is turned off during the weekend. There are many sessions on the EVCS1, of which all of them met their targets. Thanks to the good quality forecasting of the EV charging profiles accounted in the day ahead stage, there are not any curtailments in EV demand leading to 100% satisfaction of the EV consumers. Also, the batteries' SoC is within the designated range of 20 to 90% SoC.

Figure 45 shows the histogram of the dispatch error with and without control and it can be concluded that the real-time control achieves a very good accuracy in the dispatch tracking. The same can be observed by the metrics shown in Table 26.

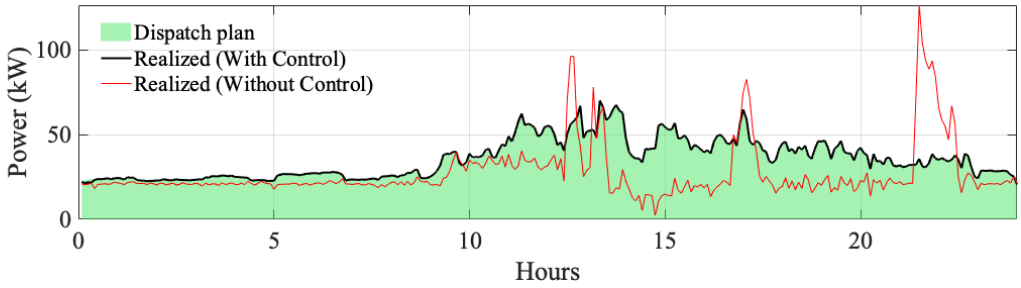

Figure 40: Dispatch plan, and power at the GCP with and without control.

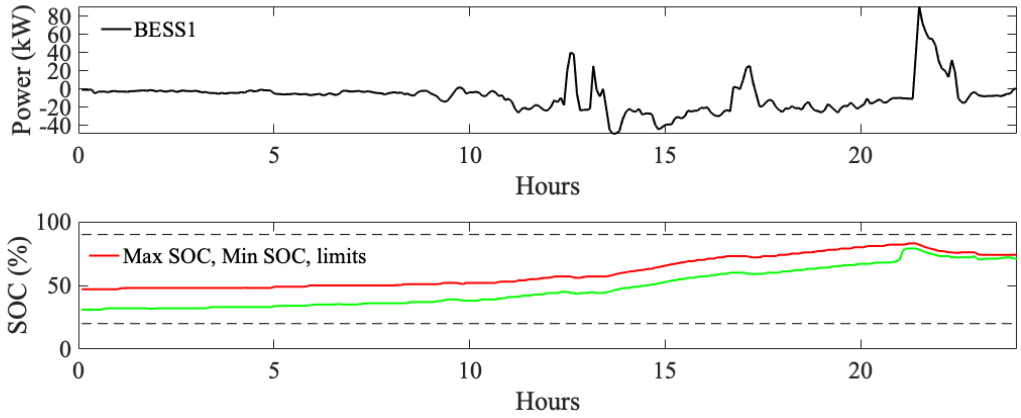

Figure 41: Active power regulation from the BESS1, and lower panel: minimum and maximum state-of-charge (SoC).

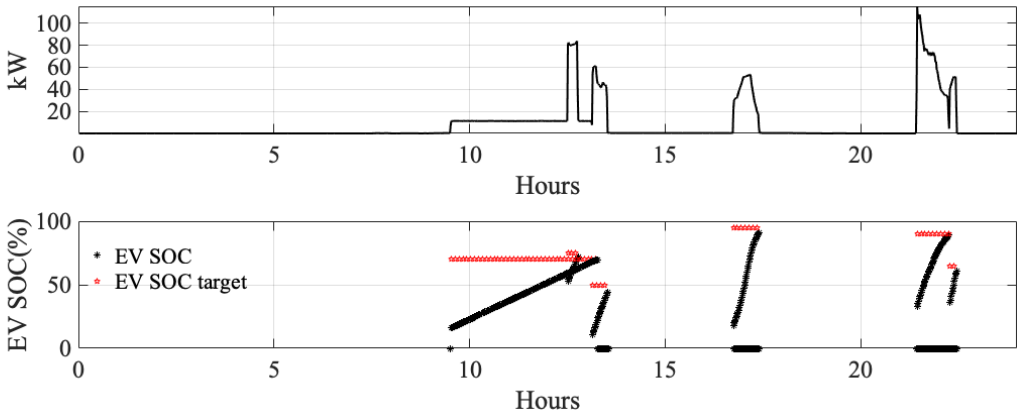

Figure 42: Upper: Controlled active power consumption by EVCS1, lower: EV SoC during the day along with the SoC target.

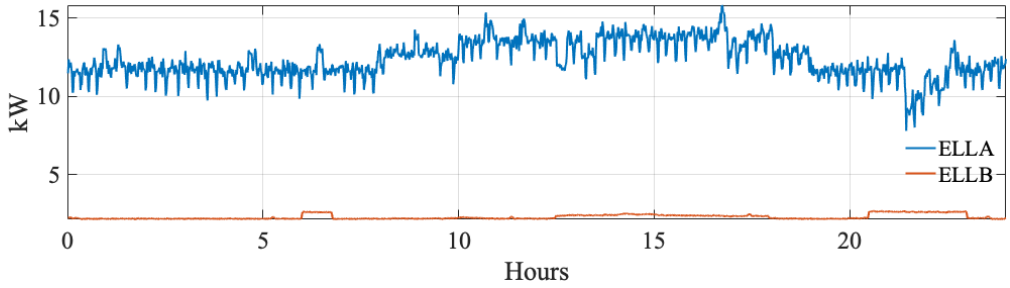

Figure 43: Demand (ELLA and ELLB) at nodes B20, and B21.

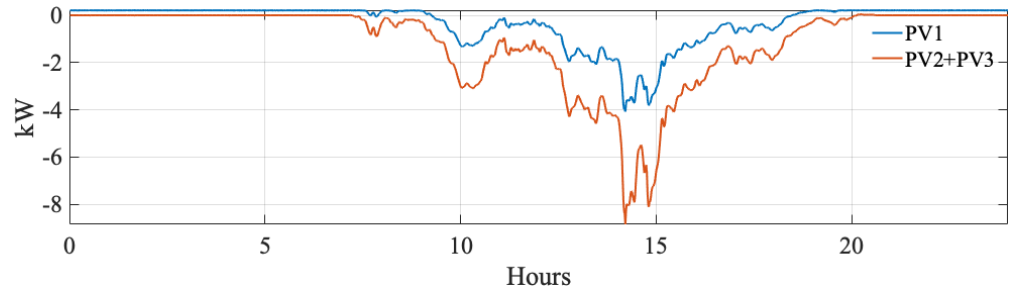

Figure 44: PV generation at nodes B14 and B16.

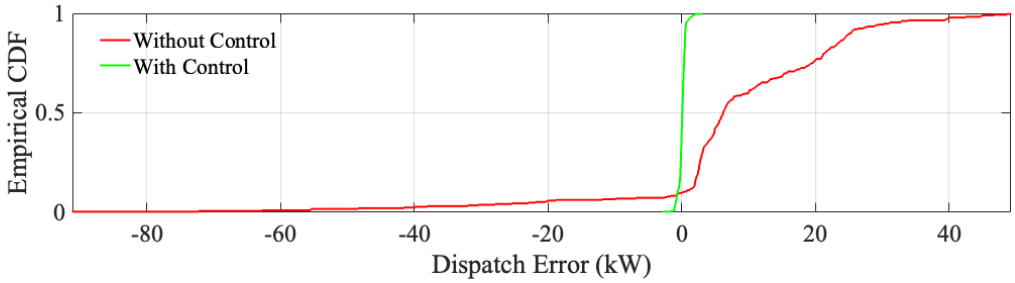

Figure 45: Cumulative distribution function (CDF) of Dispatch error with and without control.

Multiday (14-18 Apr 2023)

To demonstrate the effectiveness of the dispatching scheme, we ran the control of the BESS for four contiguous days. Figure 46 shows the dispatch plan and the measured GCP power with and without the control scheme. In Figure 47, we show the SoC evolution of BESS1 during the 4-days. The power at the GCP follows the dispatch plan and keeps the BESS SoC within a comfortable SOC so that dispatching is continued the next day.

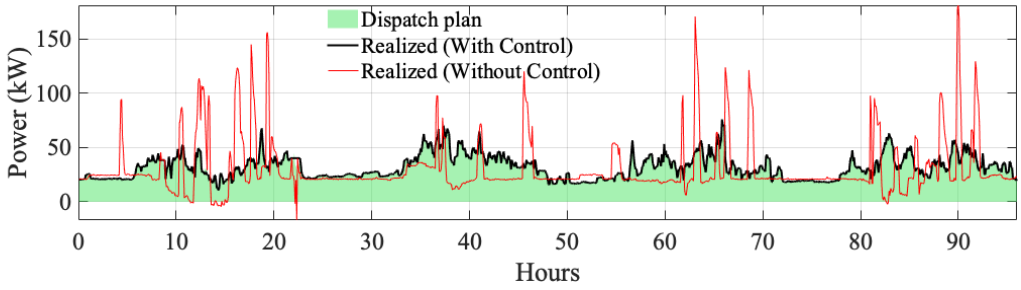

Figure 46: Dispatch plan, and power at the GCP with and without control.

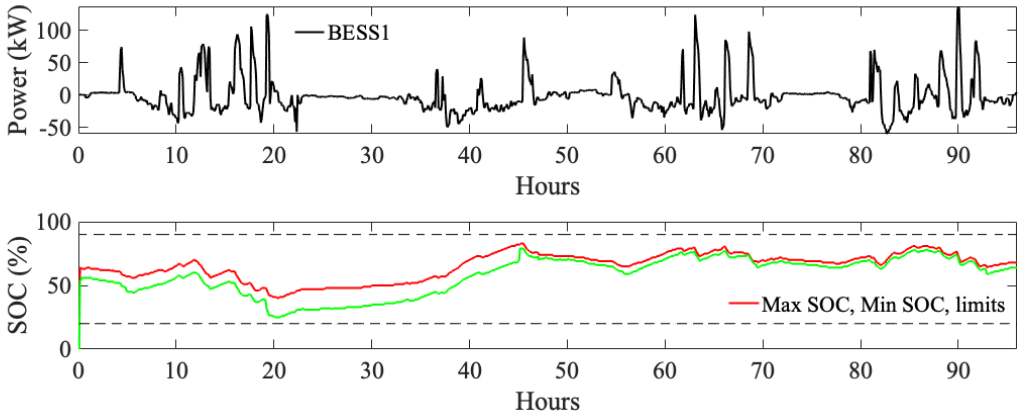

Figure 47: Active power regulation from the BESS1, and lower panel: minimum and maximum state-of-charge (SoC).

4.4. Multi-service battery control

4.4.1. Services analysis

One of the key objectives of the project is to assess market opportunities arising from flexibility provision of a setup combining fast EV charging stations and a stationary battery. Although guaranteeing dispatchability at the PCC seems to be interesting for grid operators, it is a value proposition which is currently not marketable. Therefore, GridSteer assessed alternative market opportunities of the Aigle setup via interviews with numerous companies and researchers as well as online market research. With respect to assets integrating BESSs and EV fast charging stations, the services which are the most interesting economically are peak power shaving (PPS), participation to the frequency containment reserve (FCR), backup energy storage provision, as well as reactive power management.

Peak power shaving (PPS)

In Switzerland, DSOs usually include a power price in the electricity tariff for end-users consuming more than 100 MWh/year. The billing scheme is either based on the 15 min peak power consumption of each month or on the 15 min peak consumption of the year, depending on the DSO. In that sense, to perform PPS with a limited energy reservoir such as a BESS, the controller must anticipate its peak shaving objective month/year-ahead: the smaller the shaving objective, the smaller the power bill. Note that some DSOs specify in the contract that a minimum power is billed even if the consumer does not reach it.

As an example, it is not unusual for consumers consuming a few GWh per year to have an annual power bill around 1 MIO CHF.

Frequency containment reserve (FCR)

FCR (or primary frequency regulation reserve) is a fast response mechanism of the power grid to match supply and demand. Any resource with enough flexibility can apply for a Swissgrid prequalification and participate in the FCR market. Bids are advertised day-ahead in steps of 1 MW and must be made available for slots of 4 hours (i.e., 6 slots a day). Even though the steps are of 1 MW, flexibility can be pooled. One can thus consider smaller granularity per unit if the aggregated resources in the pool allow for it. Since the bids need to be placed at least one day before activation, a day-ahead forecast of the site's prosumption (BESS excluded) is needed.

Backup energy reserve

The concerns regarding energy shortages in Switzerland are rising. More and more companies are looking into backup energy solutions such as diesel generators or BESSs. By establishing beforehand the amount of energy needed for backup, one can guarantee that amount to always be stored in the BESS and perform other services on top of it. As load shedding is often planned, a company can also reserve the battery for backup only for a specific moment while performing other services the rest of the time. This turns the backup energy resource into a revenue generating asset contributing to the energy transition.

Reactive power management

DSOs usually bill reactive power to the end-consumer if the power factor (cosφ) is smaller than a given value, often 0.9 or 0.95, but this number can significantly vary with some DSOs even setting it to 0.7. It is worth noting that even though reactive power is not what the customer pays for, it contributes to grid usage and to grid congestion just as much as active power[22] .

4.4.2. Control framework

In view of the above, GridSteer has developed a dedicated EMS for BESS to provide the identified services behind the customer meter. In this document, it is also referred to as multi-service battery controller (MSBC). Its objectives are to plan the services that the BESS performs every day and to ensure a safe operation of the BESS according to the plan. The software can be run in a physical system or in simulation mode, in which an ESR model of the battery and historical data of the load to simulate are used to assess the performance of the software on a given site. Its structure is presented in Figure 48:

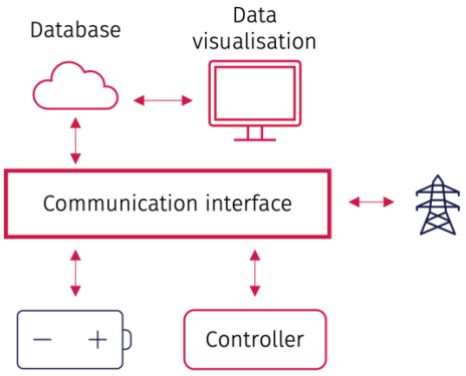

Figure 48: MSBC simplified control framework.

Communication interface

The communication interface handles all communication aspects of the system: it reads the state of the BESS, the state of the managed grid (i.e., PCC measurements, load consumption, etc), transfers them to the controller, then reads and sends the setpoints computed by the controller to the battery. It also sends data to a database to be stored and visualized.

Controller

The controller's tasks are to safely operate the BESS and maximize the revenues it generates. To do so, the controller is divided in two elements: the real-time controller and the planner.

Real-time controller

At every control cycle, the real-time controller computes the setpoints to send to the battery according to what was planned by the planner. The process is as follows:

1. Recover the latest measurements.
    a. BESS state.
    b. P, Q load consumption.
    c. P, Q at the PCC.
2. Recover the latest service schedule.
3. Check what service is scheduled for the current cycle.
4. Update the shave target, if needed (if the target value is exceeded).

[22] A transformer or a line rated for 1 MVA supplying a load with a 0.7 cosφ would not be able to distribute more than 0.7 MW, while it would be able to distribute up to 0.95 MW to a load with a cosφ of 0.95

5. Compute the setpoint.
6. Send the setpoint to the communication interface.

To compute the setpoint, the process is as follows:

1. If the current service is peak shaving.
    a. If shaving is needed, apply a proportional integral (PI) control to shave the PCC consumption.
    b. If shaving is not needed, reset the integral error of the PI control, and steer the BESS towards the maximum operating SoC.
2. If the current service is FCR.
    a. If the current cycle is the beginning of a new hour, compute the BESS charge management power (discussed in the following subsection).
    b. If the frequency deviation is smaller than 0.2Hz, compute the setpoint according to the droop control and add the charge management power.
    c. If the frequency deviation is bigger, or equal, to 0.2 Hz provide full bid power.
    d. If the SoC of the battery is not between bounds, stop performing FCR and charge or discharge the BESS to bring its SoC back between bounds.

BESS charge management

For limited energy reservoirs (LER) to participate in FCR, the asset operator must ensure that the asset can always provide the bidding power for 15 min (consumption and production). To do so, the operator can change the reference power of the asset (e.g., every hour) to maintain its SoC between the wanted limits (coined as charge management). The charge management must however not be noticed at the balance group level. This can only be done if another flexible asset within the same balance group as the BESS provides this charge management.

To compute the BESS charge management power, the MSBC forecasts (via an auto-regressive integral moving average – ARIMA – model) the average frequency deviation for the coming hour and compensates it. The frequency forecasting method is based on this method [27] co-authored by the EPFL-DESL laboratory. The current deviation with the target SoC is also compensated for.

$$P_{base} = -\alpha(\hat{\mathrm{f}} - 50) + C_{rated}\Delta SoC \quad (23)$$

Where

- α is the droop coefficient used for FCR in [W/Hz].
- $\hat{\mathrm{f}}$ is the average estimated frequency for the coming hour.
- C_{rated} rated is the rated capacity of the battery in [Wh].

Planner

The planning process is as follows:

1. Monthly/yearly:
    a. Compute a peak-shaving objective for the coming period, considering estimated FCR and PPS revenues.
2. Daily
    a. Forecast the load for the coming day.
    b. Based on the load forecast, decide in which slots of the coming day the BESS is going to perform PPS and in which slots it is going to perform FCR.

In the experimental validation of the MSBC, the forecasting part of the algorithm is not the point of focus. A seasonal ARIMA (SARIMAX) model is used for the day-ahead load forecasting. Once the forecast is computed, the service planning software computes the available margin for each slot in the day: if the margin is smaller (bigger) than zero, PPS (FCR) will be performed during that slot. The following figure illustrates this concept.

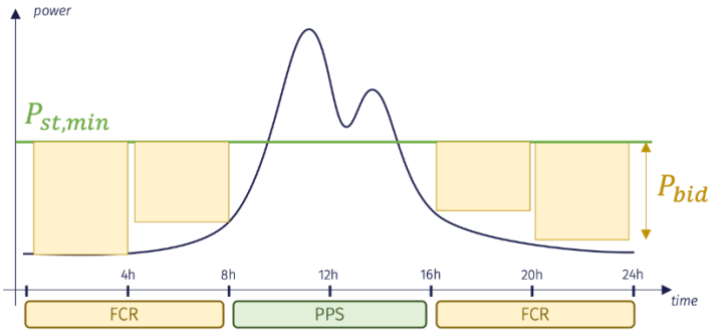

Figure 49: Illustration of FCR and PPS service planning

A commercial enhanced version of the EMS with better forecasting, increased reliability, inclusion of more services, inclusion of aggregating algorithm, is under development.

4.4.3. Simulations

The goal of the simulations is to test the performance of the MSBC and of the service planning process. To evaluate the interest of a multi-service BESS control solution, the forecasting part of the service planning algorithm is not tackled, and "perfect forecasts" are used (i.e., the realization of the coming day is used as day-ahead forecast). This allows to assess the best performance of the control framework that has been developed.

Simulation 1 - Current context

Setup

The MSBC in the context of Aigle is simulated with the following parameters.

1. Electrical network (see Figure 50):
    a. 1 x 1.6 MW rated transformer at the grid connection point
    b. 1 x 1.6 MW/2.5 MWh BESS
    c. 4 x 300 kW EVC of GoFast

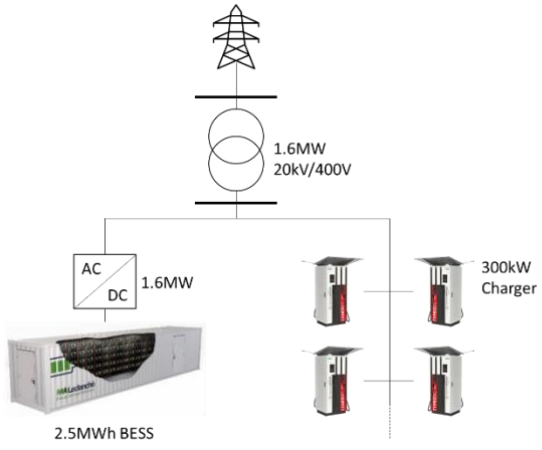

Figure 50: Simulation 1 grid schematic.

2. Tariffs of Romande Energie (2023) for a low voltage "DUP faible[23]" user located in Canton Vaud:

[23] DUP (GoFast) = Durée d'utilisation de la puissance = Annual kWh / Monthly $P_{max,15min}$
DUP faible if DUP < 3000h (this means that the prosumer has a profile with spikes)
DUP haute if DUP > 3000h (this means that the prosumer has a smooth profile)
More details on tariffs here: https://GoFast.romande-energie.ch/images/files/prix-electricite/2023_prix-electricite_bve.pdf

a. 5.63CHF / kW / month as power price component
b. 27.31 cts / kWh peak energy tariff
c. 18.97 cts / kWh off peak energy tariff
d. 18.3 cts/ kWh feed-in tariff

3. Average primary control bid price in 2022 (100 CHF/MW/4h bid)

Since the EVCSs in Aigle have not deployed, data is lacking to run a simulation. For that reason, the data of a charging station site with a similar configuration is used.

Dataset

The simulation dataset starts on January 1st of 2022 at 00h00 and ends on May the 31st of 2022 at 00h00.

The following figure shows the average hourly consumption of the site depending on the day of the week and the hour of the day. It details how the consumption of the site is distributed over a week. Every day around 12 a.m., the site is strongly active, while it is almost inactive during night-time. It also shows that the site is overall more active from Friday to Sunday than in the rest of the week.

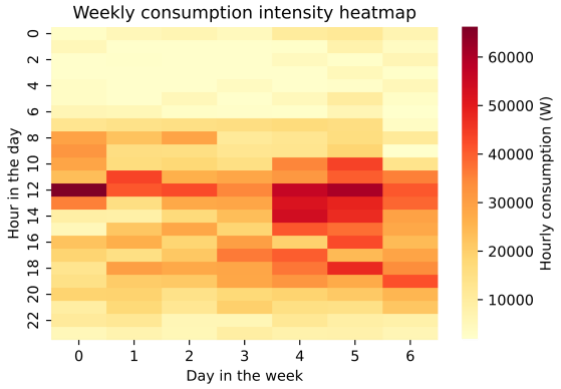

Figure 51: Simulation 1 weekly consumption of the EVCS in Aigle inferred from other GoFast EVCS with similar characteristics.

Similarly, Figure 52 shows the activity of the site for each slot where primary control can be performed.

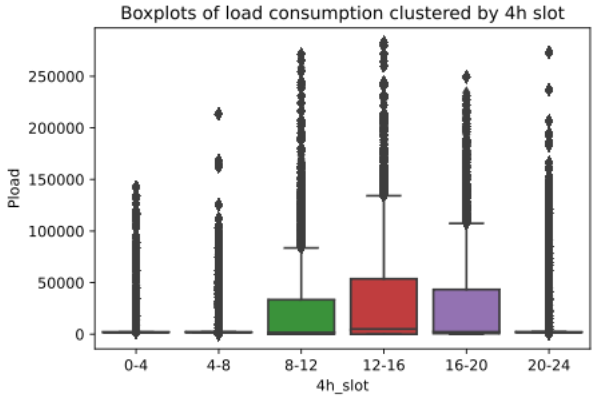

Figure 52: simulation 1 - load in 4h slot clusters

Intuitively, the service planner is expected to generally instruct the battery to perform FCR at full capacity between 8 p.m. and 8 a.m. and to reduce the FCR bids or perform peak shaving the rest of the day. It is however interesting to note that the extreme values are significant at every 4h slot, which implies that high forecasting errors are likely for any 4h slot. This will need to be accounted for when implementing the forecasting part of the service planning.

Service panel

The multi-service controller runs its planning algorithms with the following services:

1. Primary control regulation.
    a. It is assumed that the battery is aggregated in a pool containing a considerable number of resources. Therefore, the granularity in the primary bids that the battery can advertise to the pool aggregator has been set to 10 kW, although the market granularity is 1 MW (i.e., the aggregator ensures that the pool bids have a 1 MW granularity).
2. Peak-shaving.
3. 750 kWh back-up energy reserve guarantee (> 10 EV charges).

Simulation parameters

- The BESS can be safely operated between 10% and 90% of SoC.

Simulation results

Since the service planning algorithms schedules the services for the following day, the first day of the simulation is not relevant and is thus not shown in the following plots.

Power profiles

Figure 53 shows the results for a simulated period of 6 months. The service planning software decides to only perform FCR, while it sometimes needs to lower the bid power to never exceed the PPS target (which changes monthly).

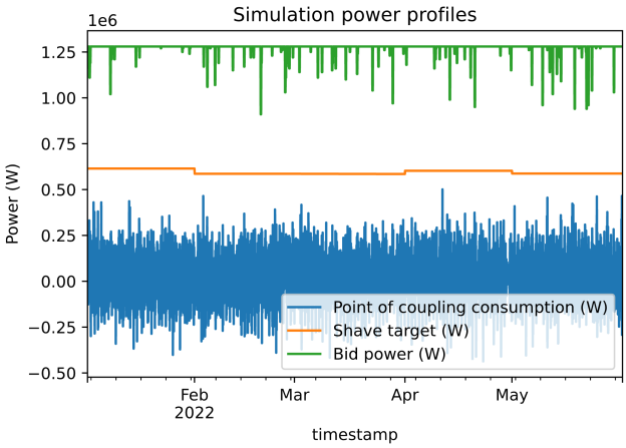

Figure 53: Simulation 1 power profiles.

To better illustrate the changes in bid power, Figure 54 shows zooms in on the simulation results for the 19th of February: between 1 and 3 p.m., the load increases and the bid power needs to be smaller to not exceed the PPS target of the month.

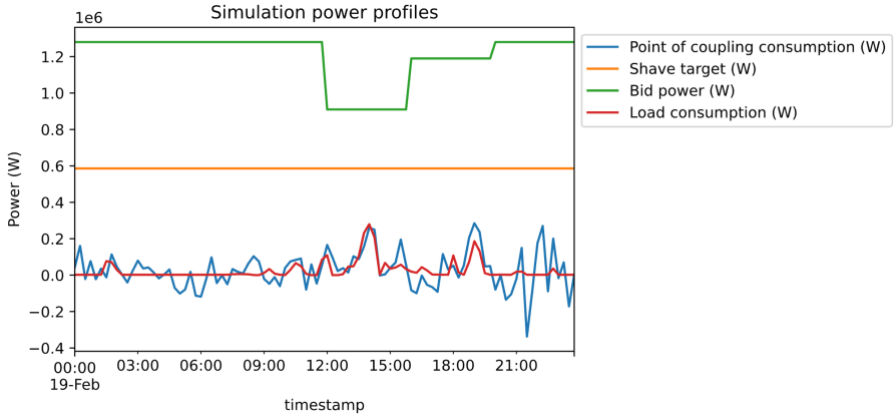

Figure 54: Simulation 1 power profiles for a single day.

BESS SoC

For a limited energy reservoir to participate in FCR, it is crucial to ensure that its SoC stays within the bounds specified by the transmission system operator. The following figure illustrates this.

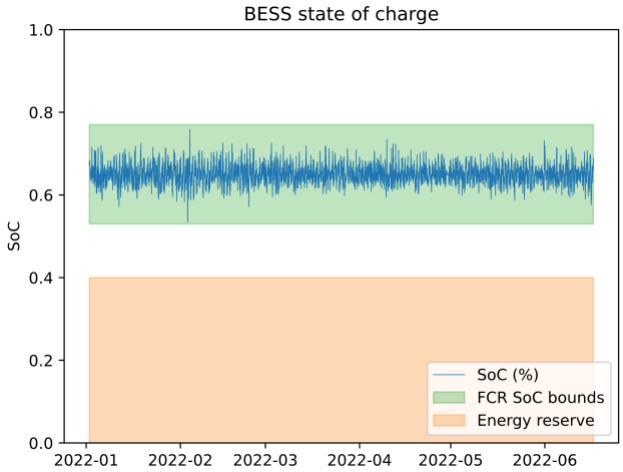

Figure 55: Simulation 1 BESS SoC.

The orange band represents the provision of 750 kWh of energy reserve. In the simulation, the battery never went below 53 % SoC (i.e., 1.325MWh of usable energy is always available in case of black-out).

The orange area shows the area in which the SoC must stay during FCR service (as per Swissgrid rules on LER participating in FCR). To ensure that the SoC stays in such bounds, the LER performs charge management: every hour, it can change its steady state operating power (i.e., the power it draws or outputs when there is no frequency deviation). Focusing on a single day, Figure 56 illustrates the BESS power profile as it performs FCR vs the hourly charge management requests.

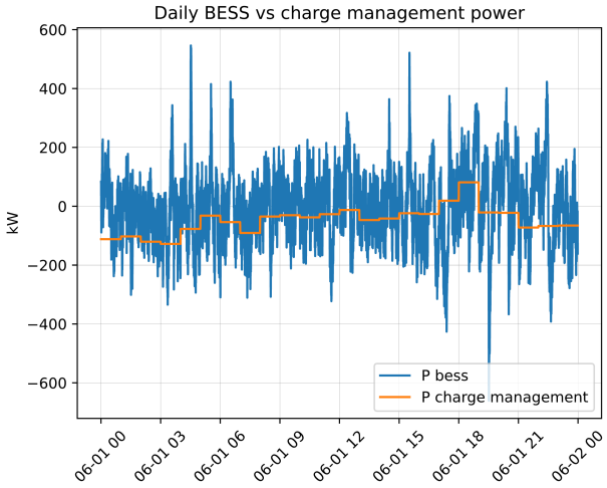

Figure 56: Simulation 1 BESS charge management.

Economics

This section shows the economical results of the simulation. On the customer side (the owner of the battery), the economics of the simulation are summarized in Table 27.

Table 27: Economics of simulation 1.

Investment cost	1625	kCHF
operation and maintenance (O&M) costs	54.5	kCHF/year
Yearly profits	103	kCHF/year

Payback time	**15.7**	**Years (without accounting the reserve and current BESS)**
	10	**Years (without accounting the reserve and downsizing the BESS)**

Table 28 shows the detailed cost and revenues of the system.

Table 28: Detailed cost and revenues of the system.

In thousand CHF per year	
Revenues	
Primary control	204
Costs	
Electricity bill increase	28.6
O&M costs	54.5

The yearly profits are computed as follows: $(204 - 28.6) * (1 - 10\%) - 54.5 \cong$ **103 kCHF/year.**

It should be mentioned that in the above equation, the BESS operator takes a 10% commission on the revenues generated by the services that the battery performs. The O&M cost is an average of all yearly recurring costs including service planning, operation, monitoring, maintenance, interventions, and insurances for a battery of this dimension.

For the BESS operator, the yearly revenues are as presented in Table 29.

Table 29: Yearly revenues for the BESS operator.

In thousand CHF per year	
Commission on services	17.5
Maintenance	50.4
Total	**67.9**

Discussion on economics

Today, the investment cost for a 2.5 MWh/1.6 MW battery is in the order of 1.6 MIO CHF. This number is based on the average cost per kWh (over the manufacturers that have been contacted) of utility-scale batteries. Additionally, operating costs include BESS operator fees, maintenance interventions, and insurances. The payback time is approximately 16 years. Note that, in this simulation, the system guarantees a backup energy reserve. It was supposed that the customer requests for a 750 kWh backup energy reserve to be resilient to shortages and the BESS operator minimizes the cost of the backup energy system. However, the value of the backup energy reserve is case specific, depending on the price that each customer is willing to pay for this reserve. Without the energy reserve, and therefore a smaller battery (around 1.75 MWh/1.6MW) that can provide only FCR, the payback time would be approximately 10 years.

It is worth noting that the system never plans to perform PPS because FCR generates significantly more income. To assess the economic feasibility of a battery performing mostly PPS, an experiment in which FCR is not in the service panel has been performed.

Simulation 2 - Without primary control

Simulation setup

This simulation is identical to the previous one except for the service panela as the BESS participation to FCR has been removed. The results of this simulation are compared with the results of the previous one.

Service panel

The service panel is identical as the previous simulation yet without FCR as a service.

Simulation parameters

- The BESS can be safely operated between 10% and 90% of SoC.

Simulation results

Figure 57 shows the results for the 6 months simulation. One can observe that the PPS targets are respected. Each month, the controller computes a PPS target for the coming month.

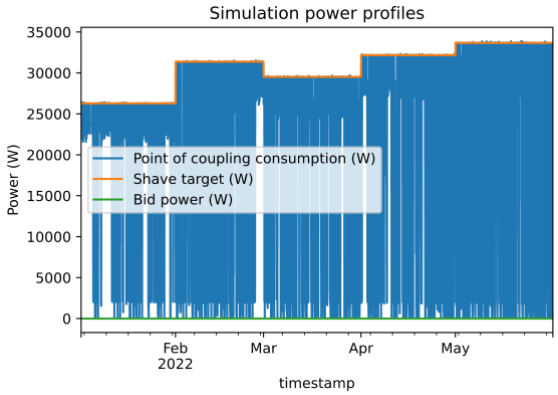

Figure 57: Simulation 2 BESS power profiles.

To better illustrate how the BESS is controlled during PPS, Figure 58 shows the BESS power profile, the load consumption profile, and the shave target on the 19th of February. One can see that the BESS compensates the load peaks when needed and charges when it can, without exceeding the PPS target.

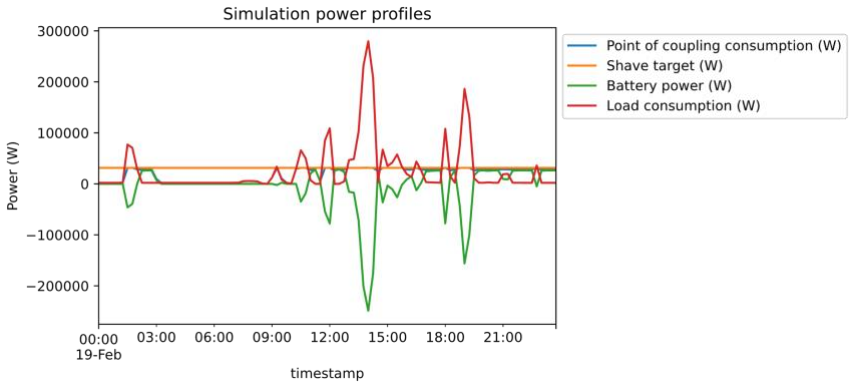

Figure 58 : Simulation 2 BESS power profiles in a single day.

BESS SoC

The SoC of the BESS stays in the specified boundaries and the backup energy reserve is always available. In fact, the lowest SoC reached during the simulation is 57.6% (i.e., 1.44 MWh are always stored in the BESS for this simulation). Figure 59 shows the evolution of the SoC over the simulation period.

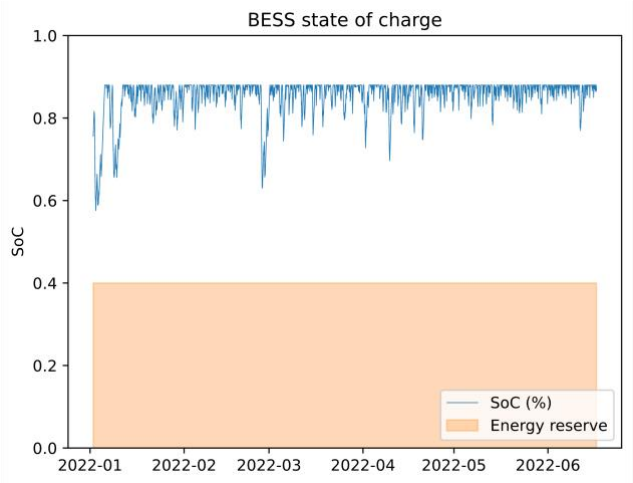

Figure 59: Simulation 2 BESS SoC.

Economics

This section shows the economical results of the simulation. On the customer side (the owner of the battery), the economics of the simulation are summarized in the following table.

For the BESS operator, the yearly revenues are as follows:

Table 30: Yearly revenues in simulation 2

Investment cost	1625	kCHF
O&M cost	54.5	kCHF/year
Yearly profits	-38.9	kCHF/year
Payback time	∞	**Years**
	30	**Years (assuming no O&M cost)**[24]

Table 31 shows the detailed cost and revenues of the system

Table 31: Detailed cost and revenues for simulation 2.

In thousand CHF per year	
Revenues	
Electricity bill decrease	17
Costs	
O&M cost	54.5

The yearly profits are computed as follows: $(15.3) * (1 - 10\%) - 54.5 \cong$ **-40.7 kCHF/year.**

Note that in the above equation it is estimated that the BESS operator would take a 10% commission on the revenues generated by the services that the battery performs.

For the battery operator, the yearly revenues are as follows.

[24] For comparison purposes.

Table 32: Yearly revenues.

In thousand CHF per year	
Commission on services	1.7
Maintenance	50.4
Total	**51.9**

Discussion on economics

For basic services of the BESS, it would not be viable to outsource the handling of this asset's operation. Indeed, BESS manufacturers often propose an EMS with simple functionalities such as PPS.

Note, however, even if the maintenance costs were fully removed (which is unrealistically optimistic) the payback time for a BESS operating in this way would be approximately 30 years, which is twice as much as the payback time obtained with the first simulation.

Discussion on current context

The current context makes a combination of PPS and FCR highly unlikely. Since the consumption peak power is much smaller than the rated powers of the BESS and of the transformer, even performing a very small amount of PPS leads to significant lost opportunities to perform FCR.

Moreover, the BESS is oversized for the current context. While this can enable substantial amounts of backup energy storage, most of the revenues that the BESS generates could be generated with an asset that has half the rated energy, which would reduce the payback time to less than 10 years.

In the medium term, the EV charging station operator aims at deploying more and more charging stations on the site. The next simulation shows the performance of the multi-service BESS controller in that situation.

Simulation 3 – Increased number of EV charging stations

Simulation setup

The medium-term objective of GoFast is to deploy other fast charging slots on the site. Such configuration would put the Aigle subnetwork under more stress and the multi-service BESS control might be used more extensively. This simulation evaluates the performance of the multi-service BESS control in the Aigle context but with 40x 300 kW DC EVC. To do so, a consumption profile of such a charging park has been generated using the EV charging session model discussed in section 4.2 EV user statistical modelling.

Dataset

From the heatmap representation of the dataset (Figure 60), one can see that the model distinguishes weekdays from weekends. Overall, in weekdays, most of the charges are generated between 7 a.m. and 8 p.m. In weekends, most charges are between 10 a.m. and 7 p.m.

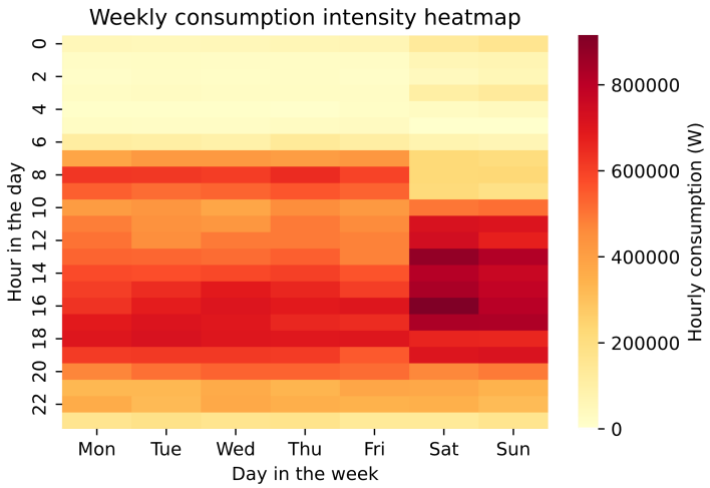

Figure 60: Simulation 3 weekly EV consumption heatmap.

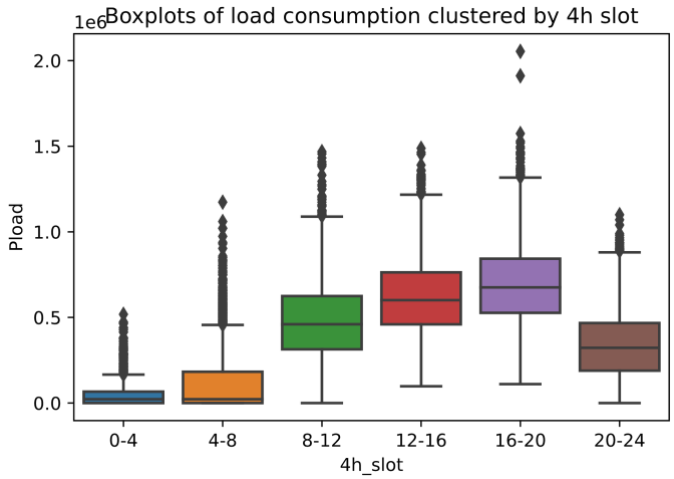

Figure 61: Simulation 3 load in 4h clustered slots.

In the boxplot representation of the model-generated data (Figure 61), the trend mentioned above is confirmed. Also, spikes going up to 2.1 MW can be identified. Note that this is larger than the transformer's rated power, meaning that either the BESS will shave such peaks, or such demand will not be satisfied by the EV charging station operator.

Power profiles

Figure 62 shows the power profiles during the simulation. One can see that the shave target is approximately set at the transformer limit (1.6 MW). The controller was able to shave the power at the point of coupling. One can see that the FCR service is performed most of the time, with bids that change to ensure that the shave target and transformer limit are always respected.

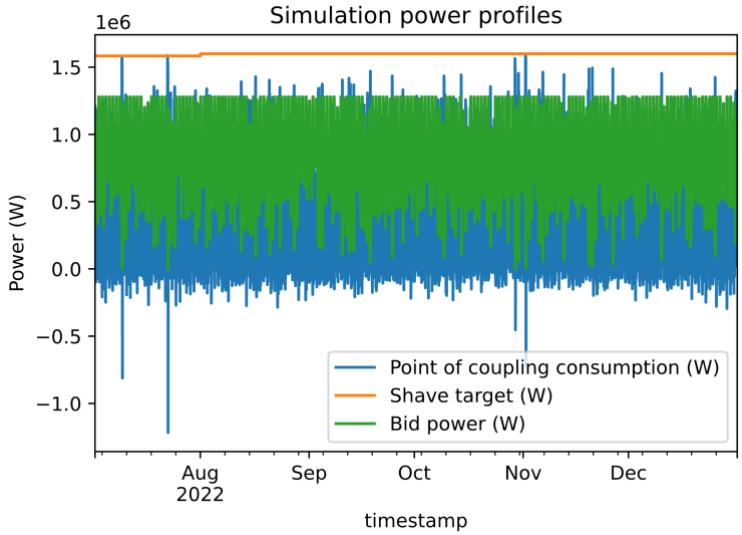

Figure 62: Simulation 3 power profiles.

Figure 63 shows a zoom on the 9th of July 2022. Here, one can observe the service stacking: between midnight and 4 p.m., the service planning algorithms decide to perform FCR with different bids. Between 4 and 8 p.m., PPS is performed (this can be seen by comparing the load and PCC consumption, also, the bid power is set to zero). Between 8 p.m. and midnight, the planer choses FCR again.

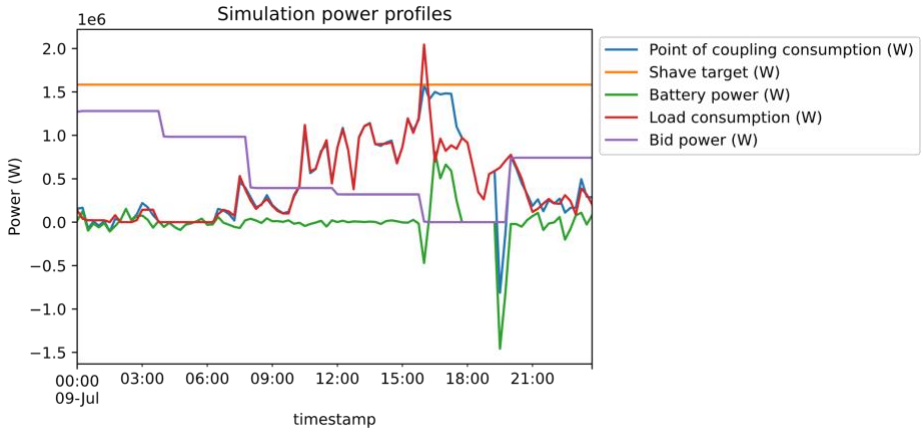

Figure 63: Simulation 3 power profiles in a single day.

BESS SoC

Figure 64 shows the evolution of the SoC of the BESS over time. The green area shows the BESS limits when performing FCR with a maximal bid (i.e., it shows the most restrictive area for the SoC). In 4 occurrences this band enlarges as the planner changes the service of the BESS towards PPS. When the BESS switches to the PPS service provision, it charges to 90% SoC to be able to perform as much PPS service as possible.

The energy reserve is satisfied since the battery never goes below 58.7% of SoC (1.467 MWh of energy is always available).

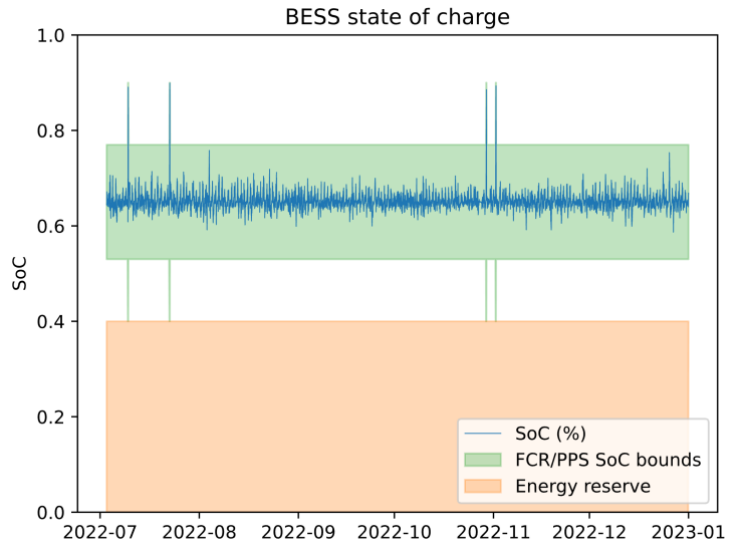

Figure 64: Simulation 3 BESS SoC.

Economics

On the customer side (the owner of the BESS), the economics of the simulation are summarized in Table 33.

Table 33: Economics of simulation 3.

Investment cost	1625	kCHF
Maintenance cost	54.5	kCHF/year
Yearly profits	70.5	kCHF/year
Payback time	**23**	**Years (without accounting the reserve and current the BESS)**
	16	**Years (without accounting the reserve and downsizing the BESS)**

Table 34 shows the detailed cost and revenues of the system

Table 34: Detailed cost and revenues in simulation 3.

In thousand CHF per year	
Revenues	
Primary regulation	136.6
Electricity bill decrease	2.3
Costs	
Maintenance + insurance cost	54.5

The yearly profits are computed as follows: $(136.6 + 2.3) * (1 - 10\%) - 54.5 \cong$ **70.5 kCHF/year.**

Note that in the above equation it is estimated that the BESS operator would take a 10% commission on the revenues generated by the services that the battery performs.

For the BESS operator, the yearly revenues are as follows:

Table 35: Yearly revenues for simulation 3

In thousand CHF per year	
Commission on services	13.9
Maintenance	50.4
Total	**64.3**

Discussion on the economics

One must note that some cost savings that the system allows have not been considered above. For instance, the customer would typically have to pay to have a backup energy system (e.g., a diesel generator set). Also, if the customer wanted to consume the power profile without having the BESS, he would need to upgrade its transformer size and increase its grid connection rating (which would result in some costs).

The transformer size that would be needed to supply the consumer load would be at least 2.1 MVA (0.5 MVA increase compared to the current transformer). By estimating the cost of an MV/LV transformer to 200 CHF/kVA [28] and supposing that the current 1.6 MVA transformer can be sold at the same price, the charging station operator would need to invest 100 kCHF to supply such a load.

Increasing the grid connection rating would cost about 100 CHF/kW and thus increase the investment by 50 kCHF.

Without the energy reserve, and therefore a smaller battery (around 1.75 MWh/1.6MW) that can provide only FCR, the payback time would be approximately 16 years.[25]

While both PPS and FCR are performed in this simulation, this happens only because of the transformer limit. This means that if the customer were to choose which service to perform on economics only and did not have a limiting transformer limit, he would only perform FCR (i.e., the incentive to perform PPS is not enough to not perform FCR with the BESS).

Ultimately, DSOs might want to incentivize EV charging station operators to perform PPS to avoid upcoming grid congestions and infrastructure reinforcements. To do so, they would need to increase the cost of power with respect to the revenues of FCR. Hence, a power cost sensitivity analysis is presented below to show the impact of higher peak power prices on the service planning.

[25] An alternative way of estimating the return of investment for the BESS without downsizing it, it would be to consider the value of the reserve. While this is case specific, a simplified consideration is based on the cost of alternative technologies that can provide this reserve. Considering backup storage with 8h runtime, a comparable system would be a 100 kW diesel generator (750 kWh are ensured to be stored in the BESS which means ~100 kW can be provided during 8 h). Typically, diesel generators cost around 800 CHF/kW which would lead to an 80 kCHF investment [29] (ignoring the rare occasions of diesel consumption costs). Taking this investment avoidance factor, the payback time would be approximately 20 years.

Simulation 4 - Peak power cost sensitivity analysis

Until now the peak power price has been fixed at 5.63chf/kW/month as discussed above. Below are the results of a peak power price set at 13 CHF/kW/month. Note that several operators in Switzerland already apply these tariffs to certain customers.

Power profiles results

Figure 65 shows the power profiles for the simulation with a 13 CHF/kW/month peak power price. One can see that the PPS target is re-computed every month and is 1.5 MW at maximum. As the transformer limit is 1.6 MW, we can conclude that PPS was performed.

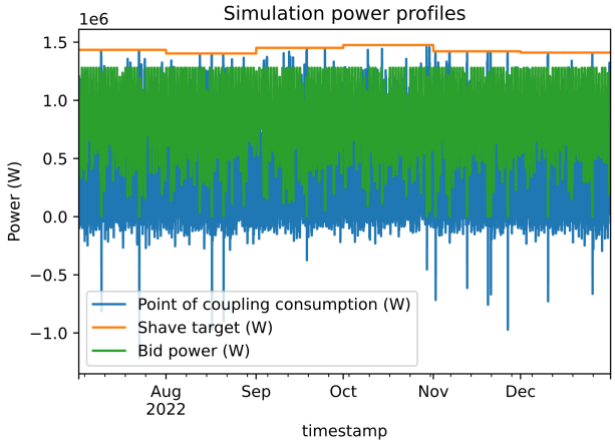

Figure 65: Simulation 4 power profiles.

Zooming on the 22nd of July better shows the PPS service being performed, with a PPS target of less than 1.5 MW (Figure 66).

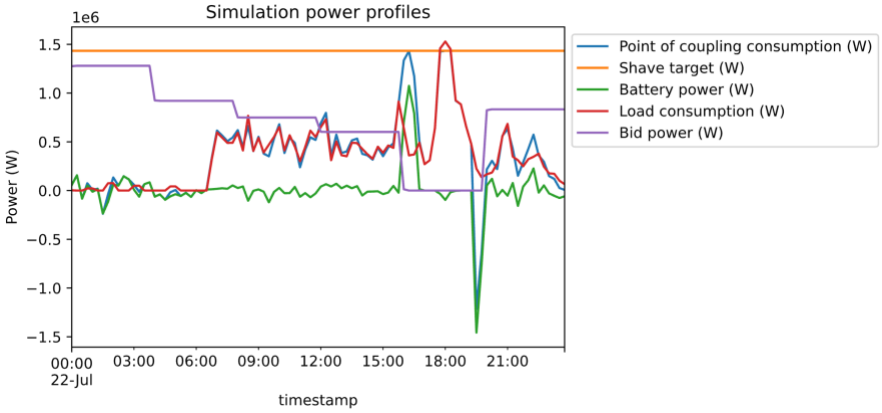

Figure 66: Simulation 4 power profiles in a single day

BESS SoC

As shown in Figure 67, the previously considered 750 kWh energy reserve limit is guaranteed. The lowest SoC reached during the simulation is 58% (i.e., 1.45 MWh always stored in the battery). It can be observed that more occurrences of PPS have been applied in order to remain within transformer limits.

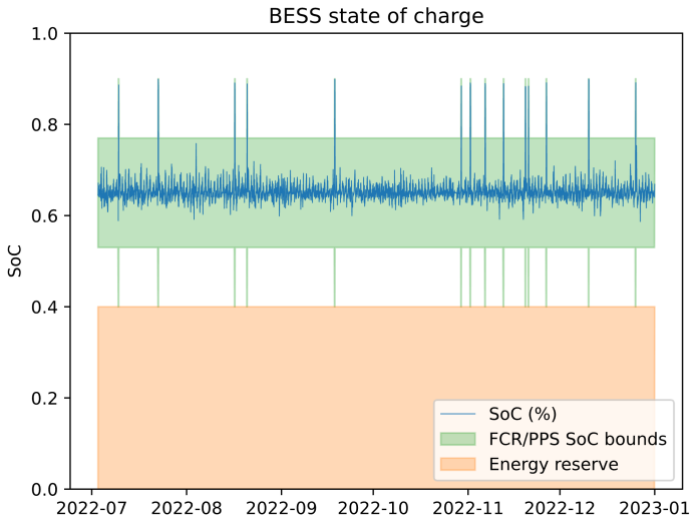

Figure 67: Simulation 4 BESS SoC.

Economics

On the customer side (the owner of the BESS), the economics of the simulation are summarized in Table 36.

Table 36: Economics of the simulation 4.

Investment cost	1625	kCHF
Maintenance cost	54.5	kCHF/year
Yearly profits	87.3	kCHF/year
Payback time	**18.6**	**Years (Without accounting energy reserve and current BESS)**
	16	**Years (accounting energy reserve revenue and grid upgrade costs)**
	13	**Years (without accounting the reserve and downsizing the BESS)**

Table 37 shows the detailed cost and revenues of the system.

Table 37: Detailed cost and revenues.

In thousand CHF per year	
Revenues	
Primary regulation	136.4
Electricity bill decrease	21
Costs	
Maintenance + insurance cost	54.5

The yearly profits are computed as follows: $(136.4 + 21) * (1 - 10\%) - 54.5 \cong$ 87.3 kCHF/year.

For the BESS operator, the yearly revenues are as follows:

Table 38: Yearly revenues in simulation 4.

In thousand CHF per year	
Commission on services	13.9
Maintenance	50.4
Total	**64.3**

If the energy reserve cost and grid upgrade costs are considered, the payback time is approx. 16 years.

Price sensitivity discussion

Further increasing the peak power price would increase the amount of PPS shaving performed and decrease the payback time for the battery. For example, running the experiment with a 20 CHF/kW/month leads to a payback time of 13 years.

To make BESS coupled with EV charging stations performing PPS, the distribution grid operator should increase the price of the power component: the energy component can be reduced so that the overall bill of a charging station operator (without the use of batteries) does not change.

In some specific cases, BESSs can be economical even with the current prices. For example, in remote places, where upgrading the infrastructure to supply the rated power of the charging stations would lead to huge investment costs, batteries can be deployed to take care of the consumption peaks.

Conclusion

In Table 39 the first simulation shows a BESS that has a break-even at about the same time than its lifetime without accounting for the economic benefit of 750kWh reserve. This means that the constant reserve of 750kWh can be considered as cost-free.

In the second simulation, it can be concluded that a battery in this context cannot be profitable without FCR as a service.

The third simulation, a tenfold increase of EVC shows lower profitability of the BESS. The reason is that with an increased load, a fixed transformer size limits the possibilities of FCR participation from the BESS.

Finally, the last simulation indicates that only if the power price triples its current value, then EV charging station operators would consider performing PPS instead of only FCR. This indicates a suggested pricing scheme for grid operators to incentivise PPS when grid congestions will arise. It is important to note that EV charging station operators may be forced to perform PPS despite any peak power price if it avoids costly grid connection reinforcement requirements.

All in all, BESS profitability alongside a charging station is possible yet not a given. To reach an attractive break-even cost, a careful dimensioning of the BESS must consider numerous parameters which also vary during its lifetime. These parameters include market prices, number of EVCs, transformer size and others.

Table 39: Cost and revenues for all 4 simulations

Simulation	4 EVC Services: FCR + PPS + Reserve	4 EVC Services: PPS + Reserve	40 EVC Services: FCR + PPS + Reserve Power price: 5.6chf/kW/month	40 EVC Services: FCR + PPS + Reserve Power price: 13chf/kW/month	
Investment	-1625	-1625	-1625	-1625	*kCHF*
O&M	-54.5	-54.5	-54.5	-54.5	*kCHF/year*
Primary control revenues	204	0	136.6	136.4	*kCHF/year*
Electricity bill savings	-28.6	17	2.3	21	*kCHF/year*
Yearly profits*	103	-38.9	70.5	87.3	*kCHF/year*
Payback time 1*	15.7	∞	23	18.6	*years*
Payback time 2**	10	30***	16	13	*years*

**Without considering the economic benefits of constant 750kWh reserve nor avoidance of transformer upgrade*
Considering a smaller BESS which does not provide an energy reserve except for *
**** Assuming no O&M cost for comparison purposes*

4.4.4. Experiment

Replicated setup

To experimentally validate the multi-service battery controller of Gridsteer, it was decided to replicate the setup of “Simulation 3 - With additional charging stations” and a power price increase at 13chf/kW/month.

Experimental setup

Since the Aigle setup is not ready for such experiment, it was replicated at EPFL by scaling down the ratings of the hardware in Aigle by a factor of 62.5. This limitation is due to the rated power of the controllable load being 30kVA. That is to say:

1. the replicated charging station load reaches 24.5 kW at maximum. In Aigle, it would reach 1.53 MW.
2. The scale-down replica of the Aigle BESS has a 40 kWh / 25.6 kW rating. The EPFL BESS SoC range is limited by the software to match these ratings (i.e., the usable SoC range is [17.7 %, 82.2%]). The power rating is replicated by setting a virtual limit in the software.
3. The transformer limit is replicated by setting a virtual limit at 25.6 kW.
4. The PPS target and FCR bids are scaled down accordingly.

The following hardware was used:

1. 1 string of a 9 string 740 kVA/560 kWh BESS, resulting in an 80 kVA/62 kWh battery virtually capped at [17.7 %, 82.2%].
2. 1 controllable electronic load (30 kVA).

Note that other nodes are also part of this network but have been ignored for the experiment.

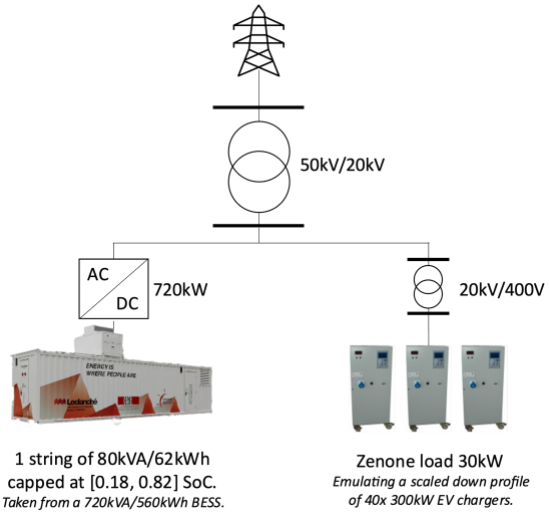

Figure 68: Experiment grid schematic

Results

The BESS performed FCR at all times except from 4pm to 8pm for PPS as planned. This respects the scheduled services and the profile curves match the simulation well as shown in Figure 69.

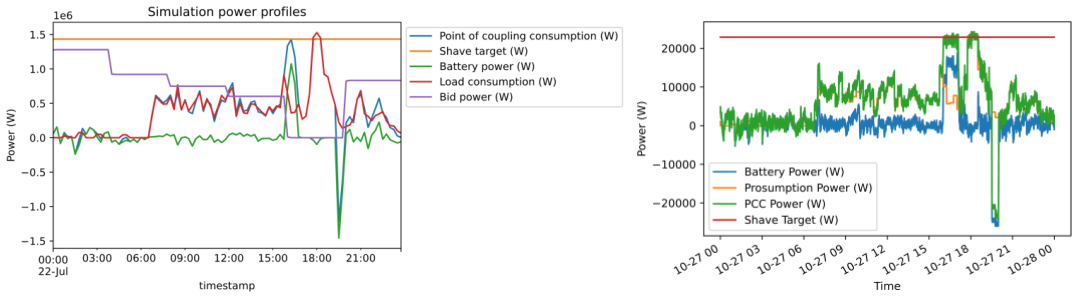

Figure 69: Simulation vs experiment power profiles.

An example of adequate FCR support for the slot of 0-4am is shown in Figure 70. The BESS power follows the frequency with a pre-defined scaled-down droop coefficient of 0.1MW/Hz (which changes for every 4h slot). Additionally, the charge management is applied to keep the BESS within a tight SoC range as shown in Figure 71.

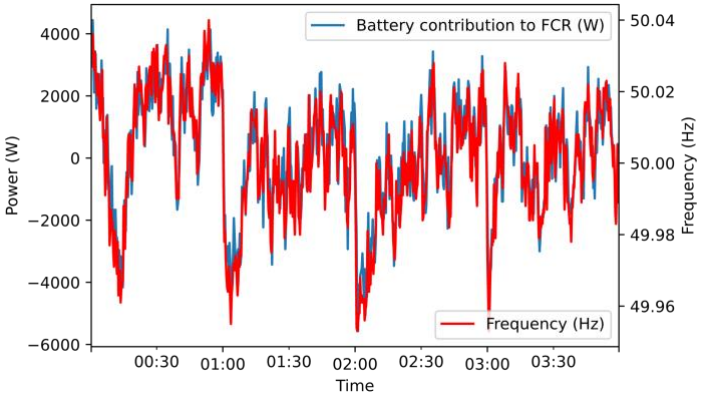

Figure 70: Experiment of BESS FCR provision.

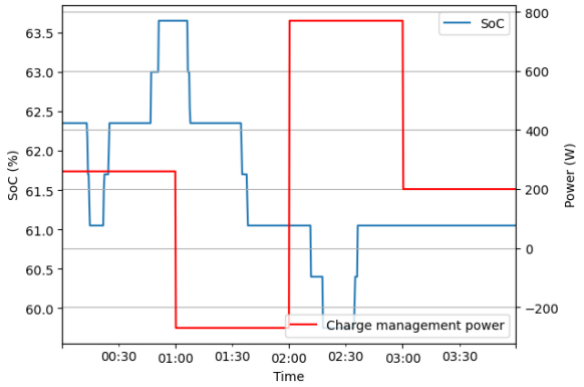

Figure 71: Experiment BESS SoC and charge management during FCR provision.

In between 4pm and 8pm, PPS operated as expected to keep the PCC power within transformer limits (see Figure 72).

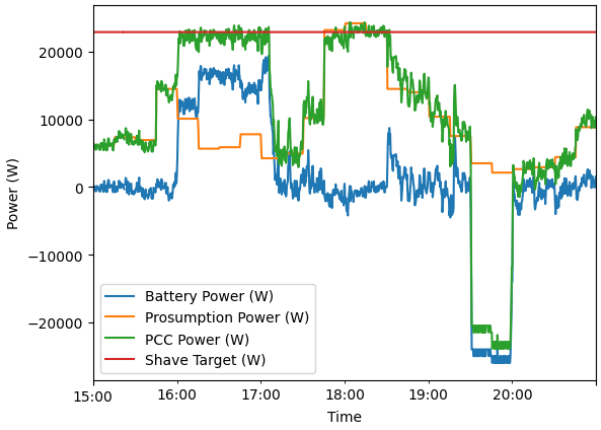

Figure 72: Experiment BESS power profiles during PPS.

The SoC during the experiment was well kept between 60 and 65% during FCR and up to 90% during PPS as show in Figure 73.

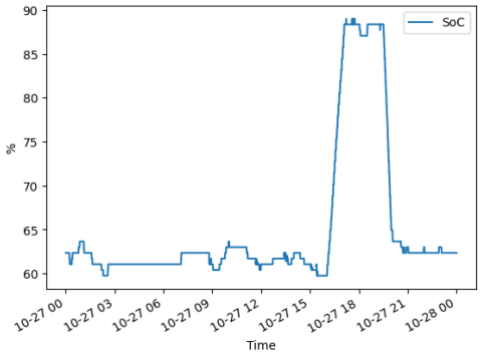

Figure 73: BESS SoC during experiment.

All in all, the results show that the scaled down battery operated in the same way as in the simulation which displays the physical feasibility of the MSBC control framework.

5. Conclusion and outlook

The key takeaway messages of this project are the given here below.

A. EVs charging profiles can be controlled for the benefit of the grid without significantly changing users satisfaction. The control framework should consider that: (i) customers tend to receive more energy than targeted (4% more); (ii) customers leave later than anticipated (10% later); (iii) customers are ready to extend their charge duration (by a few minutes) to help the grid (32% against a discount and 35% even without a monetary discount), and (iv) most users (65%) plan their EV charge based on SoC rather than a target stay duration or cost.

B. Controlling EV fast charging stations is not suitable for sub-second control frameworks and their dynamic needs to be accounted for in sub-minute control frameworks. By testing the GoFAST EVTEC charging station with a Tesla Model S90D, one can observe response times varying between the second to minute range depending on the amplitude of the setpoint power variation. Moreover, one can observe that the implementation error follows a quadratic trend, where the error is largest for low and high setpoints. However, the car model might contribute to these characteristics, thus implying that other car models might lead to significantly different results.

C. Combining a controllable EVCS and a BESS has measurable benefits for grid management and control. The control of EVCS alone in the day-ahead stage already provides several measurable benefits in terms of reduction of the untracked energy error, and shaving the peak PCC injections, without penalizing EV users' satisfaction. However, it does not guarantee that the flexibility will be available when it is needed since it is uncertain when the EV(s) will be present at the charger. Therefore, the installation of a BESS is required. Even more, when EVCS and BESS are controlled in real-time, notably by the control framework developed in the MESH4U project, all error metrics are reduced by more than tenfold compared to a without-control scenario.

D. The control of EVCS can reduce the need for BESS investment without affecting EVCS user's satisfaction. At the same time, the increase of the BESS's energy and apparent power capacity has a limited impact on the dispatching cumulative energy uncertainty (at least in our case study).

E. The adoption of controlled EVCS can lower their impact to the grid. It is ubiquitous that adding fast EVCS is inevitable to promote the transition towards electric mobility. It is also known that their deployments are viewed as a risk for the grid from the added stochasticity and peak power demands. However, with adequate control of the stations, one can not only lower their impact on the grid but also provide useful grid support (e.g., day-ahead dispatching). Public fast charging stations can therefore not only help the electric mobility transition but also provide grid flexibility to the condition that they are both controllable and controlled. It is thus important to consider this aspect in the selection process of future charging station providers.

F. Commercial fleet charging stations (CFCS) can support the electrification of the mobility sector in a more cost-efficient way than the public fleet charging stations (PFCS). For the same CS energy demand, the required battery size to track the dispatch plan is ten times smaller for a CFCS. In terms of required infrastructure and investments, one can achieve more grid predictability and flexibility with lower investments by implementing dispatch plans on nodes encapsulating schedulable and controllable commercial fleet charging stations. Due to the significantly higher stationary battery investment costs, when truly necessary for the grid, tracking a PCC node encapsulating highly stochastic PFCSs can be achieved. Figure 74 qualitatively shows the grid support versus cost analysis between different levels of prediction/scheduling and control for both PFCS and CFCS:

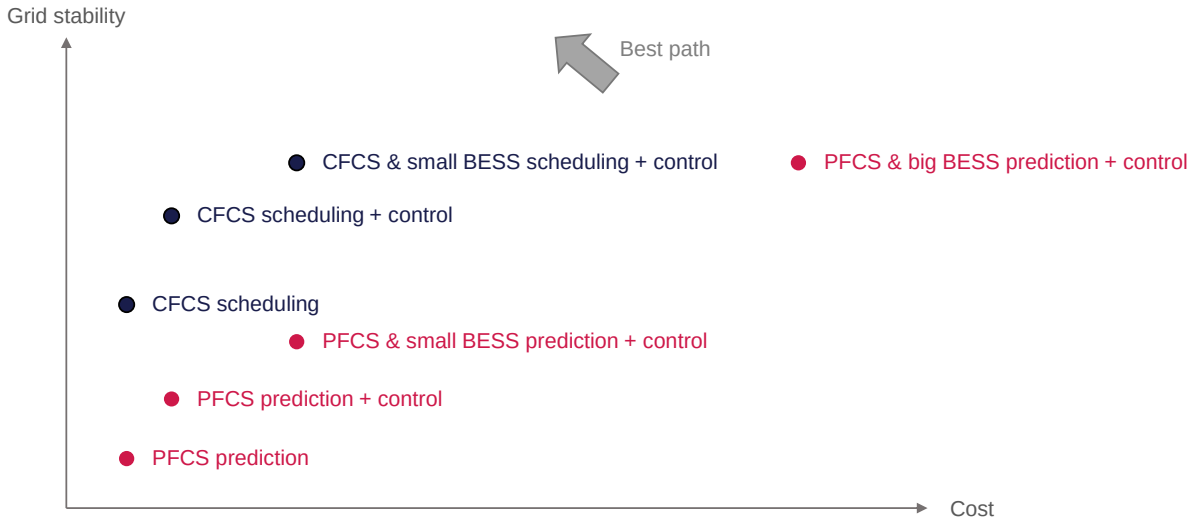

Figure 74: CFCS vs PFCS measures analysis in grid stability and cost.

G. The profitability of an investment in BESS coupled with EVCS is case specific. To make BESS coupled with EVCS economically worth performing peak power shaving (PPS), the distribution grid operator should increase the price of the power component. Note that the energy component can be reduced so that the overall bill of a charging station operator (without the use of batteries) does not change. While for the case of the Aigle setup, using the battery to perform PPS is not economical, in some specific cases, BESSs can be economically worth even with the existing prices. For example, in remote places, where upgrading the infrastructure to supply the rated power of the charging stations would lead to huge investment costs, batteries can be deployed to take care of the consumption peaks. Other locations with significant PV production and low feed-in tariffs can also make BESS profitable as self-consumption would be added to the panel of services. To reach an attractive break-even cost, a careful dimensioning of the BESS must consider numerous parameters which vary during its lifetime. These parameters include market prices, number of EVCs, transformer size, the load evolution and others.

6. National and international cooperation

This project was undertaken under the international collaboration framework ERA-Net Smart Energy Systems' focus initiatives Smart Grid Plus and Integrated, Regional Energy Systems. The ERA-Net project, entitled Multi Energy Storage Hub For reliable and commercial systems Utilization (MESH4U), aimed to develop, and test multi energy storage hub solutions for flexibility operation from end customers in the local grids, via SMEs/Industry up to the Energy/Distribution System Operator. The objective was to enhance the reliability and economic advantage of energy supply as well as to offer more flexibility and cost efficiency to the modern distribution power grids. The MESH4U solutions was implemented in 4 demonstrators in different countries, namely Germany, Italy, Poland and Switzerland, in order to test several use cases and applications of multi energy storage hubs within different infrastructures, size of the systems, regulatory and market conditions.

EPFL-DESL was leading the WP2 on the Development of methodologies and algorithms for optimal planning and operation of Flexibility Hub and provided contributions to WP1 and WP4 while ensuring the transfer of information and knowledge among Swiss and European partners. WP1 was on the analysis and modeling of different storage technologies and their dependencies in multi-storage system, while WP4 on the implementation and operation of Mesh4U in demonstrators PL, DE, CH, IT.

Concrete research activities were also undertaken notably with the MESH4U project partners of the University of Rome Tor Vergata (see section *4.3.4*).

7. Publications

Fahmy, S. (2022). *Efficient Methods for the Operation of Microgrids in Unsymmetric and Uncertain states* (PhD thesis). EPFL, 2022.

Chevron, Max (2021) *Day-ahead grid-aware dispatcher for active distribution networks embedding stochastic electric vehicle charging stations* (Master Thesis) EPFL, 2021.

Gupta Rahul, Sherif Fahmy, Max Chevron, Riccardo Vassapolo, Enea Fagini, Mario Paolone, Grid-aware Scheduling and Control of Electric Vehicle Charging Stations for Dispatching ADNs. Part-I: Dayahead and Numerical Validation *[submitted for the publication to the IEEE Transaction of Smart Grids, under review].*

Gupta Rahul, Sherif Fahmy, Max Chevron, Enea Fagini, Mario Paolone, Grid-aware Scheduling and Control of Electric Vehicle Charging Stations for Dispatching ADNs. Part-II: Intraday and Experimental Validation *[submitted for the publication to the IEEE Transaction of Smart Grids, under review].*

8. References

[1] United Nations Framework for Climate Change. The Paris Agreement. Retrieved 16 May 2023 from https://unfccc.int/process-and-meetings/the-paris-agreement

[2] FOEN, F. (2021). Long-term climate strategy to 2050. Retrieved 13 December 2021, from https://www.bafu.admin.ch/bafu/en/home/topics/climate/info-specialists/emission-reduction/reduction-targets/2050-target/climate-strategy-2050.html

[3] FOEN, F (2023). Evolution of Switzerland's greenhouse gas emissions since 1990 (April 2023). Retrieved 16 May 2023, from https://www.bafu.admin.ch/dam/bafu/en/dokumente/klima/fachinfo-daten/THG_Inventar_Daten.xlsx.download.xlsx/Evolution_GHG_since_1990_2023-04.xlsx

[4] FOEN, F (2022). Evolution of Switzerland's greenhouse gas emissions since 1990 (April 2022). Retrieved 10 February 2023, from https://www.bafu.admin.ch/dam/bafu/en/dokumente/klima/fachinfo-daten/THG_Inventar_Daten.xlsx.download.xlsx/Evolution_GHG_since_1990_2022-04.xlsx

[5] Swiss confederation-STAT. New registrations of road vehicles by vehicle group and type. Retrieved 16 May 2023 from https://www.pxweb.bfs.admin.ch/pxweb/fr/px-x-1103020200_120/px-x-1103020200_120/px-x-1103020200_120.px/table/tableViewLayout2/

[6] FOEN, F. (2021). Indicator Climate. Retrieved 13 December 2021, from https://www.bafu.admin.ch/bafu/en/home/themen/thema-klima/klima--daten--indikatoren-und-karten/klima--indikatoren/indikator-klima.pt.html

[7] Swiss Federal Office of Energy, “Kennzahlen alternative Antriebe Neuwagen”, 2019, https://www.bfe.admin.ch/bfe/en/home/supply/statistics-and-geodata/key-vehicle-data/key-data-relating-to-alternative-drives.html

[8] F. Sossan and al. « Achieving the Dispatchability of Distribution Feeders Through Prosumers Data Driven Forecasting and Model Predictive Control of Electrochemical Storage ». In: (2016).

[9] R. Gupta and al. « Grid-aware Distributed Model Predictive Control of Heterogeneous Resources in a Distribution Network: Theory and Experimental Validation ». In: (2020).

[10] A. Bernstein and al. « A composable method for real-time control of active distribution networks with explicit power setpoints. Part I: Framework ». In: (2015).

[11] L. Reyes-Chamoro and al. « A composable method for real-time control of active distribution networks with explicit power setpoints. Part II: Implementation and validation ». In: (2015).

[12] R. Rudnik and al. \Real-Time Control of an Electric-Vehicle Charging Station While Tracking an Aggregated Power-Setpoint". In: (2020).

[13] Transmission Code et Balancing Concept Suisse. Swissgrid. (n.d.). Retrieved December 13, 2021, from https://www.swissgrid.ch/fr/home/customers/topics.html#transmission-code-et.

[14] Fahmy, S. (2022). *Efficient Methods for the Operation of Microgrids in Unsymmetric and Uncertain states* (No. THESIS). EPFL.

[15] Refaeilzadeh, P., Tang, L., & Liu, W. (2009). Cross-validation. *Encyclopedia of database systems*, *5*, 532-538.

[16] Reynolds, D. A. (2009). Gaussian mixture models. *Encyclopedia of biometrics*, *741*(659-663).

[17] Sedgwick, P. (2012). Pearson's correlation coefficient. *Bmj*, *345*.

[18] Berger, V. W., & Zhou, W. (2014). Kolmogorov–smirnov test: Overview. *Wiley statsref: Statistics reference online*.

[19] Fahmy, S., Gupta, R., & Paolone, M. (2020). Grid-aware distributed control of electric vehicle charging stations in active distribution grids. *Electric Power Systems Research*, *189*, 106697.

[20] Likas, A., Vlassis, N., & Verbeek, J. J. (2003). The global k-means clustering algorithm. *Pattern recognition*, *36*(2), 451-461.

[21] Arthur, D., & Vassilvitskii, S. (2006). *k-means++: The advantages of careful seeding*. Stanford.

[22] Leehter Yao, Wei Hong Lim, and Teng Shih Tsai. A real-time charging scheme for demand response in electric vehicle parking station. IEEE Transactions on Smart Grid, 8(1):52–62, 2016.

[23] Fahmy, S., & Paolone, M. (2021, June). Analytical Computation of Power Grids' Sensitivity Coefficients with Voltage-Dependent Injections. In *2021 IEEE Madrid PowerTech* (pp. 1-6). IEEE.

[24] Namor, E., Sossan, F., Scolari, E., Cherkaoui, R., & Paolone, M. (2018, October). Experimental assessment of the prediction performance of dynamic equivalent circuit models of grid-connected battery energy storage systems. In *2018 IEEE PES innovative smart grid technologies conference Europe (ISGT-Europe)* (pp. 1-6). IEEE.

[25] Gupta, R., Fahmy, S., & Paolone, M. (2022). Coordinated day-ahead dispatch of multiple power distribution grids hosting stochastic resources: An ADMM-based framework. *Electric Power Systems Research*, *212*, 108555.

[26] Fahmy, S., Walger, Q., & Paolone, M. (2022). Resynchronization of islanded unbalanced ADNs: Control, synchrocheck and experimental validation. *Electric Power Systems Research*, *211*, 108496.

[27] Schiapparelli, G.P., Massucco, S., Namor, E., Sossan, F., Cherkaoui, R., & Paolone, M (2018). Quantification of Primary Frequency Control Provision from Battery Energy Storage Systems Connected to Active Distribution Networks. *2018 Power Systems Computation Conference (PSCC)*

[28] Pertes du transformateur, Energie Retrieved Oct 13, 2022, from https://energieplus-lesite.be/concevoir/reseau-electrique55/choisir-un-transformateur/

[29] Kurtz, J., Saur, G., Sprik, S., & Ainscough, C. (2014) Backup Power Cost of Ownership Analysis and Incumbent Technology Comparison. NREL https://www.nrel.gov/docs/fy14osti/60732.pdf

[30] Gupta, R., Sossan, F., & Paolone, M., (2021) Countrywide PV hosting capacity and energy storage requirements for distribution networks: The case of Switzerland *Applied Energy*, vol. 281, 2021, 116010.

[31] R. Gupta, A. Zecchino, J. -H. Yi and M. Paolone, "Reliable Dispatch of Active Distribution Networks via a Two-Layer Grid-Aware Model Predictive Control: Theory and Experimental Validation," in *IEEE Open Access Journal of Power and Energy*, vol. 9, pp. 465-478, 2022, doi: 10.1109/OAJPE.2022.3216072.

[32] L. Bartolucci et al., "Grid service potential from optimal sizing and scheduling the charging hub of a commercial Electric Vehicle fleet," 2020 IEEE International Conference on Environment and Electrical Engineering and 2020 *IEEE Industrial and Commercial Power Systems Europe (EEEIC / I&CPS Europe), Madrid, Spain, 2020*, pp. 1-6, doi: 10.1109/EEEIC/ICPSEurope49358.2020.9160695.